Identification of critical epigenetic modifiers in prostate cancer

by

Bengül GÖKBAYRAK

A Dissertation Submitted to the
Graduate School of Sciences and Engineering in
Partial Fulfillment of the Requirements for the Degree of

Doctor of Philosophy

in

Molecular Biology and Genetics

KOÇ ÜNİVERSİTESİ

January 21, 2022

Identification of critical epigenetic modifiers in prostate cancer

Koc University

Graduate School of Science and Engineering

This is to certify that I have examined this copy of a doctoral dissertation by

Bengül GÖKBAYRAK

and have found that is complete and satisfactory in all respects, and that any and all revisions required by the final examining committee have been made.

Committee Members:

Associate Professor Nathan A. Lack (Advisor)

Associate Professor Tuğba Bağcı-Önder

Associate Professor N.C. Tolga Emre

Associate Professor Ceyda Açılan-Ayhan

Assistant Professor Ahmet Acar

Date: January 21, 2022

I dedicate my thesis

to my parents, Fatma and Halim Çetin,

to my sister, Nilgün,

to my husband, Onur,

who supported me endlessly and encouraged me in every step of the way.

I couldn't have done this without you.

ABSTRACT

Identification of critical epigenetic modifiers in prostate cancer

Bengül GÖKBAYRAK

Doctor of Philosophy in Molecular Biology and Genetics

January 21, 2022

Prostate cancer (PCa) is the second leading cause of cancer-related death in men. The introduction of potent second-generation antiandrogens such as enzalutamide (ENZA) has improved overall survival for patients with recurrent or metastatic PCa. Yet, while patients initially respond to treatment, the vast majority eventually develop resistance. ENZA-resistant PCa is almost invariably lethal, and few treatment options are available. Clinical and basic studies have demonstrated that epigenetic events play a critical role in the development of ENZA resistance by changing the genome accessibility through DNA methylation, histone modifications, and chromatin remodeling. Considering their critical function and druggability, epigenetic modifiers offer a promising pharmacological target to treat ENZA-resistant PCa.

This study aims to identify critical epigenetic modifiers in late-stage ENZA-resistant PCa. Due to the availability of lysine demethylase (KDM) inhibitors, we tested the essentiality of all KDM enzymes to provide preclinical evidence that would support further drug development. We performed an arrayed screen using a KDM-focused shRNA library in multiple PCa cell lines. Despite previous literature, we observed that the knockdown of KDM enzymes largely had little effect on PCa proliferation, potentially due to genetic redundancies. To expand the focus of the project and screen all epigenetic modifiers, we, therefore, generated an epigenetic-focused CRISPR library and performed unbiased CRISPR-Cas9 dropout screens in multiple PCa and ENZA-resistant cell lines. Although shRNA screen results were inconclusive, our epigenome-wide CRISPR-Cas9 screens (EPIKOL) identified both known and novel epigenetic targets in ENZA-resistant PCa. From this, we focused on SMARCC2, a core subunit of the SWI/SNF complex as a potential candidate for ENZA-resistant prostate cancer. We confirmed SMARCC2-dependency on multiple ENZA-resistant models with orthogonal proliferation assays. We found that the SMARCC2 cistrome was significantly expanded in ENZA-resistant cells with marked differences in transcription factor occupancy. These gained binding sites correlated with increased chromatin structures in PDX and clinical CRPC samples. Collectively, these findings suggest that the SMARCC2-dependent SWI/SNF complex gains an essential role in ENZA resistance by expanding its chromatin regulation. This dependency could be exploited for the treatment of ENZA-resistant CRPC by SWI/SNF inhibitors.

OZETCE

Prostat kanserinde önemli olan epigenetik düzenleyicilerin saptanması

Bengül GÖKBAYRAK

Moleküler Biyoloji ve Genetik, Doktora

21 Ocak 2022

Prostat kanseri (PK), erkeklerde kansere bağlı ölümlerin ikinci önde gelen nedenidir. Enzalutamid (ENZA) gibi güçlü ikinci nesil antiandrojenlerin piyasaya sürülmesi, tekrarlayan veya metastatik PK'lı hastalar için genel sağkalımı iyileştirmiştir. Hastalar başlangıçta tedaviye yanıt vermesine rağmen, büyük çoğunluğu sonunda direnç geliştirir. ENZA'ya dirençli PK neredeyse her zaman ölümcüldür ve çok az tedavi seçeneği mevcuttur. Klinik ve temel çalışmalar, epigenetik olayların, DNA metilasyonu, histon modifikasyonları ve kromatin şekillenmesi yoluyla genom erişilebilirliğini değiştirerek ENZA direncinin gelişmesinde kritik bir rol oynadığını göstermiştir. Kritik işlevleri ve ilaç geliştirilebilecek yapıları göz önüne alındığında, epigenetik düzenleyiciler, ENZA'ya dirençli PK'yı tedavi etmek için umut verici bir farmakolojik hedef sunar.

Bu çalışma, geç evre ENZA'ya dirençli PK'daki kritik epigenetik düzenleyicileri belirlemeyi amaçlamaktadır. Lizin demetilaz (KDM) inhibitörlerinin geliştirilmiş olması nedeniyle, ilaç geliştirmeyi daha fazla destekleyecek klinik öncesi kanıtlar sağlamak için tüm KDM enzimlerinin gerekliliğini test ettik. Birden fazla PK hücre hattında KDM odaklı bir shRNA kitaplığı kullanarak dizili bir tarama gerçekleştirdik. Önceki literatüre rağmen, KDM enzimlerinin susturulmasının, potansiyel olarak genetik benzerlikler nedeniyle PK proliferasyonu üzerinde genel olarak çok az etkisi olduğunu gözlemledik. Projenin odağını genişletmek ve tüm epigenetik düzenleyicileri taramak için, epigenetik odaklı bir CRISPR kitaplığı oluşturduk ve birden fazla PK ve ENZA'ya dirençli hücre hattında tarafsız CRISPR-Cas9 taramaları gerçekleştirdik. shRNA tarama sonuçları yetersiz olmasına rağmen, epigenom çapındaki CRISPR-Cas9 taramalarımız (EPIKOL), ENZA'ya dirençli PK'da hem bilinen hem de yeni epigenetik hedefleri tanımladı. Bundan yola çıkarak, ENZA'ya dirençli prostat kanseri için potansiyel bir aday olarak SWI/SNF kompleksinin bir çekirdek alt birimi olan SMARCC2'ye odaklandık. Ortogonal proliferasyon deneyleri ile birden fazla ENZA dirençli modelde SMARCC2 bağımlılığını doğruladık. SMARCC2 kromatin bağlanma bölgelerinin ENZA'ya dirençli hücrelerde önemli ölçüde genişlediğini ve bu yerlere bağlı transkripsiyon faktörü profilinde belirgin farklılıklar olduğunu bulduk. Kazanılan bağlanma bölgeleri, PDX ve klinik CRPC numunelerinde artan kromatin erişilebilirliği ile ilişkilendirilebilir. Özet olarak, bu bulgular SMARCC2'ye bağlı SWI/SNF kompleksinin kromatin düzenlemesini genişleterek ENZA direncinde önemli bir rol kazandığını göstermektedir. Bu bağımlılık, ENZA'ya dirençli kastrasyon dirençli PK'nin SWI/SNF inhibitörleri tarafından tedavisi için kullanılabilir.

ACKNOWLEDGEMENT

I started my PhD right after my Bachelor's degree. I had no idea what is on my path or where it is taking me. I would like to thank Dr. Nathan Lack for his guidance and his encouragement on this path both academically and personally. He entirely changed my life in multiple ways by inviting me to Vancouver Prostate Centre (VPC) to conduct my experiments. He understands the struggle we are in, empathizes and encourages us to do better. He is inspiring us in every aspect to become a well-accomplished scientist. I feel extremely privileged to be a part of his team.

I would like to thank my thesis monitoring committee members Dr. Tuğba Bağcı-Önder and Dr. N.C. Tolga Emre for their time and insightful discussions. I would like to thank Dr. Ceyda Açılan-Ayhan and Dr. Ahmet Acar for accepting the invitation to be a part of my PhD defense jury. Additionally, I express my sincere gratitude to Dr. James Lynch from AstraZeneca UK for our regular discussions and his insightful comments.

I would like to thank KUSOM, KUTTAM and VPC for providing a cutting-edge research environment and their administrative staff for their help and support to arrange my transfer between two labs. I would like to thank AstraZeneca Turkey, KUTTAM and VPC for their financial support during my PhD studies.

I would like to thank everyone who contributed to the both versions of the library, to the current and previous members of Önder and Bağcı-Önder's lab; Fidan, Ezgi, Filiz, Alisan, Ozlem, Derya, Can, Kenan, Firat and Tunc, and many others. I would like to thank Dr. Tamer Önder for the shRNA library, and Dr. Ceyda Açılan-Ayhan, Dr. Amina Zoubeidi and Dr. Martin Gleave for the cell lines. Dr. Ahmet Cingoz and Betul Ersoy provided extreme help with the ongoing animal studies. Tunc Morova did the initial NGS analysis in CRISPR screens. Dr. Shreyas Lingadahalli performed ChIP-seq experiments. Umut Berkay Altintas analyzed ChIP-seq, RNA-seq and clinical ATAC-seq data. Elif Demirtas and Erinc Barcin, previous undergrad students in our lab, helped with experiments in shRNA screen and cloning of validation vectors. I am grateful for their time, help and patience.

I was lucky enough to work in two stunning academic institutions during my PhD, with groups of people who support and help each other continuously both at work and outside of work. I would like to thank previous and current members of Lack Lab. Hilal, Fatma, Nil, Tunc, Dogancan, Zeynep and Ceren provided a supportive and friendly Lack Lab spirit from the very beginning of this long journey. I will always appreciate our memories in the small coffee breaks, in multiple weddings including mine. The Lack Lab spirit later on followed me in Vancouver Prostate Centre. When we first established our lab in VPC, it was only me, Flora Huang and Nathan. I cannot thank Flora enough for all the moments we shared along the way; her kindness and modesty, the long night talks after a long day in the lab, our car rides with my amateur co-piloting, her wonderful and thoughtful gestures to everyone in the lab. Tunc later on joined us in VPC boosting up our energy here as well. He encouraged me to use RStudio which become a very essential tool to me after a while due to managing large datasets. Our lab in VPC grew in last 4 years, and I had a chance to meet these wonderful people and work with them. Ivan is a wonderful scientist, a great listener and a great neighbor, very sophisticated young man with lots of virtues. Shreyas always inspired me by his quick-thinking and deep knowledge of literature, and also a good taste of beer. Meric is very determined with his decisions and very persistent which makes him a perfect match for protein crystallization work. Having Dogancan in VPC is a great contribution to VPC district. People that I met in VPC, Mitali Pandey, Eliana Beraldi, Helene Morin and many others, were extremely supportive and friendly. They all inspired me for better versions of myself. I would like to thank you all for this productive, competitive, cooperative working environment and also for your support and friendship outside of work. I can't state this enough; I feel very lucky to work with all these people during my PhD.

I would like to thank my best friends Gozde and Izel, for their support beyond 10,000km distance and also beyond years considering that we know each other for at least 15 years. Lastly, the family of Cetin Ceviz! All I can think of is how lucky I am to be a daughter of two very capable, hardworking, loving people, and to be the sister of a young woman who is very creative, thoughtful and loving. Thank you for your unconditional love and growing support over the years. I feel so proud to be a part of my family. My husband… who decided to join me in my Vancouver journey without thinking twice, and being on my side in every occasion with lots of sacrifices. I couldn't make it without you. Thank you for everything.

TABLE OF CONTENTS

LIST OF TABLES

LIST OF FIGURES

ABBREVIATIONS

ADD	ATRX-DNMT3-DNMT3L
ADT	Androgen Deprivation Therapy
AF1	Activation Function-1
AF2	Activation Function-2
AR	Androgen Receptor
AR-V	Androgen Receptor Splice Variant
ARE	Androgen Response Elements
BAF	BRG1/BRM-Associated Factor
BET	Bromodomain And Extra-Terminal Motif
bHLH	Basic-Helix-Loop-Helix
BPH	Benign Prostate Hyperplasia
cBAF complex	Canonical BAF Complex
CHD	Chromodomain Helicase DNA-Binding Domain
ChIP	Chromatin Immunoprecipitation
CHROMO	Chromodomain
CRISPR	Clustered Regularly Interspaced Short Palindromic Repeats
CRPC	Castration Resistant Prostate Cancer
CTE	Carboxy Terminal Extension
DBD	DNA-Binding Domain
DE	Differentially Expressed
DHT	Dihydrotestosterone
DNA	Deoxyribonucleic Acid
DNMT	DNA Methyltransferase
DRE	Digital Rectal Examination
dsRNA	Double Stranded RNA
DUB	Deubiquitinating Enzymes
ENZA	Enzalutamide
EPIKOL	Epigenetic Knockout Library
ER	Estrogen Receptor
FSH	Follicle-Stimulating Hormone
gBAF	Gained BAF
GnRH	Gonadotropin-Releasing Hormone

GR	Glucocorticoid Receptor
gSMA	Gained SMARCC2
H3K27ac	Histone 3 Lysine 27 Acetylation
H3K27me1/2/3	Histone 3 Lysine 27 Mono-/Di-/Tri-Methylation
H3K4me1/2/3	Histone 3 Lysine 4 Mono-/Di-/Tri-Methylation
HDAC	Histone Deacetylase
HDR	Homology Directed Repair
HPG axis	Hypothalamic-Pituitary-Gonadal Axis
HSA domain	Helicase/SANT-Associated Domain
HSPC	Hormone-Sensitive Prostate Cancer
HSS domain	Hand-Sant-Slide Domain
ISWI	Imitation Switch
KAT	Lysine Acetyltransferase
KDM	Lysine Demethylase
KMT	Lysine Methyltransferase
LBD	Ligand-Binding Domain
LH	Luetinizing Hormone
LHRH	Luetinizing Hormone-Releasing Hormone
MBD	Methyl-Binding Domain
MBT domain	Malignant Brain Tumor Domain
miRNA	Micro RNA
MOI	Multiplicity of Infection
MR	Mineralocorticoid Receptor
ncBAF complex	Non Canonical BAF Complex
NES	Nuclear Export Signal
NHEJ	Non-Homologous End Joining
NLS	Nuclear Localization Signal
NTD	N-Terminal Domain
NUC lobe	Nuclease Lobe
PAM	Protospacer Adjacent Motif
PBAF complex	Polybromo-Associated BAF Complex
PCa	Prostate Cancer
PCR	Polymerase Chain Reaction

PHD	Plant Homeodomain
PI domain	Pam-Interacting Domain
PIP2	Phosphatidylinositol-4,5-Bisphosphate
PIP3	Phosphatidylinositol-3,4,5-Trisphosphate
PR	Progesterone Receptor
PRC2	Polycomb Repressive Complex 2
PRMT	Protein Arginine Methyltransferases
PSA	Prostate-Specific Antigen
rBAF	Retained BAF
REC lobe	Recognition Lobe
RIME	Rapid Immunoprecipitation Mass Spectrometry of Endogenous Proteins
RNA	Ribonucleic Acid
RNAi	RNA Interference
RRA	Robust Rank Aggregation
RT-qPCR	Reverse-Transcriptase Quantitative PCR
SAM	S-Adenosyl-L-Methionine
sgRNA	Single Guide RNA
SHBG	Sex-Hormone Binding Globulin
shRNA	Short Hairpin RNA
siRNA	Small-Interfering RNA
SUMO	Small Ubiquitin-Like Modifier
SWI/SNF	Switch/Sucrose Non-Fermentable
t-NEPC	Treatment-Induced Neuroendocrine Prostate Cancer
TALEN	Transcription-Activator Like Effector Nuclease
TET	Ten-Eleven Translocation
ZFN	Zinc Finger Nuclease

Chapter 1 INTRODUCTION

1.1 Prostate Gland

The prostate gland is a walnut-sized, endoderm-derived secretory gland in the male reproductive system. It produces and secretes prostatic fluid during ejaculation, which contributes to male fertility by semen liquefaction, sperm motility, and sperm capacitation [1–3]. Prostatic fluid contains prostate-specific antigen (PSA) which digests semen-coagulating proteins, thereby promotes semen liquefaction and sperm motility [1–3].

1.1.1 Anatomy and Structure of Prostate Gland

The human prostate is a unilobular gland anatomically divided into the central, transitional, and peripheral zones (**Figure 1.1a**) [1,3,4]. The zones are covered anteriorly by fibromuscular zone and exteriorly by fibrous capsule [1]. The central zone makes up 20-25% of the prostate gland [1]. It surrounds the ejaculatory duct and extends to the bladder base. The transitional zone surrounds the urethra and constitutes approximately 5-10% of the gland [1]. The peripheral zone is the largest zone making up 70-75% of the gland and it spans the prostate's apical, posterior and lateral sides. This zone is commonly affected by chronic prostatitis [1]. Benign prostatic hyperplasia (BPH), a non-malignant tissue enlargement, is typically observed in transitional zone [5]. Prostate cancer (PCa) primarily occurs in the peripheral zone (70%) though it is also observed in the central zone (1-5%) and transitional zone (20%) [1].

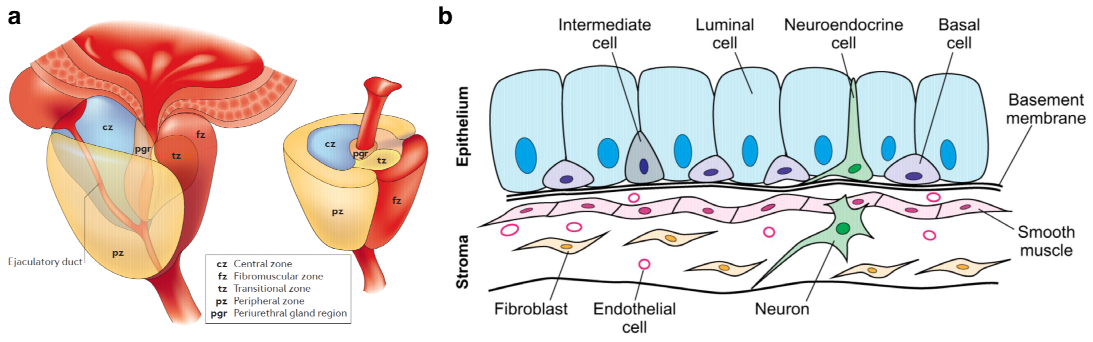

Figure 1.1 (a) The anatomy and (b) cellular structure of prostate tissue. Figures taken from [2,3].

The adult prostate is composed of ducts layered with epithelial cells that sit on a basement membrane supported by stromal cells (**Figure 1.1b**) [1–3]. The prostate epithelium consists of different cell types including luminal, neuroendocrine, basal and intermediate cells. Luminal cells are the most abundant terminally-differentiated cell type in the prostate epithelium [1,2]. They express luminal markers cytokeratin 8 and 18, PSA, prostatic acid phosphatase, and androgen receptor (AR) [2,3]. The connection between luminal cells is mediated through cell-cell adhesion molecules concentrated in desmosomes and tight junctions. These luminal cells are also connected to the basement membrane through integrins, which help the integrity of the epithelium. Neuroendocrine cells are rare, terminally-differentiated cells with a low proliferation index [1,2]. They reside among secretory luminal cells and contribute to epithelial growth and differentiation. Neuroendocrine cells release peptide hormones or prohormones that are important for the paracrine and autocrine activity of the prostate gland [1,2]. They have no or undetectable levels of AR and PSA. Basal cells are small, pyramid-shaped, undifferentiated cells that reside on the basement membrane and have a low proliferative index. They express high levels of basal markers cytokeratin 5 and 14, and no expression of AR, PSA, or prostatic acid phosphatase [1,2]. Intermediate cells express both basal and luminal cell markers. They are highly proliferative, and their proliferation is androgen-dependent [1,2]. A stromal compartment flanks the prostatic duct, supports and maintains the local microenvironment. It consists of both extracellular matrix and stromal cells such as fibroblasts, capillaries, lymphatic endothelial cells, smooth muscle cells, neuroendocrine cells, and axons [2,3]. The communication between the stromal and epithelial compartments regulates cell adhesion, proliferation, differentiation, growth, and migration [2,3].

1.1.2 Endocrinology of Testosterone

The male reproductive system is tightly controlled by testosterone [1,6]. In men, testosterone production is regulated by the hypothalamic-pituitary-gonadal axis (HPG axis). This complex process is initiated by hypothalamus stimulation, which causes the secretion of luteinizing hormone-releasing hormone (LHRH), also known as gonadotropin-releasing hormone (GnRH). In the anterior pituitary gland, LHRH then induces gonadotrophs to secrete decapeptide hormones, luteinizing hormone (LH) and follicle-stimulating hormone (FSH) [6,7]. Finally, LH stimulates Leydig cells in the testes

to produce testosterone. This site synthesizes 95% of all testosterone produced in the male body. Adrenal glands synthesize the other 5% under the control of adrenocorticotropic hormone [1,6]. Testosterone production has both annual and daily pulses that peak in springs and in the mornings [8]. Testosterone production pulses are disrupted by aging [1]. Due to its hydrophobicity, the vast majority of secreted testosterone is protein bound in the bloodstream with 67% loosely bound to albumin or other serum proteins, 30% tightly bound to sex hormone-binding globulin (SHBG), and only 0.5-3% circulating unbound [1]. Testosterone that is free/unbound or albumin-bound is considered bioavailable. Therefore, the ratio of SHBG to albumin determines the relative bioavailable testosterone levels in blood [1]. Bioavailable testosterone can freely pass through the cellular membrane because of its lipophilic structure. Once inside the prostate cell, it is irreversibly converted to the more active androgen, dihydrotestosterone (DHT), by 5α-reductase type II (SRD5A2) [1,6].

1.1.3 Androgen Receptor

Testosterone and its potent form DHT bind to AR and induce its conformational change, which leads to AR translocation into the nucleus and transcription of AR-target genes [9]. The prostate gland depends on androgen receptor (AR) activity for organ development and maintenance. Androgen receptor (NR3C4) is a member of steroid hormone receptors which is part of the nuclear receptor superfamily [9]. Other steroid hormone receptors include the glucocorticoid receptor (GR/NR3C1), mineralocorticoid receptor (MR/NR3C2), progesterone receptor (PR/NR3C3) and oestrogen receptor α and β (ERα/NR3A1 and ERβ/NR3A2). These steroid hormone receptors share both an evolutionarily conserved structure and a similar mechanism of action [10,11]. The *AR* gene is located at the X chromosome at Xq11-12. As there is only a single gene copy of the *AR* gene in males, it is more susceptible to mutations that can alter AR activity. *AR* gene is a 90 kb DNA segment and contains eight exons that code for 10.6 kb mRNA that makes up the 2757 base pair open reading frame (**Figure 1.2**). The gene encodes for a 110 kDa protein with 919 amino acids [9].

Androgen Receptor Structure

Similar to all steroid receptors the AR protein has distinct domains: N-terminal domain (NTD), DNA-binding domain (DBD), hinge-domain and ligand-binding domain (LBD) (**Figure 1.2**)[9,10,12].

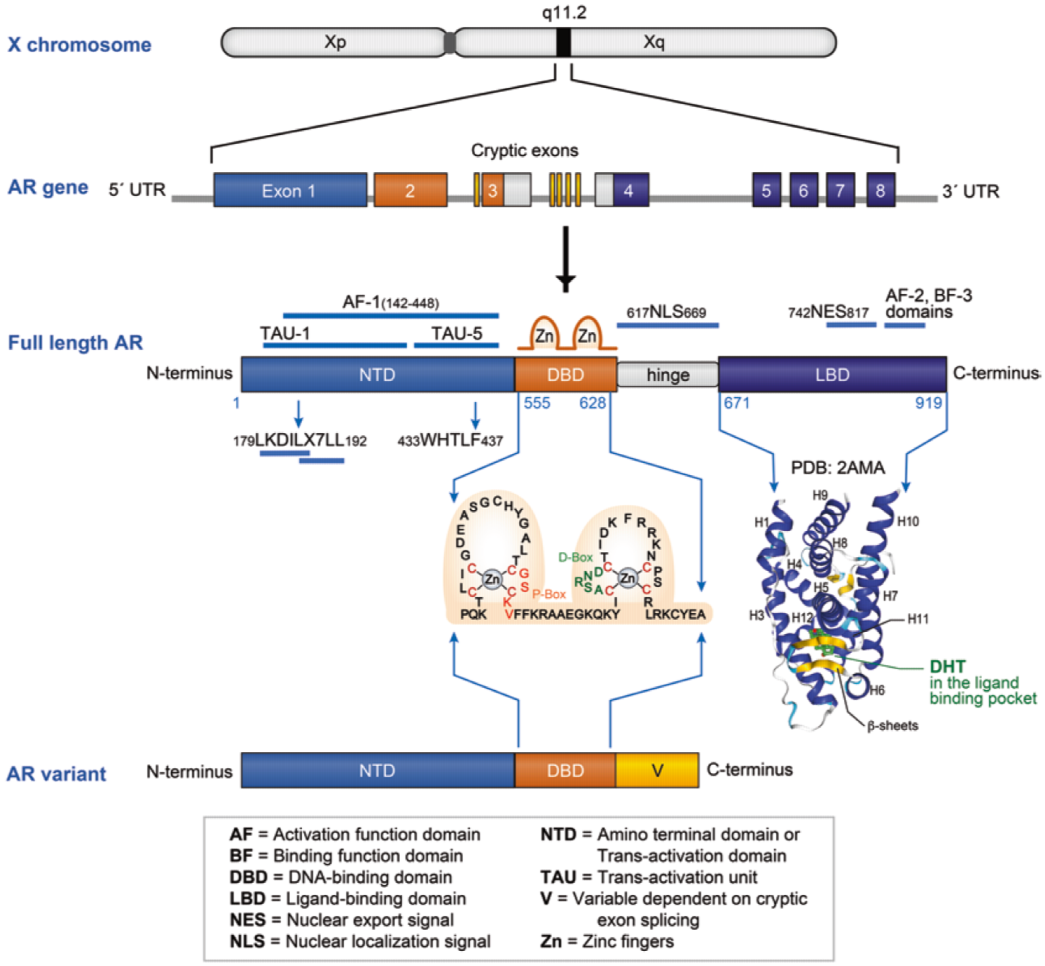

Figure 1.2 Androgen receptor genomic location and structure. AR is located at Xq11.2, encompasses 90kb DNA segment containing 8 exons which encodes 110kDa protein. It has NTD, DBD, hinge and LBD, similar to other nuclear receptors. AF-1 and AF-2 regions are important for N/C interaction and cofactor binding. Most AR-Vs have cryptic LBD, thereby become activated independent of ligand presence. Figure taken from [12].

N-Terminal Domain: The NTD (residues 1-555) transcribed from exon 1, is the largest and the least conserved domain (**Figure 1.2**). Thought to be intrinsically disordered, the NTD contains the activation function 1 (AF1) region that is necessary and sufficient for AR transactivation [13,14]. Unusual for other steroid receptors, LBD-truncated AR is

constitutively active [15,16]. Within the AF1, the Tau-1 and Tau-5 region are crucial for both N-terminus and C-terminus interaction of AR (N/C interaction) and coregulator interactions [14]. Further the NTD has a 20-22 glutamine repeats region starting from residue 57 [17]. The repeat length affects NTD folding, in turn, the transcriptional activity of AR [18].

DNA-binding domain: The DBD (residues 556-623) is the most conserved region among steroid receptors. DBD is a 70 amino acid cysteine-rich domain that is transcribed from exon 2 and 3 **(Figure 1.2**). It binds as a dimer to androgen response elements (ARE) that occur in the genome [11]. The canonical ARE has palindromic hexameric half-sites separated by three nucleotides (5'-AGAACAnnnTGTTCT-3')[11,19]. As nuclear receptors have very closely related DBD structures and DNA-binding motifs, it is unclear how each receptor has distinct binding sites throughout the genome [20–22].

Hinge region: The hinge region (residues 624-665) is the flexible region between DBD and LBD (**Figure 1.2**). It contains a bipartite nuclear localization signal (NLS), carboxy-terminal extension (CTE) and PEST sequence. The NLS sequence is located at the junction of the DBD and hinge region and only becomes accessible when ligand-bound AR undergoes conformational changes [23,24].

Ligand-binding domain: The LBD (residues 666-919) is well-structured domain with numerous crystal structures (e.g. PDB 1E3G[25], 5JJM[26], 2AMA[27]) (**Figure 1.2**). LBD binds androgens such as testosterone or DHT at the ligand binding site [28–30]. Given this critical function, most AR antagonists or antiandrogen drugs have been designed to target the ligand binding site and prevent androgen binding [31–34]. Like other steroid receptors, the ligand-binding pocket is capped by an alpha-helix, which upon ligand binding forms a hydrophobic cleft known as activation function 2 (AF2) region [25]. AF2 is a docking site for coactivators and the N/C interaction via a FxxLF motif [35–37].

1.2 Prostate Cancer

1.2.1 Epidemiology of Prostate Cancer

Prostate cancer (PCa) is the second most common cause of cancer-related death in men in developed countries [38]. Fortunately, the majority of cases are localized primary PCa (**Figure 1.3c**) that can often be successfully treated with surgery or radiotherapy. However, advanced or metastatic PCa is very difficult to treat and has a high rate of mortality [39]. The incidence rate of the disease is influenced by age, ethnicity, and family history. Both incidence and death rates are highest for African-American men and the lowest for Asian and Native American men (**Figure 1.3a**)[40]. For all ethnicities, the incidence rate dramatically increases with age and men >65 have a significantly higher chance of being diagnosed with PCa (**Figure 1.3b**)[40]. The genetic background of the patient also influences the prevalence of the disease. Men with a family history of PCa have a nearly two-fold higher chance of being diagnosed than men with no family history [41]. Genome-wide association studies showed that specific genetic loci are associated with PCa susceptibility [42,43]. New guidelines include BRCA2 mutation as a risk factor

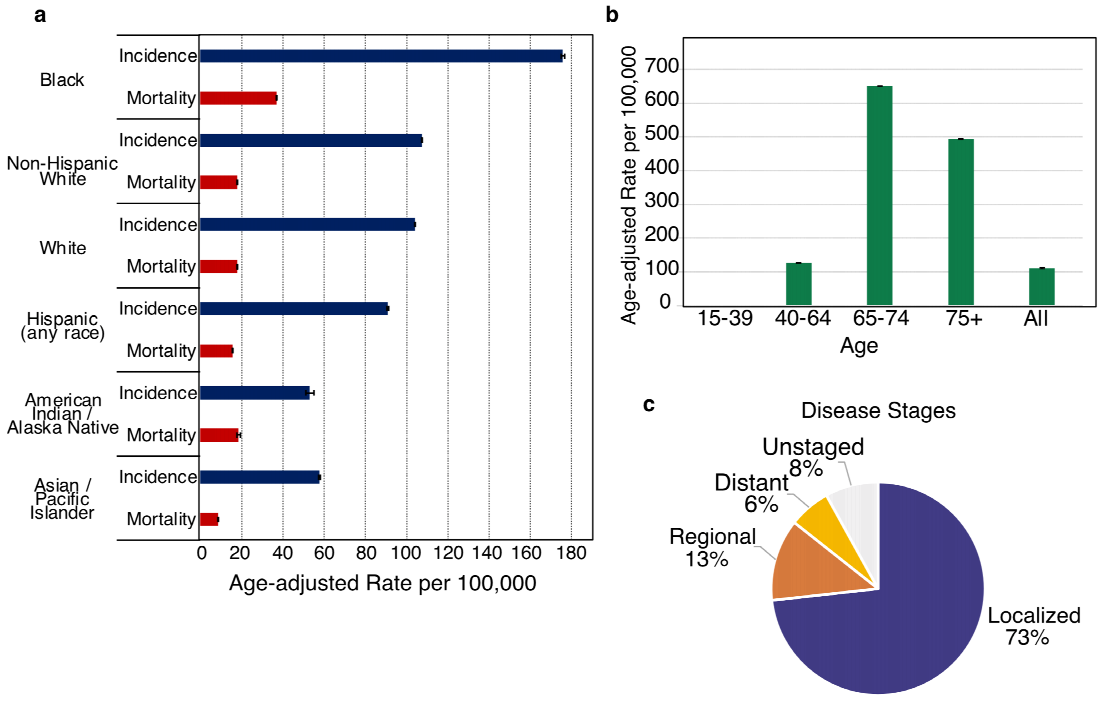

Figure 1.3 The incident rates of prostate cancer based on (a) ethnicity, (b) age and (c) disease stages. Incidence rates between 2014-2018 based on (a) ethnicity, (b) age, and (c) disease stage during diagnosis. Mortality rates between 2015-2019 based on (a) age. The data retrieved from SEER database. (https://seer.cancer.gov/statfacts/html/prost.html) and it refers to age-adjusted rates per 100,000 cases.

for PCa development in men above 40 years of age [44]. Dietary habits, physical activity, and smoking also impact the incident rate and the progression of the disease [39].

1.2.2 Diagnosis and Treatment of Prostate Cancer

PCa is suspected when a patient has high PSA levels and a palpable prostate in a digital rectal examination (DRE). For these patients, biopsy samples are collected from different prostate regions and graded by the Gleason grading system [45,46]. This grading system is from 1 to 5, based on the level of differentiation in cancerous tissue, and consists of the sum of the most prevalent pattern and second most prevalent pattern in biopsy samples [44,47]. Patients are categorized into different risk groups based on their Gleason Score, PSA level, stage in diagnosis and Tumor-Node-Metastasis (TNM) evaluation listed in **Table 1.1** [45,46]. The classification helps to determine the method of cancer management, which is typically discussed with a multidisciplinary group including urologists, radiologists, oncologists and pathologists [45,46].

Table 1.1 Risk groups for biochemical recurrence of localized and locally advanced PCa

	Low Risk	**Intermediate Risk**	**High Risk**	
PSA level (ng/mL)	<10	10-20	>20	Any PSA
Gleason Score	<7	7	>7	Any GS
Stage in diagnosis	Localized	Localized	Localized	Locally advanced
Clinical Tumor Node Metastasis classification	cT1-T2a	cT2b	cT2c	cT3-T4 or cN+
T values are based on DRE only. T1: Tumor is not palpable T2: Tumor is palpable and confined in prostate (a: one half of lobe or less, b; more than one half of one lobe but not both lobes, c: both lobes) T3: Tumor extends through the prostatic capsule (a: extracapsular extension (unilateral or bilateral), b: tumor invades seminal vesicle(s)) T4: Tumor is fixed or invades adjacent structures other than seminal vesicles: external sphincter, rectum, levator muscles and/or pelvic wall N: regional (pelvic) lymph nodes (N0: no regional LN metastasis, N1: regional LN metastasis) M: distant metastasis (M0: no distant metastasis, M1: distal metastasis)				

Localized or Locally Advanced PCa Therapy Options

The most common therapy for localized PCa includes watchful waiting, active surveillance, radical prostatectomy, radiotherapy and brachytherapy (**Figure 1.4b**) [44,45]. The selection of the specific therapy depends on the risk group summarized in **Table 1.1**. Active surveillance is offered to low-risk patients to prevent overtreatment,

while watchful waiting is offered for the patients with a life expectancy of less than ten years [44]. For patients with mid-grade PCa radical prostatectomy and radiotherapy are the most common treatments [44]. Following prostatectomy, patients undergo regular PSA monitoring to determine biochemical recurrence which is the state where increased PSA levels have been observed in two consecutive tests (>0.2ng/ml) [44,45,48]. Patients with biochemical recurrence are more likely to develop distant metastasis and resistance to first-line therapies and have a decreased overall survival [44,49,50].

Those patients with recurrent, high-risk or metastatic PCa are typically given androgen deprivation therapy (ADT) [44]. Most commonly, this is performed by chemical castration through LHRH agonists/antagonists. LHRH agonist overstimulates the anterior pituitary gland and causes a temporary increase in testosterone levels in serum known as "testosterone flare" [51]. Eventually, continuous stimulation triggers the negative feedback mechanism, which lowers the levels of LHRH receptors and desensitizes gonadotrophs, thereby lowering testosterone levels [52,53]. In contrast, LHRH antagonist directly blocks the activity of LHRH receptors in the anterior pituitary gland resulting in a decrease in LH release that prevents testosterone secretion from Leydig cells [52,53]. While primarily given as a monotherapy, there is increasing evidence that in metastatic hormone-sensitive PCa, combining ADT with AR targeting therapeutics like enzalutamide (ENZA) and abiraterone or docetaxel, a cytotoxic chemotherapeutic, can improve progression-free survival and overall survival [44,54–56].

Castration Resistant PCa and Therapy Options

Even though most patients respond to ADT, the tumor almost always adapts to castration conditions and progresses into a castration-resistant state (**Figure 1.4a**). This castration-resistant prostate cancer (CRPC) has a poor prognosis with a median survival of less than three years [57,58]. The management of CRPC is still evolving with the recent approval of several new treatment options (**Figure 1.4b**) [59–61]. Common treatment for CRPC includes second-generation androgen receptor signaling inhibitors such as abiraterone or ENZA, or docetaxel chemotherapy [59]. Abiraterone acetate inhibits androgen biosynthesis by targeting CYP17A1, an enzyme essential in androgen biosynthesis [62]. In chemo-naïve metastatic CRPC patients, abiraterone acetate treatment improves overall survival and delays chemotherapy or bone lesion formation [63,64]. Antiandrogens

directly block AR activity by primarily competing with DHT for AR binding. The limited potency and agonistic-like activity of first-generation antiandrogens [65–67] led to the development of second-generation antiandrogens apalutamide [68], darolutamide [69], or ENZA [70]. These are preferred for CRPC treatment [59] due to their improved effect in progression-free survival [71–73]. ENZA has been shown to delay the disease progression, and increases the overall survival in docetaxel-naive, metastatic CRPC patients [74]. However, in almost all patients, the disease develops resistance and current therapies have limited effect on overall survival and progression-free survival in CRPC. There is, therefore, a need for new therapeutics to treat late-stage PCa.

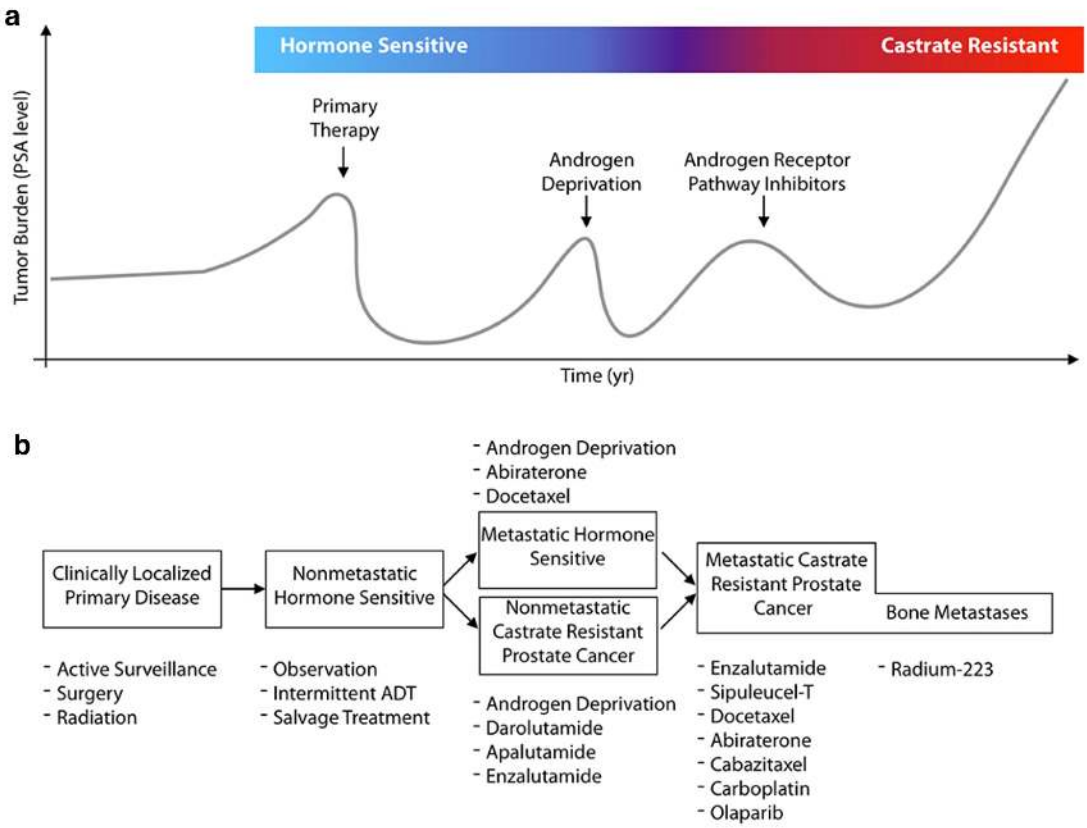

Figure 1.4 (a) Prostate cancer (a) progression and (b) available therapy options. (a) General disease progression presented by hypothetical disease burden measured as PSA level. (b) Some therapy options available at different disease stage. Figure taken from [66].

1.2.3 Mechanisms of Castration Resistance

It is crucial to understand the mechanisms of treatment resistance in order to develop better therapeutic options. There is extensive clinical evidence that the majority of CRPC

tumors remain dependent on AR, and loss of activity causes a significant decrease in cell proliferation of both primary PCa [75] and CRPC [76,77] models. Tumor cells adapt or become hypersensitized to castrate conditions through multiple resistance mechanisms that re-activates the AR signaling axis. This can include AR amplification, AR mutations, AR splice variants, intratumoral *de novo* steroidogenesis, alternative ligand binding, activation of alternate pathways, genetic and epigenetic alterations [78–82].

AR amplification: Amplification of the *AR* gene or enhancer increases expression of AR that sensitizes the nuclear receptor to castrate androgen levels [83–85]. This increases proliferation in cell line models and decreases sensitivity to antiandrogens [86].

AR mutations: Point mutations in the *AR* hinge region or LBD allow a large spectrum of ligands to interact with AR and alter transactivation [87,88]. Mutated AR has been shown to be responsive to adrenal androgens [89], other steroids [90], certain growth factors such as IGF-1 and EGF [91]. Further, mutations to the AR can cause antiandrogens to act as agonists and actually increase proliferation [29,30,92–94].

AR splice variants: Androgen receptor splice variants (AR-Vs) are lowly expressed in primary PCa and then increase in CRPC [95,96]. Most AR variants lack an LBD and are constitutively active in the absence of a ligand. Given that they do not need androgen to be activated, AR-Vs are intrinsically resistant to ADT and antiandrogens [97–100] and correlate with clinical antiandrogen resistance [101–103]. AR-V7 is the most commonly observed splice variant detected by both mRNA and protein levels in neoplastic prostatic tissues [95,96,104]. AR-V7 forms homodimers or heterodimers with full-length AR [99,105,106]. Although the DNA occupancy of AR-V7 and AR mostly overlaps [107,108], they induce the transcription of different gene sets [99,107,109], suggesting that the co-regulators for AR-Vs might play a role in differential gene expression contributing to CRPC.

Intratumoral de novo steroidogenesis: Despite androgen blockade, CRPC patients have higher intratumoral androgen levels than primary PCa patients [110]. It has been demonstrated that the PCa tumour itself can produce androgens *de novo*. In this, enzymes involved in the steroidogenesis pathway such as CYP17A1 and AKR1C3 are

overexpressed leading to a so-called “backdoor” synthetic route [110,111]. Removal of adrenal glands reduces the testosterone levels in castrated mice; however, recurrence is observed in AR-positive cells that express *de novo* steroidogenesis enzymes [89].

Alternative pathways of AR activation: Alternate pathways also contribute to treatment resistance. Commonly observed mutations in clinical CRPC samples are clustered in major pathways including PI3K pathway, WNT pathway and DNA repair in addition to AR pathway [112–114].

Epigenetic modifications: In addition to frequent mutations in epigenetic modifiers, multiple studies on CRPC epigenome and AR co-regulators revealed an important role for epigenetic modifiers in disease progression through epigenetic reprogramming and cistrome alterations [22,115–117]. DNA methylation, histone modification and chromatin accessibility strongly correlate with clinical outcome. Multiple epigenetic modifiers have been shown to be essential for androgen-dependent transcription or DNA recruitment [118,119]. Additionally epigenetic vulnerabilities are observed in preclinical studies which can be exploited for cancer therapy [120,121]. Due to their druggable structure, epigenetic modifiers emerge as potential drug targets to re-sensitize tumor cells for readily available therapies.

1.3 Epigenetics and Epigenetic Modifications

Epigenetics are heritable changes that induce a phenotype without altering the DNA sequence. These can affect multiple biological processes including DNA repair, pluripotency, differentiation, genomic imprinting, transcriptional regulation, splicing, spreading of heterochromatic state and X chromosome inactivation [122–125].

Epigenetic information is commonly stored as either DNA chemical modifications or histone post-translational modifications. DNA in eukaryotic genomes is wrapped around a histone octamer that is composed of one H3-H4 tetramer and two dimers of H2A-H2B [124]. Histone proteins are rich in positively charged amino acids lysine and arginine, which neutralize negatively charged sugar phosphate backbone of DNA [124]. This nucleosome core contains 147 hydrogen bonds between the backbones of DNA and histone [124]. Linker histone H1 is mostly responsible for further compaction into multi-

nucleosomal structures [124]. The relative compaction of these nucleosomes strongly influences the accessibility of transcription factors and other proteins to chromatin. Thus, the crosstalk between epigenetic modifications on DNA and histones functionally regulates transcriptional machinery and gene expression. Given this critical role, epigenetic dysregulation has been associated with complex human disorders, metabolism changes, cancer and drug resistance [126–128].

1.3.1 DNA Methylation

In eukaryotes DNA methylation is an epigenetic event where a methyl group is transferred to the 5th carbon in the pyrimidine ring of cytosine nucleotides to form 5-methylcytosine. The major function of DNA methylation is to induce heterochromatin formation and transcriptional repression to regulate genomic imprinting, X chromosome inactivation, repression of mobile genetic elements and tissue-specific gene expression [129]. DNA methylation is controlled by the activity of DNA-methyltransferases (DNMT) and Ten-eleven translocation (TET) family proteins. In humans, methylated cytosines are primarily found on cytosine nucleotides followed by guanine nucleotides (CpG), and less frequently in other cytosine-containing sites [129]. Aberrant DNA methylation is observed in many different cancers [130].

DNA methylation: DNA methylation patterns are maintained during cell division as epigenetic memory or generated *de novo*. During DNA replication, DNMT1 interacts with UHRF1 E3-ubiquitin ligase that is bound to hemimethylated CpG nucleotides in the replication fork that is di-/tri-methylated at H3K9. UHRF1 ubiquitinates H3 tails and activates DNMT1 which, in turn, methylates the daughter strand and helps maintaining DNA methylation [129]. *De novo* DNA methylation is mediated by DNA methyltransferases DNMT3A and DNMT3B. These writer proteins contain a highly conserved DNA methyltransferase domain (DNMT) and two reader domains namely ATRX-DNMT3-DNMT3L (ADD) and PWWP [129]. ADD domain interacts with unmethylated H3K4, thereby triggering the DNA-methyltransferase activity [129]. Transcriptionally active promoter sites are methylated at H3K4 which repels ADD from that region and prevents DNA methylation [129].

DNA demethylation: TET proteins (TET1, TET2, TET3) are Fe (II) and α-ketoglutarate dependent dioxygenases. They oxidize 5'-methylcytosine to an intermediate form that can be removed during replication or excised and repaired by base excision repair machinery [129,131]. TET1 and TET3 proteins have CXXC domains that tend to bind CpG-rich regions, whereas TET2 has different preferences due to the lack of this domain [131]. Additionally, 5-methylcytosine can be converted to thymidine either passively or actively by deamination leading to the depletion of CpG with time [150,154].

Readers of methylated DNA: Multiple protein domains can "read" DNA methylation including methyl-binding domain (MBD), C2H2 or zinc finger-containing proteins and p53 [132]. Also basic-helix-loop-helix (bHLH) transcription factors such as MYC and MAX are responsive to TET-modified CpGs [132]. Basic leucine-zipper and homeodomain transcription factor families can also recognize methylated DNA [132].

1.3.2 Histone Modifications

The N-terminus of histones commonly undergo posttranslational modifications by epigenetic modifying enzymes. These modifications are heritable, reversible and dynamic [133]. The "writer" enzymes covalently attach posttranslational modifications to histone residues, while "eraser" enzymes remove these modifications. "Readers" are the proteins that recognize the epigenetic marks and interpret them. The epigenetic state and transcription are regulated in cooperation with either writers or erasers that are in complex with readers, other chromatin remodelers or transcription factors [125,133]. Study of posttranslational modifications in histone tails have focused on methylation, acetylation, phosphorylation, ubiquitination and sumoylation [125,133]. Histone lysine methylation will be discussed in *Section 1.3.3*.

Histone arginine methylation: Arginine methylation is observed in both histone and non-histone proteins, and contributes to multiple cellular processes including transcriptional regulation, alternative splicing and DNA damage response [134,135]. Methylation is catalyzed by protein arginine methyltransferases (PRMTs) using S-adenosyl-L-Methionine (SAM or AdoMet) as the methyl source. Arginine residues can be monomethylated, asymmetrically or symmetrically di-methylated [134,136]. PRMTs are classified into three groups based on their activity. Type I PRMTs include PRMT1 to

PRMT4, PRMT6 and PRMT8, which generate monomethyl-arginine and asymmetric dimethylarginine [135]. PRMT5 and PRMT9 are Type II PRMTs, which transfer the methyl groups to unmethylated arginine or mono-methylated arginine resulting in symmetric dimethylarginine [135]. PRMT7 is the only member of Type III PRMT, and generates mono-methylated arginine residues on histones [135,137]. PRMT1 and PRMT5 are responsible for the majority of methyl-arginines. In addition, JMJD6 and certain JmjC-domain containing lysine demethylases (KDM3A, KDM4E, KDM5C and KDM6B) have been reported to catalyze the removal of methyl-groups from arginine [138].

Histone acetylation: Histone acetylation is a highly dynamic and redundant PTM. It occurs in the ε-amino group of lysine residues with acetyl CoA providing the acetyl source [139]. Lysine acetyltransferases (KATs) and histone deacetylases (HDACs) are responsible for the balance of acetylation. Being negatively charged, acetyl group neutralizes the positive charge in lysine residue on histone, and weakens the interaction between histone and DNA [139]. Type-B KATs are mostly cytoplasmic where they modify newly synthesized histone H4 at lysine 5 and lysine 12 which will be removed after the nucleosome incorporation [139]. Type-A KATs are mostly nuclear and are classified into three groups based on their sequence homology including GNAT, MYST and CBP/p300 families. They are often found in large protein complexes and can modify multiple lysine residues in histone N-terminus [140]. GCN5 and PCAF are members of the GNAT family that acetylate H3K9 residues. MYST family includes Tip60, MOZ, MORF, HBO1 and MOF [141]. Tip60 is part of NuA4 acetyltransferase complex and has multiple roles including acting as a co-activator of nuclear receptors, β-catenin, c-MYC, E2F and p53 [142]. CBP and p300 can acetylate all histone subtypes [143]. Other KATs include steroid receptor coactivators (SRC1-4) [139].

Histone deacetylation: Removal of acetylation from lysine histone residues are mediated by histone deacetylases (HDACs) which cause chromatin compaction and transcriptional repression. There are four HDAC classes. Class I (HDAC1, -2, -3, -8), Class II (HDAC4 to HDAC7 , HDAC9 and HDAC10), Class III (Sirtuins, SIRT1 to SIRT7) and Class IV (HDAC11)[144]. HDAC1, HDAC2 and HDAC3 also participate in co-repressor

complexes including NuRD, Sin3, CoREST, NCoR and SMRT [145,146]. HDAC inhibitors are clinically tested for cancer treatments [144].

Readers of acetylated histones: Bromodomain, YEATS domain and double PHD finger (DPF) domain can recognize acetylated lysine residues [147–150]. Bromodomain and external domain (BET) family includes BRD2, BRD3, BRD4 and BRDT. BRD4 actively participates in transcription and enhancer activity [151]. Inhibitors and proteolysis targeting chimera are designed against BET proteins and tested in preclinical and clinical settings [149,152].

Other common epigenetic modifications: Other histone post-translational modifications include -but not limited to phosphorylation, ubiquitination, sumoylation. Histone tails are phosphorylated at serine, tyrosine and threonine residues by kinases and dephosphorylated by phosphatases. Phosphorylation is a dynamic event and the details are not well characterized. Histone ubiquitination occurs in lysine residues and requires sequential reactions mediated by ubiquitin ligases [153]. Transcriptional regulation by histone ubiquitination is location-dependent. H2AK119 ubiquitination by BMI and RING1A/B works together with H3K27me3 for gene silencing [154], whereas H2BK120 ubiquitination by RNF20/40 is associated with active transcription [155,156]. H2A ubiquitination by RNF8 and RNF168 marks damaged DNA regions for repair [157]. Histone ubiquitination is reversed by deubiquitinating enzymes (DUB) such as USP22, USP16, BAP1-ASXL1/2 complexes [158,159]. Sumoylation is similar to ubiquitination and requires E1, E2, E3 ligases to covalently attach small ubiquitin-like modifiers (SUMO) [160] and is generally associated with gene silencing [161].

1.3.3 Histone Lysine Methylation

Lysine residues on histones are reversibly methylated using SAM as the methyl source [162]. As this modification does not change the overall electric charge of the amino acid chain, the effect of the methylation on the chromatin accessibility strongly depends on the residue position (**Figure 1.5**). Overall, the methylation of H3K4, H3K36 and H3K79 is associated with transcriptionally active regions [133], while the methylation of H3K9, H3K27 and H4K20 is associated with transcriptionally repressed regions [133]. Bivalent

methylation marks on H3K4 and H3K27 co-exist to facilitate the shift of gene expression from poised state to transcriptionally active state [163].

Histone lysine methyltransferases: Histone lysine methyltransferases (KMTs) are categorized based on the SET domain presence. SET-domain containing KMTs include KMT1 to KMT8 and introduce mono-/di-/tri-methyl groups into lysine residues [162].

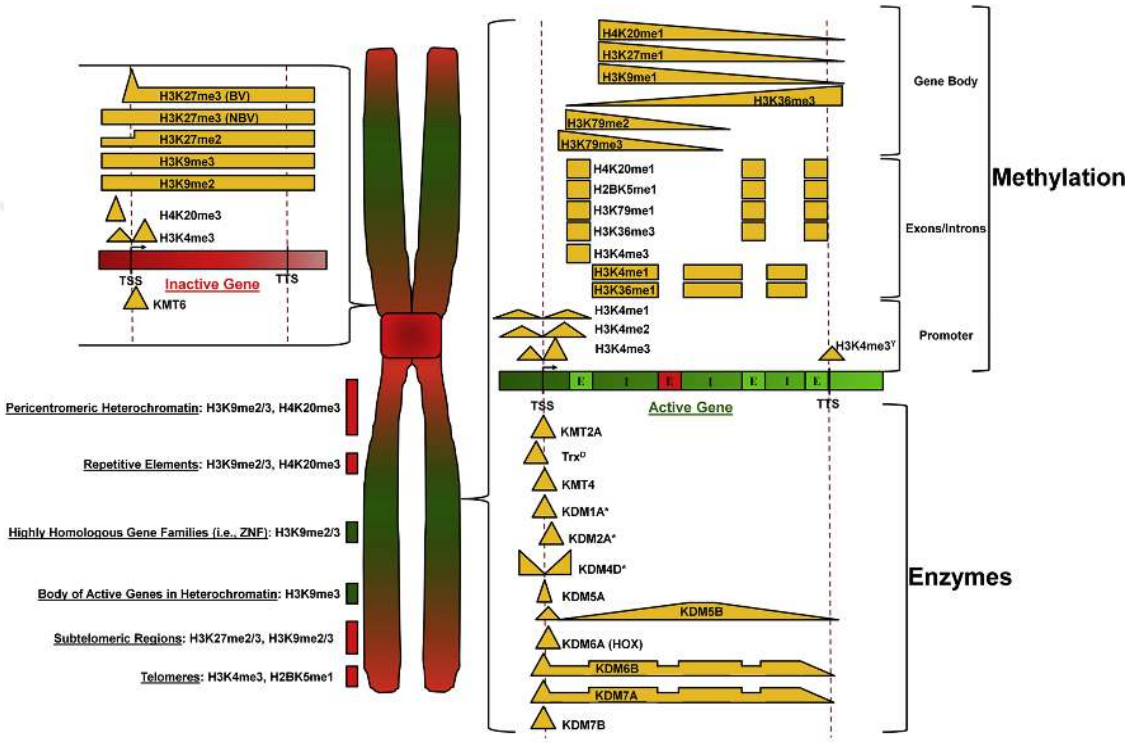

Figure 1.5 The distribution of histone lysine methylation and its effect on gene expression. Green: euchromatin regions. Red: heterochromatin regions. BV: Bivalent. E: Exon. I: Intron. the methylation of H3K4, H3K36 and H3K79 is associated with transcriptionally active regions, while the methylation of H3K9, H3K27 and H4K20 is associated with transcriptionally repressed regions. Bivalent methylation marks on H3K4 and H3K27 co-exist to facilitate the shift of gene expression from poised state to transcriptionally active state. Figure taken from [157].

SET-domain containing KMTs can be further divided into SUV39, EZH, SET2, PRDM, SMYD and SET1 families. SUV39 family methylates H3K9, which is observed in constitutive or facultative heterochromatin regions such as promoters, pericentromeric regions and long terminal repeats [162]. EZH family joins Polycomb group protein complexes and introduce H3K27me1 in gene bodies and H3K27me2/3 in transcription start sites [162,164]. SET2 family methylates H3K9, H3K27 and H4K20 [162]. PRDM

family is thought to methylate H3K9 [162]. Unlike other KMTs, SET1 proteins are associated with transcriptional activation and methylate H3K4 residues in promoter and enhancer regions [165,166]. DOT1L is the only non-SET domain containing KMT and it methylates H3K79, which has conflicting roles in transcription [167].

Readers of methylated histones: Lysine methylation is recognized by diverse reader domains including PHD, chromo, TUDOR, PWWP, WD40, BAH, ADD, ankyrin repeats, MBT and zn-CW domains [162].

Histone Lysine Demethylases

Histone lysine demethylases (KDMs) are divided into two groups based on their cofactor requirement for demethylase activity (**Figure 1.6a,b**). Besides their demethylase activity, most KDMs have reader domains and join large protein complexes that contribute to the tight regulation of histone-modifications [168].

FAD-dependent lysine demethylases: KDM1A (also known as LSD1) and KDM1B are amine oxidases which require flavin adenine dinucleotide (FAD) for their activity [169,170] (**Figure 1.6a,c,d**). KDM1A was the first KDM discovered and also demonstrated the reversible nature of histone methylation [169]. KDM1A demethylates mono- and di-methyl H3K4 [169]. Although *in vitro* studies suggests that it cannot work on H3K9me2 peptides [169], H3K9me2 demethylase activity has been observed when interacting with AR [171]. Amine oxidases are incapable of using trimethylated lysine residues as substrates [172]. Specific KDM1A inhibitors are clinically in development due to their *in vitro* efficacy against certain cancer types including PCa [173].

JmjC-domain containing lysine demethylases: The lysine demethylases KDM2 to KDM8 all contain a JmjC domain and require both Fe(II) and 2-ketoglutarate to oxygenate methyllysine to hydroxymethyl-lysine (**Figure 1.6b,c,d**) [170]. H3K9 demethylation is mediated by KDM3, KDM4 and KDM7 families which can thereby act as transcriptional activators. KDM3/JHDM2 family can demethylate H3K9me1 and H3K9me2 [174]. KDM4/JHDM3 family demethylates H3K9me2/me3 and H3K27me2/me3 [175,176]. KDM7 family, structurally related to KDM2 family, can act on H3K9me1, H3K9me2 and also on H3K27me2 [177,178], KDM7B, also known as PHF8, recognizes H3K4me3

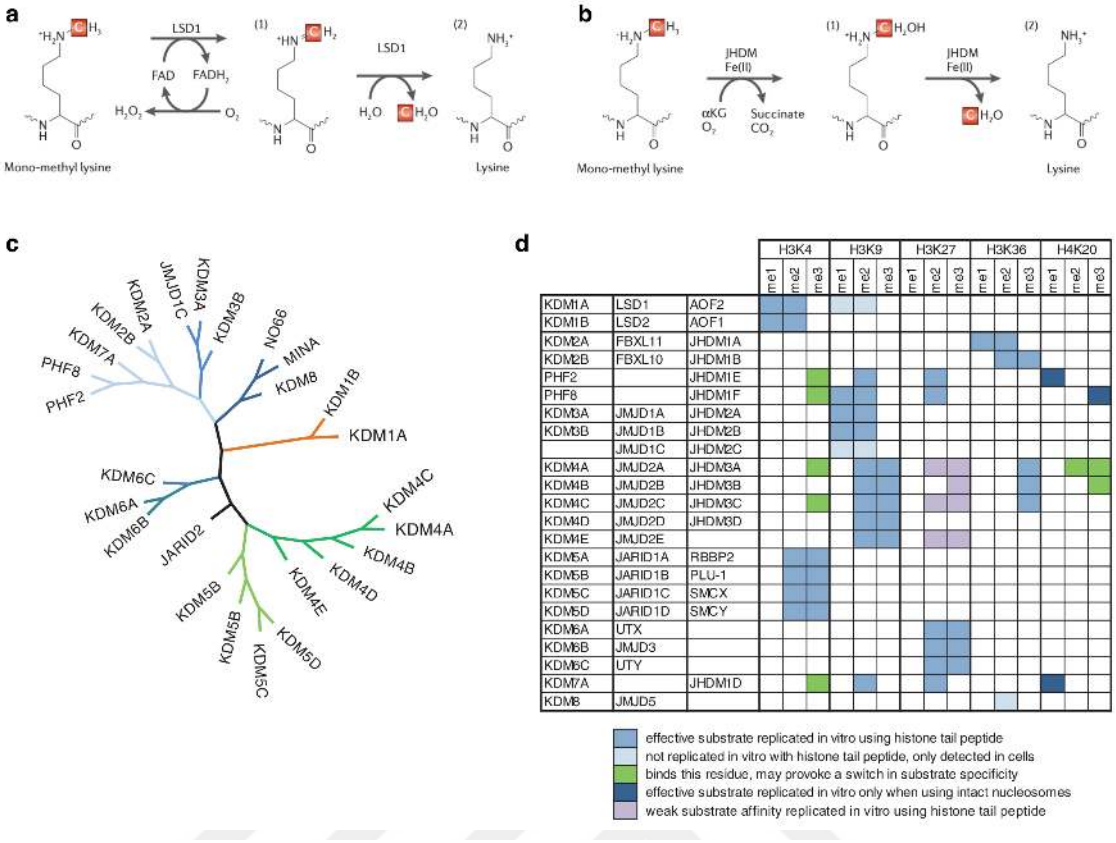

Figure 1.6 Histone lysine demethylases, their cofactor requirement and substrate specificity. The representative demethylase reaction of (a) FAD-dependent and (b) Fe(II) and 2-ketoglutarate-dependent KDMs. (c) Phylogenetic tree of KDMs and (d) their methyl-histone substrates. Figures taken from [162,168].

regions and removes mono- and di-methyl groups from nearby H3K9 thereby contributing to the exclusive distribution of H3K4 and H3K9 methylation [178]. KDM6 family (UTX, UTY and JMJD3) demethylate H3K27me2 and H3K27me3 [179]. Other KDM families act on transcriptionally active marks and contribute to transcriptional gene silencing. KDM5/JARID1 family demethylates H3K4me2 and H3K4me3 found in promoter regions [180,181]. KDM2 and KDM4 families removes methyl groups from transcriptionally active H3K36 marks [162,176]. MINA53 and NO66 have been suggested to remove H3K4 methylation, however this has not been validated with peptide substrates [176]. There is accumulated evidence for the role of KDMs in different cancer types [127,174,182,183]. This has led to the development of numerous KDM inhibitors. Initial studies focused on amine-oxidase inhibitors and 2-ketoglutarate analogs that targeted a broad range of KDMs [184,185]. However, recent studies have led to the development of inhibitors with increased specificity [186,187].

1.3.4 Chromatin remodeling

ATP-dependent chromatin remodelers are highly conserved among species, and are involved in nucleosome editing, chromatin accessibility, nucleosome assembly and organization [188]. They belong to the SF2 superfamily of DEAD/H-box helicases and contain ATPase domains DEXX and HELIC. They are grouped into four subcategories based on their ATPase activity and subunit compositions: imitation switch (ISWI), chromodomain helicase DNA-binding (CHD), switch/sucrose non-fermentable (SWI/SNF) and INO80 (**Figure 1.7**)[189].

ISWI family has an ATPase domain with two RecA-like lobes separated by a short sequence and a C-terminal HAND-SANT-SLIDE (HSS) domain that binds to unmodified H3 tail and linker DNA [188]. It organizes the nucleosome assembly and the spacing between nucleosomes [188]. The CHD family has N-terminal tandem chromodomains, C-terminal DBD and the ATPase domain similar to that of ISWI [188]. It functions in nucleosome assembly, chromatin accessibility, and nucleosome editing [188]. INO80 family has two RecA-like lobes separated by a large insertion and an N-terminal HSA [188]. It regulates nucleosome editing by removing and inserting new histones independent of DNA replication [188].

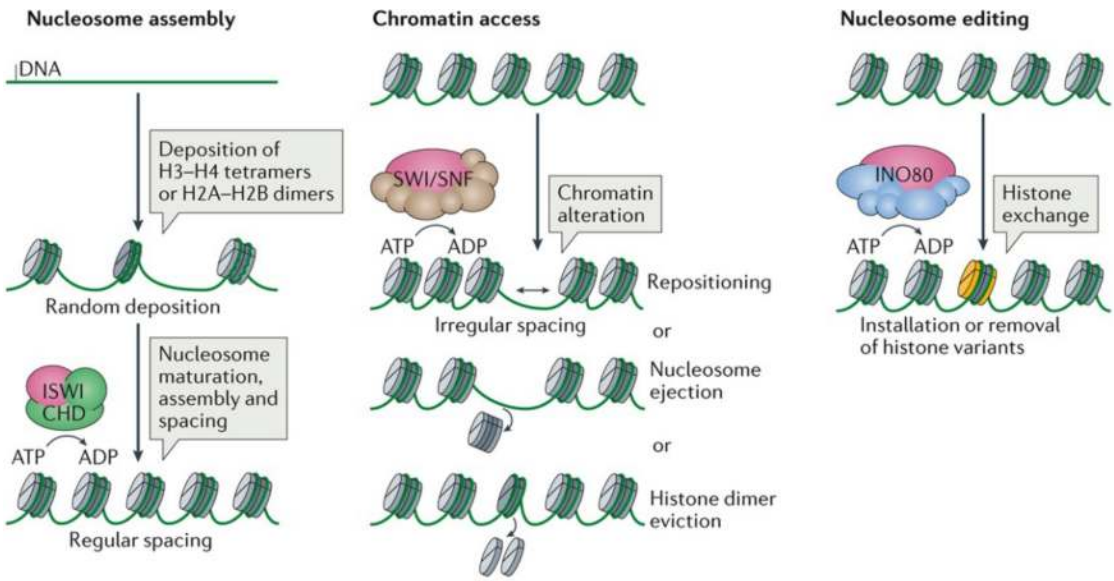

Figure 1.7 ATPase-dependent chromatin remodelers and their role on chromatin regulation. ISWI and CHD remodellers regulate nucleosome spacing, SWI/SNF changes chromatin accessibility, and INO80 involves in nucleosome editing. Figure taken from [181].

SWI/SNF complex

The SWI/SNF complex is primarily involved in altering chromatin accessibility and associated with both transcriptional activation and repression[166,188]. SWI/SNF family members have two RecA-like lobes separated by a small insertion, an N-terminal helicase/SANT-associated (HSA) domain that interacts with actin-related proteins, post-HSA domain, AT-hooks and a C-terminal bromodomain [188]. There are more than 25 genes that transcribe SWI/SNF complex subunits [190]. These subunits form different complexes composed of at least 15 proteins. There are three well-defined SWI/SNF complexes: canonical BAF complex (cBAF), polybromo-associated BAF complex (PBAF), and non-canonical BAF complex (ncBAF) (**Figure 1.8**)[190–192]. The distinct composition of SWI/SNF complex also affects its affinity toward histone modifications highlighting their functional differences [193]. It is still unclear how their distinct composition is regulated or whether modules have independent activities. However, as the SWI/SNF complex doesn't have any DNA sequence requirement, it is primarily recruited to the regions by other transcription factors [188]. Proteins in the complex can recognize acetylated histone regions through bromodomains or double PHD-finger domains [193]. Each SWI/SNF complex requires the ATPase domain for chromatin remodeling activity [194,195]. The distinct SWI/SNF complex compositions have specific roles in neuronal differentiation [196,197] and self-renewal [198]. Inhibitors and

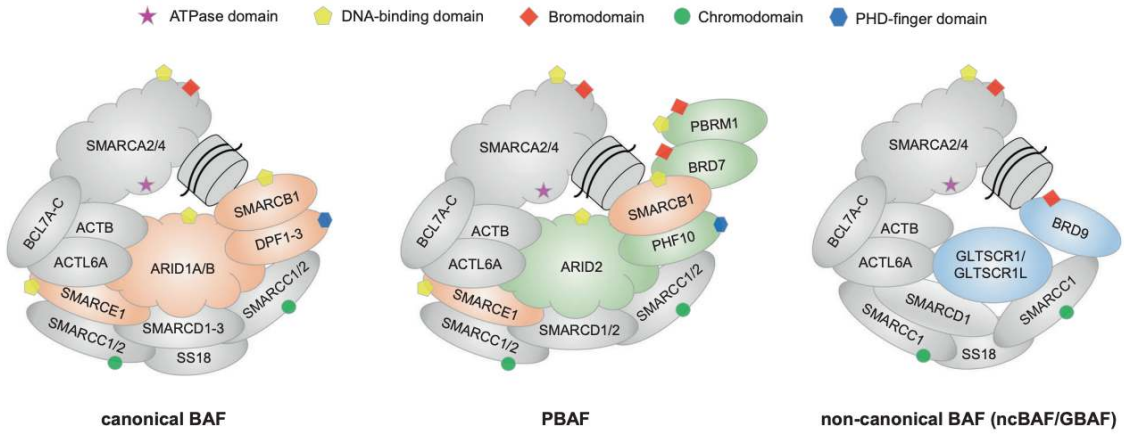

Figure 1.8 The subunits of SWI/SNF complex and functionally important domains of subunits. SWI/SNF complexes are mainly categorized into three groups based on the protein composition, namely canonical BAF, PBAF and ncBAF. Shared subunits are colored in grey. Orange-pink color represents the subunits that do not exist in ncBAF. Green subunits are specific to PBAF and blue subunits are specific to ncBAF. Figure taken from [192].

synthetic lethal interactions of SWI/SNF subunits have become interesting targets for cancer therapy [199].

These SWI/SNF complexes are composed of modules, including the BAF core module, ARID/BAF core intermediate and ATPase-module, that have specialized roles in the complex (**Figure 1.8**) [190,194,200]. The BAF core module is formed by homo- or hetero- dimerization of either SMARCC1 and SMARCC2 proteins that in turn interacts with SMARCD1/2/3 [194]. The core interacts with either SMARCB1 and SMARCE1 to form the BAF core [201], or GLTSCR1/1L to form ncBAF core [194]. The ARID/BAF core intermediate contains either ARID1A/B for cBAF complex, ARID2 for PBAF complex, or no AT-rich protein for ncBAF complex [194]. The subcomplex then interacts with other proteins, before recruiting the ATPase module. Certain subunits are unique to particular SWI/SNF complexes such as ARID1A/B and DPF2 to cBAF, PBRM1 and ARID2 to PBAF, GLTRSCL and GLTRSCL1 to ncBAF (**Figure 1.8**) (**Table 1.2**) [190,196]. Proteins occupying the same space in the complex structure are mutually exclusively but can compensate the loss of one protein [202].

Table 1.2 Defining subunits of SWI/SNF complex and their functional domains. esBAF: pluripotent stem cell BAF, npBAF: neuronal progenitor BAF, nBAF:postmitotic neuron BAF [190,203]

Module	Specificity	Gene	Alias	Important Domains
ATPase module	cBAF/ncBAF	SS18L1	CREST	
ATPase module	cBAF/ncBAF	SS18	SYT	
ATPase module	PBAF-specific	PBRM1	BAF180	Bromodomain/BAH/ HMG
BAF core	Forms homodimer in esBAF	SMARCC1	BAF155	Chromodomain/ SWIRM/SANT
BAF core	cBAF/PBAF-specific, not found in esBAF and ncBAF	SMARCC2	BAF170	Chromodomain/ SWIRM/SANT
BAF core	Not found in ncBAF	SMARCB1	BAF47	Winged helix DBD
BAF core	Not found in ncBAF	SMARCE1	BAF57	HMG box
BAF core	Found in npBAF	SMARCD1	BAF60a	SWIB
BAF core	Defining subunit in hematopoetic stem cells	SMARCD2	BAF60b	SWIB
BAF core	Defining subunit in cardiac progenitors BAF complex and hematopoetic stem cells	SMARCD3	BAF60c	SWIB
ARID/ BAF	cBAF-specific	ARID1A/B	BAF250a/b	ARID (AT-rich interactive domain)

ARID/ BAF	PBAF-specific	ARID2	BAF200	ARID/zinc finger
ARID/ BAF	cBAF-specific, also found in nBAF	DPF1	BAF45b	Zinc finger/ PHD finger
ARID/ BAF	cBAF-specific, also found in nBAF	DPF2	BAF45c	Zinc finger/ PHD finger
ARID/ BAF	cBAF-specific, also found in esBAF/npBAF	DPF3	BAF45d	Zinc finger/ PHD finger
ARID/ BAF	PBAF-specific, also found in esBAF/npBAF	PHF10	BAF45a	PHD finger
ARID/ BAF	PBAF-specific	BRD7		Bromodomain
ARID/ BAF	ncBAF-specific	BRD9		Bromodomain
ARID/ BAF	ncBAF-specific	GLTSCR1	BICRA	
ARID/ BAF	ncBAF-specific	GLTSCR1L	BICRAL	

1.3.5 Epigenetics in Prostate Cancer

Prostate cancer is a disease with a long tail of mutations that is dominated by AR gene alterations and the loss of known tumor suppressors *TP53*, *RB*, and *PTEN* genes [112,113,204]. Both genetic and epigenetic alterations contribute to the disease progression [205–207]. As in the case of most cancer types, aberrations in DNA methylation and histone marks are observed in prostate cancer [83,208–212]. Additionally, endogenous AR interactome profiling has revealed multiple epigenetic modifiers as AR interactors [213–215], some of which have been validated by other studies or tested in the context of cancer cell fitness [205–207,216].

Overall DNA methylation level decreases by the disease progression; clinical samples of CRPC are hypomethylated compared to the samples of primary cancer and benign prostate [210]. Hypomethylated regions mostly contain regulatory regions and are more prone to somatic mutations causing dysregulations [210]. Locus-specific DNA hypermethylation is observed especially in the genes associated with cell cycle, DNA repair, apoptosis, and hormone response promoting cancer growth [217–220]. The loss of DNA demethylase TET2 promotes cell proliferation and migration observed with an increase in AR-targeted gene expression [221]. The overexpression of miR-29 family which targets TET2 for its depletion is correlated with poor prognosis in CRPC patients [222]. Global changes in histone modifications are observed in the disease progression and have a diagnostic and prognostic value in PCa [223,224]. EZH2-related H3K27

methylation signature with poor outcome and CRPC-specific enrichment in H3K27ac in metastatic AR-binding sites have been reported [225,226].

EZH2 is overexpressed in advanced PCa along with other PRC2 components BMI1 and RING1 [227] and these expression levels are predictive of biochemical recurrence [228]. BMI1 increases the stability of AR by preventing its ubiquitination through protein interaction [229]. EZH2 loss reduces cell fitness in both AR-positive and AR-negative cell lines [230–232]. N-MYC promotes the DNA binding of EZH2 in AR-null cells [233], while AR transcription depends on EZH2 activity in AR-positive cells [234], showing cell line-specific roles of EZH2. CHD1 loss is frequently observed in clinical samples [112,113,204], which redistributes AR binding in cell culture to a cistrome similar to that of clinical samples [116]. Additionally, *in vivo* shRNA screen on frequently altered genes in PCa revealed that CHD1 loss contributes ENZA resistance [235]. CHD1 loss induces changes in chromatin accessibility and transcription, resulting an heterogenous population dictated by different transcription factors activating lineage differentiation in ENZA resistance [235]. Acetyltransferases MLL, MLL2 and CBP/p300 interact with AR for androgen-mediated transcription, and contribute to cell proliferation and tumor growth [236–239]. Arginine methyltransferase PRMT5 is selectively essential in prostate cancer cell lines with TMPRSS2-ERG fusion [240]. ERG competes with AR, requires PRMT5 to bind AR-target genes and negatively regulates AR-targeted gene expression [240].

BRD4 belongs to BET family which recognizes acetylated histones and positively regulates transcription. Its activity can be disrupted by BET inhibitors (BETi) such as JQ1. BRD4 inhibition decreases cell proliferation and invasion *in vitro* and *in vivo* experiments in different PCa models accompanied by cell cycle arrest and apoptosis [120,241]. BET proteins promote c-MYC expression, however the decrease in cell proliferation by BETi can be partially rescued by c-MYC overexpression [241]. BRD4 interacts and co-localizes with AR, which is abrogated by BETi treatment [120]. JQ1 treatment also abrogates BRD4 and AR-Vs interaction and represses the androgen-independent cell growth [242]. JQ1 inhibits AR recruitment to target genes, thereby AR-mediated transcription [120]. Acquired BETi resistance is observed in the cells with

restored MYC expression and hyperactive AR, which can be overcome by antiandrogen treatment and PARP inhibition [243].

Histone Lysine Demethylases in Prostate Cancer

Lysine demethylases have been and shown to be important for cell viability and AR transcriptional activity in CRPC. Given the importance of KDMs in PCa based on the literature, KDM inhibitors hold great potential to treat advanced PCa.

KDM1 family: KDM1A demethylates H3K4me1 and H3K4me2, and forms repressor complex with CoREST and HDACs [244,245]. Interestingly, it also demethylates repressive H3K9me1 and H3K9me2 marks when interacting with AR, and functions as a transcriptional coactivator in AR-targeted genes [171,244,246]. The dual activity of KDM1A is regulated by H3 phosphorylation which causes a switch from H3K4 to H3K9 [247,248]. Another layer of regulation comes from KDM1A methylation itself at lysine 144 by G9a, which is recognized by CHD1 [249]. Methylated KDM1A colocalizes with CHD1 in AR-bound regions, and differentially regulates gene expression [249]. Loss of KDM1A has minimal effect on androgen-induced AR recruitment to the target genes, but partially affects AR-dependent transcription of a gene subset [244,250]. KDM1A loss or inhibition decreases cell viability in multiple different PCa cell lines, including the AR-null cells [171,251,252]. KDM1A regulates the expression of cell-cycle related genes in CRPC cell line [253]. While poorly understood, demethylase-independent roles for KDM1A have been shown to be essential for cell viability [251]. KDM1A inhibitors offer promising results in preclinical testing for advanced PCa treatment and other cancers [173].

KDM3 family: KDM3 family catalyze demethylation of H3K9me1 and H3K9me2. KDM3A has an LxxLL motif and interacts with AR in a ligand-dependent manner [254]. KDM3A knockdown reduces H3K9me2 in some AR-targeted regions without impacting AR binding [118,254]. It affects HK9 trimethylation and acetylation around these regions suggesting its requirement for the recruitment of other epigenetic modifiers [254]. KDM3A maintains its activity in hypoxic conditions, interacts with p300, HP1α and AR for transcriptional activity [255]. Loss of KDM3A [118,256] and KDM3B [257] reduces cell fitness *in vitro* and *in vivo*. KDM3A can recruit splicing factors to promote AR variant

expression [258]. In line with this observation, the depletion of ubiquitin ligase targeting KDM3A yields an increase in ARv7 expression [238]. KDM3A increases oncogenic c-MYC levels by promoting AR-dependent transcription and protein stability [256]. Interestingly, KDM3A is ubiquitinated at non-canonical sites by HUWE1, which increase its transcriptional activity in DNA repair genes with c-MYC and p300 [259]. Mutations in KDM3A ubiquitination sites sensitize the cancer cells for radiotherapy and PARP inhibitor [238].

KDM4 family: KDM4C colocalizes with AR and works with KDM1A to remove repressive H3K9 methylation marks [246]. KDM4C loss impairs cell proliferation and reduces the expression of genes in both AKT signaling and the MYC pathway [260]. Other trimethyl-H3K9 demethylases KDM4A and KMD4D have been shown to interact with AR [261]. *KDM4A* overexpression is correlated with a high Gleason score and promotes abnormal prostate growth in mice [262]. KDM4A is recruited to the promoter of oncogenic YAP1 by the ETS transcription factors ERG and ETV1, and promotes YAP1 expression in different cell line models [262,263]. KDM4A depletion reduces the viability of tumor cells, which can be rescued by YAP1 expression [262,263]. KDM4A and KDM4B knockdown induce cell-cycle arrest in the G1/S phase in AR-dependent and AR-null cells, which is also observed with KDM4 inhibitors [264]. PLK1 expression is differentially regulated by KDM4 inhibitor treatment, and reporter assay with PLK1 promoter validated the requirement of KDM4B demethylase activity [264]. Independent of its demethylase activity, KDM4B is suggested to increase AR stability by preventing AR ubiquitination through protein-protein interaction [265]. KDM4B knockdown reduces cell proliferation in AR-positive cell lines [265].

KDM5 family: KDM5 family removes H3K4 methylation and silences gene expression. Although it doesn't affect cell proliferation or migration, KDM5D represses cell invasion by silencing invasion-related genes in PCa cell line [266]. Low *KDM5D* expression levels are associated with poor prognosis [266] and docetaxel resistance in CRPC [267]. In contrast, *KDM5B* and *KDM5C* are upregulated in advanced PCa [268,269]. Reporter assays show enhanced AR transcriptional activity by enzymatically active KDM5B [268]. KDM5B expression is induced under low oxygen conditions and it can remain active up to extreme hypoxic conditions [255].

KDM6 family: The KDM6 family demethylates di-/tri-methylated H3K27 thereby reversing the effect of EZH2[176]. KDM6A/B inhibitor is shown to decrease proliferation in multiple PCa cell lines [270–272]. The role of KDM6B in PCa is controversial. It is upregulated in PCa [179,272] while other work suggests that it may have a tumor suppressor role [273]. *KDM6B* expression is proposed to be regulated by NKX3.1 and G9a during prostate differentiation [274].

KDM7 family: PHF8, a member of the KDM7 family, demethylates H3K9me2/me3, H3K27me2 and H4K20me1. High *PHF8* expression are associated with disease progression and poor prognosis in PCa [275–277]. Hypoxia induces the expression of PHF8 which remains active in these conditions [277]. PHF8 interacts with AR and mediates AR-mediated transcriptional activation unless demethylation activity is suppressed [277]. KDM7A is overexpressed in ENZA-resistant cells, and its inhibition induces cell death [278].

Other KDMs: KDM2B has been shown to be important for spermatogenesis [279] and it has anti-apoptotic roles in prostate cancer [280]. KDM8 removes H3K36 dimethylation. It is overexpressed in clinical samples which correlates with high Gleason score [281]. It decreases proliferation in CRPC and ENZA-resistant cell lines, and regulates metabolic activities through PKM2 and HIF1α interaction [281]. NO66 is also upregulated in advanced PCa, loss of which reduces cell proliferation and increases docetaxel sensitivity in AR-null cells [282].

Most of the studies revealed the differential expression of KDMs in a moderate number of clinical samples. The KDM4 family and KDM1A are the most studied KDMs; however, the comprehensive role of KDMs is still yet to be understood. Their direct role in transcription and their druggable nature hold great potential to be exploited for cancer treatment. The development of KDM inhibitors have been successful with increased specificity. Validated KDM dependency in late-stage PCa could further initiate a small molecule development program for the treatment of CRPC.

SWI/SNF Complex in Prostate Cancer

The SWI/SNF complex accounts for 20% of overall mutations in many cancer types including ovarian clear-cell carcinoma, clear-cell renal cell carcinoma, hepatocellular carcinoma, gastric cancer and synovial sarcoma [190,203,283]. However, the frequency of SWI/SNF mutations is very low for PCa [113,284,285]. BRG1, ATPase subunit of SWI/SNF complex, is overexpressed in CRPC with a moderate correlation to Gleason score [284,286,287]. Enzymatically active BRG1 promotes cell invasion [286] and it is essential for cell proliferation in multiple cell lines validated by siRNA, sgRNA and inhibitor treatments in different studies [119,213,287–289]. BRG1 and PTEN have synthetic lethal interaction in cell line, organoid and mice models; and BRG1 depletion induces apoptosis and growth arrest in PTEN-null cells [288]. It was proposed that PTEN loss results in AKT activation which phosphorylates GSK3β [288]. This phosphorylated GSK3β cannot phosphorylate BRG1 which is necessary for its proteasomal degradation, thereby increasing BRG1 stability [288]. Another study shows that BRG1 and HMGB1 promotes AKT phosphorylation and thereby promotes oncogenic activity including cell migration, cell invasion and cell proliferation [290]. Interestingly, BRG1 loss is suggested to impair antiandrogen-induced transcriptional repression [291]. BRG1 depletion also results in decreased proliferation in PCa cell lines with the loss of *TP53, RB1* or both genes [284]. Dual degradation of SMARCA4 and SMARCA2 results in chromatin compaction on the regions where PCa-associated transcription factors bound, and leading to tumor growth inhibition and increased response to ENZA treatment [121].

Three independent studies demonstrated that BRG1, ARID1A and multiple SWI/SNF subunits are endogenous AR interactors [213–215]. Although BRG1 chromatin binding sites overlap with AR and FOXA1 [119,213], BRG1 has been shown to interact with AR but not FOXA1 [119]. Upon BRG1 loss, the chromatin accessibility changes in AR-binding sites including both androgen-dependent and androgen-independent locations [213]. The comparison between AR-regulated and BRG1-regulated differentially expressed genes shows a small overlap upon androgen treatment, further supporting its regulatory role outside of androgen-regulated genes [213]. However, the BRG1-mediated decrease in cell proliferation is accentuated upon androgen treatment [213]. Multiple SWI/SNF complex subunits including BRG1, SMARCC1, SMARCC2 and ARID1A interact with ERG in a DNA-independent manner [289]. Interestingly, PBAF-specific

subunits are less enriched in proteomic analysis for ERG interactome [289]. In addition to ERG, other ETS factors ETV1 and ETV5 also interact with BRG1 and SMARCC1/2 [289]. Chromatin binding profiles of ERG and SMARCC1 show an enrichment of the ERG motif in overlapping regions, whereas regions only occupied by SMARCC1 enrich for an AR motif [289]. Ectopic expression of ERG or ETV1 has been shown to affect the SMARCC1 binding [289]. Although SWI/SNF cistrome is not altered by DNA-binding mutant ERG, ERG-mediated gene expression is impaired in regions co-occupied by SWI/SNF and mutant ERG [289]. Both ERG and SMARCC1 occupancy are lost upon ARID1A depletion [289]. ERG-mediated transcriptional activity is highly dependent on enzymatically active BRG1 [289]. BRM is the other ATPase subunit which is present in the SWI/SNF complex mutually exclusively to BRG1 [202]. BRM is heterogeneously expressed in clinical samples [286]. Its loss induces abnormal growth of the prostate in mice and increased proliferation in *in vitro* assays [292], suggesting a tumor-suppressor role for BRM. No effect on androgen-regulated genes is observed upon BRM loss [292]. BRG1 is generally found bound to active or bivalent promoters and active/poised enhancer sites, whereas BRM is located in facultative or constitutively repressed promoter and bivalent promoter sites [293].

SMARCC1 is upregulated in clinical samples and partially correlates with Gleason score [294]. Controversially, another study reported prolonged survival in localized PCa in patients with high expression of SMARCC1 [295]. PBRM1, PBAF-specific subunit, regulates the expression of epithelial-to-mesenchymal transition-related genes EpCAM, TGF-β and N-cadherin [296]. SMARCD1 is identified as an androgen-dependent AR interactor from *in silico* screens based on the FxxLF motif [297]. SMARCD1 loss reduces the expression of androgen-regulated target genes, whereas structurally related SMARCD2 and SMARCD3 have a moderate effect on AR-response gene expression [297].

A recent study compared the expression levels of SWI/SNF subunits in different PCa clinical cohorts and demonstrated that there neuroendocrine prostate cancer has a distinct SWI/SNF complex composition [284]. Non-canonical BAF complex component BRD9 interacts with AR and it is required for cell viability and tumor growth [298]. BRD9 chromatin binding shows overlaps with BET proteins and regulates AR-driven gene

expression [298]. Overall, this work suggests an essential role for the SWI/SNF complex in PCa progression which could be targeted by ATPase or bromodomain inhibitors.

1.4 Functional screens using genetic perturbations

1.4.1 RNA interference and large-scale shRNA screens

RNA interference (RNAi) is a sequence-specific gene silencing mechanism driven by double-stranded RNA at transcriptional level. RNAi protects against foreign RNA and also regulates gene expression by transcript degradation or translation blockade [299]. This system induces gene silencing by small interfering RNAs (siRNAs) and microRNAs (miRNAs) through sequence-specific cleavage of complementary or partially complementary mRNAs. Primary miRNAs are transcribed by RNA polymerase II or III, and cleaved by Drosha and DCGR8 into smaller precursors namely pre-miRNAs at the base of hairpin structure which leaves 2-3 nucleotide 3'overhangs [300]. In the cytoplasm both pre-miRNAs and long double-stranded RNA (dsRNAs) are further processed by Dicer, PACT and TRBP into miRNA and siRNA duplexes respectively. The duplex binds to Argonaute protein within the RNAi-induced silencing complex (RISC) and one of the duplex strands is removed [301–304]. The remained guide strand in the RISC directs the complex to complementary mRNA for post-transcriptional gene regulation [301–304]. Loaded RISC complex can repeat the mRNA cleavage multiple times mediating a strong post-transcriptional gene regulation [303]. Artificial siRNAs that mimic Dicer-digested siRNAs can effectively knockdown the gene expression [302]. Short hairpin RNAs (shRNAs) are structurally more related to the miRNA, and their processing is similar to the described miRNA processing [302]. Vector-based RNAi uses self-contained RNA polymerase III promoters such as U6 promoter for effective shRNA processing [302]. Stable shRNA expression systems have enabled large scale pooled screens to investigate the role of coding regions in different biological concepts [305–307], however non-coding regions cannot be investigated by RNAi method. In addition, a single copy integration in pooled shRNA screen may not be sufficient to induce significant knockdown levels resulting in false negative results [308]. Multiple copy insertions could oversaturate the proteins in RNAi processing [309], and could induce interferon response [310].

1.4.2 CRISPR-Cas9 system and CRISPR-Cas9 screens

Genome editing technologies are powerful tools to explore the function of individual genes or non-coding regions. Multiple methods are available for targeted genome editing such as transcription-activator like effector nucleases (TALENs), zinc finger nucleases (ZFNs) and meganucleases [311,312]. However, due to the difficulty in designing and cloning these genome editors, these have largely been supplement by Clustered Regularly Interspaced Short Palindromic Repeats (CRISPR)[313,314]. This system is easier to design, suitable for high-throughput assays and can be multiplexed in different cell types.

CRISPR is a part of prokaryotic adaptive immunity which provides sequence-specific protection against foreign bacteriophages [315–317]. CRISPR array in bacteria includes short direct repeats interspaced by non-repetitive spacers derived from foreign DNAs (protospacers)[315]. Spacer incorporation works as an immunological memory for invading pathogens and can provide immune adaptation [315–318]. Each CRISPR array is transcribed as a long precursor pre-CRISPR RNA (pre-crRNA) that is processed into smaller crRNAs by RNase III [315,316,318]. Trans-acting crRNA helps crRNA loading to Cas protein by forming double stranded RNA duplex with crRNA [315,316]. The Cas endonuclease is then guided by crRNA to a target region which has a specific protospacer adjacent motif (PAM) downstream of target sequence [315–317]. When this complex hybridizes, the Cas protein introduces double stranded DNA breaks into the target region [315,316]. The PAM sequence is important to distinguish self-genetic material from non-self-genetic material, and is determined by PAM-interacting (PI) domain that is specific to each Cas protein [319,320]. Multiple Cas family proteins have been identified in prokaryotes [317]. Of these, Type II CRISPR-Cas9 is the simplest and relies on a single multidomain Cas9 protein [314]. Currently, codon optimized *Streptococcus pyogenes* Cas9 protein with nuclear localization signal is a common tool for mammalian gene editing. Although eukaryotic systems don't require bacterial RNase III to process crRNA, the system is even more simplified by the substitution of crRNA-tracrRNA duplex with a chimeric RNA (sgRNA) which includes 20nt guide RNA (gRNA) sequence that can be designed based on the specific target sequence [321,322].

Once the double stranded DNA breaks is made by Cas9, the cell will repair them by either homology directed repair (HDR) or non-homologous end joining (NHEJ) [313]. NHEJ

predominantly repairs double stranded DNA breaks, generates insertions or deletions (indels) in the region and frequently causes loss-of-function mutations [313]. HDR occurs less frequently but with high fidelity when the repair template is present [313]. HDR is exploited for introducing specific mutations in specific loci in cell culture and in animal models [323–327].

While robust and easy to work with, the limitation of the *S. pyogenes* CRISPR-Cas9 system is the availability of the Cas9 specific 5'-NGG-3' PAM sequence. Recent studies have developed mutant Cas9 proteins that have broader PAM sequence recognition with less off-targets compared to wildtype *S.* pyogenes Cas9 [328]. Cas9 can tolerate mismatches outside of its seed sequence, and target regions with alternative PAM sequence (5'-NAG-3'), which causes the off-target activity [329]. There is currently extensive work ongoing to develop safer CRISPR-Cas systems with more precision for clinical work [330].

Overall, CRISPR-Cas9 genome engineering has been established as a powerful tool for genetic manipulations of both coding and non-coding regions. Its power resides in its ease to design, execute, validate and multiplex. Given this strength, highly multiplexed and pooled genetic screens have been developed to systematically test the function of genomic regions to identify essential genes, synthetic lethal genes or cancer co-dependencies [331–343].

Chapter 2 AIM OF THE STUDY

Despite the approval of several life-prolonging drugs in advanced PCa, resistance invariably emerges. There is an unmet clinical need for new therapeutics to control CRPC. There is accumulated evidence that epigenetic events play a critical role in disease progression by altering the genome accessibility through DNA methylation, histone modifications and chromatin remodeling. In addition to their important role in PCa and other cancers, epigenetic modifiers have recently been shown to be "druggable" with several compounds in late-stage clinical development.

This study aims to identify critical epigenetic modifiers in late-stage PCa by two different methods summarized below, and investigate the mechanism of "hits".

Aim1: Investigation of essential lysine demethylases in PCa by performing an arrayed screen using KDM-focused shRNA library (**Chapter 4**)

Aim2: Epigenome-wide CRISPR-Cas9 drop-out screen in PCa which systematically tests all epigenetic modifiers to identify epigenetic dependencies in different stages of PCa with a focus in ENZA-resistance (**Chapter 5**).

Chapter 3 MATERIALS AND METHODS

3.1 Cell Culture

3.1.1 Cell Lines

Cell lines used in this thesis are listed in **Table 3.1**. Cells were maintained in humidified incubators at 37°C with 5% CO_2. Cells are regularly tested for mycoplasma. MR49F cells were a kind gift from Dr. Amina Zoubeidi and Dr. Martin Gleave from Vancouver Prostate Centre. LNCaP-enzaR, 22Rv1-DoceR, 22Rv1-CabaR cell lines are a kind gift from Dr. Ceyda Açılan-Ayhan from KUTTAM. All cell lines except DU145 and RWPE-1 express AR. RWPE-1 cell line represent non-neoplastic epithelial prostate cells, and were used as normal-like prostate control in screening experiments. LNCaP represents advanced prostate adenocarcinoma. Other cell lines are models of castration resistance. MR49F and LNCaP-enzaR are enzalutamide-resistant CRPC cell lines. 22Rv1-DoceR cells are docetaxel-resistant, 22Rv1-CabaR cells are cabazitaxel-resistant. Culturing media, origin, androgen sensitivity and doubling time are summarized in **Table 3.1**.

Table 3.1 List of cell lines with their origin, culturing conditions and certain characteristics

Cell line	Origin	Culture Media	Androgen sensitivity	Doubling time
LNCaP	Human PCa cells derived from lymph node metastasis [345]	RPMI 1640 suppl. with 10% fetal bovine serum (FBS) and 1% Penicillin/Streptomycin	Sensitive	34 hrs
LNCaP-abl	LNCaP cells propagated in androgen free media for 10 months in cell culture [346]	RPMI 1640 suppl. with 10% charcoal-stripped serum (CSS) and 1% Penicillin/Streptomycin	Insensitive	34 hrs
LNAI	LNCaP cells propagated in castrated mice for several months	RPMI 1640 suppl. with 10% CSS and 1% Penicillin/Streptomycin	Insensitive	34 hrs
MR49F	LNCaP cells propagated in castrated mice and then reinjected into castrated and ENZA-treated mice [347]	RPMI 1640 suppl. with 10% FBS and 1% Penicillin/Streptomycin and 10 μM MDV-3100	Sensitive	34 hrs
LNCaP-enzaR	LNCaP cells propagated in ENZA-containing media for several months in cell culture	RPMI 1640 suppl. with 10% FBS and 1% Penicillin/Streptomycin and 10 μM MDV-3100	Sensitive	42 hrs
22Rv1	CWR22 xenograft propagated in castrated mice [348]	RPMI 1640 suppl. with 10% FBS and 1% Penicillin/Streptomycin	Sensitive	40 hrs

22Rv1-DoceR	22Rv1 cells propagated in docetaxel-containing media for several months in cell culture	RPMI 1640 suppl. with 10% FBS and 1% Penicillin/Streptomycin and 25 nM docetaxel		47 hrs
22Rv1-CabaR	22Rv1 cells propagated in cabazitaxel-containing media for several months in cell culture	RPMI 1640 suppl. with 10% FBS and 1% Penicillin/Streptomycin and 10 nM cabazitaxel		46 hrs
DU145	Human PCa cells derived from brain metastatic site [349]	RPMI 1640 suppl. with 10% FBS and 1% Penicillin/Streptomycin	Insensitive	36 hrs
RWPE-1	Immortalized human prostate epithelial cells by human papilloma virus 18 (HPV-18) transfection [350]	Keratinocyte Serum Free Medium (K-SFM) suppl. with 0.05 mg/ml BPE and 5 ng/ml EGF	Sensitive	58 hrs

3.1.2 Antibiotic selection

Each cell line has different tolerance levels for different antibiotics. Therefore, the optimal conditions for each antibiotic were determined for each cell line. Cells were seeded onto either 6 or 12 multiwell plates and treated with varying concentrations of antibiotics. Cells are grown in selective media for three days for puromycin selection, and for five days for blasticidin S HCl selection. After the selection, the concentration that kills more than 90% of the cell population was selected as the working antibiotic concentration for that cell line. The concentrations are indicated in **Table 3.2** for each cell line.

Table 3.2 Optimal antibiotic concentrations of different cell lines

Cell Line	Puromycin concentration	Blasticidin S HCl concentration
LNCaP	2 µg/mL	8 µg/mL
LNCaP-abl	1 µg/mL	10 µg/mL
LNAI	2 µg/mL	Not needed
MR49F	4 µg/mL	30 µg/mL
LNCaP-enzaR	16 µg/mL	10 µg/mL
DU-145	1.5 µg/mL	8 µg/mL
22Rv1	1.5 µg/mL	10 µg/mL
22Rv1-DoceR	8 µg/mL	8 µg/mL
22Rv1-CabaR	32 µg/mL	8 µg/mL
RWPE-1	1 µg/mL	10 µg/mL

3.2 KDM-focused arrayed shRNA screen

3.2.1 KDM-focused shRNA Library

Our KDM-focused shRNA library contains 62 shRNA targeting 23 KDMs (2-3 shRNA per gene). AR targeting shRNA (shAR) was used as positive control, and shRNA targeting Firefly Luciferase (shFF) was included as negative control. We subgrouped 37 shRNAs targeting 14 KDMs from a broader library which was a kind gift from Dr. Tamer Onder. To cover all known KDMs, we searched the literature for KDMs and identified 9 KDMs that are not targeted in our library. 26 shRNAs targeting 9 KDMs were designed and cloned individually into pMSCV- pm [305] retroviral backbone. shRNA sequences are listed in **Table 3.3**.

Table 3.3 The content and the sequences of lysine demethylase-focused shRNA library

Targeted Gene	Oligo #	Hairpin sequence
KDM1A	101	TGCTGTTGACAGTGAGCGCCCTCTCAGAAGATGAGTATTATAGTGAAGCCACAGATGTATAATACTC ATCTTCTGAGAGGTTGCCTACTGCCTCGGA
KDM1A	102	TGCTGTTGACAGTGAGCGAGCTCCACGAGTCAAACCTTTATAGTGAAGCCACAGATGTATAAAGGTT TGACTCGTGGAGCGTGCCTACTGCCTCGGA
KDM1A	103	TGCTGTTGACAGTGAGCGCGGCCTAGACATTAAACTGAATTAGTGAAGCCACAGATGTAATTCAGTT TAATGTCTAGGCCTTGCCTACTGCCTCGGA
KDM2A	104	TGCTGTTGACAGTGAGCGCGGAGTCAACCTGGATTATGATTAGTGAAGCCACAGATGTAATCATAAT CCAGGTTGACTCCATGCCTACTGCCTCGGA
KDM2A	105	TGCTGTTGACAGTGAGCGAGCAGAGAACTTTGTGAATGTATAGTGAAGCCACAGATGTATACATTCA CAAAGTTCTCTGCGTGCCTACTGCCTCGGA
KDM2A	106	TGCTGTTGACAGTGAGCGCGCCCTCACTGGAGTTCCTATATAGTGAAGCCACAGATGTATATAGGAA CTCCAGTGAGGGCTTGCCTACTGCCTCGGA
KDM2B	107	TGCTGTTGACAGTGAGCGAACCCTGGATGCCTTAAGATTATAGTGAAGCCACAGATGTATAATCTTA AGGCATCCAGGGTGTGCCTACTGCCTCGGA
KDM2B	108	TGCTGTTGACAGTGAGCGCCCTGAACCACTGCAAGTCTATTAGTGAAGCCACAGATGTAATAGACTT GCAGTGGTTCAGGTTGCCTACTGCCTCGGA
KDM2B	109	TGCTGTTGACAGTGAGCGCTCAACCTGTCTGACTGCAATATAGTGAAGCCACAGATGTATATTGCAG TCAGACAGGTTGATTGCCTACTGCCTCGGA
KDM3A	110	TGCTGTTGACAGTGAGCGCGCACAGTCCTCCATACGTTTATAGTGAAGCCACAGATGTATAAACGTA TGGAGGACTGTGCTTGCCTACTGCCTCGGA
KDM3A	112	TGCTGTTGACAGTGAGCGACCCTAATAACTGTTCAGGAAATAGTGAAGCCACAGATGTATTTCCTGA ACAGTTATTAGGGCTGCCTACTGCCTCGGA
KDM3B	113	TGCTGTTGACAGTGAGCGCGGTTTCGAGATCATATGCAAATAGTGAAGCCACAGATGTATTTGCATA TGATCTCGAAACCATGCCTACTGCCTCGGA
KDM3B	114	TGCTGTTGACAGTGAGCGACCAATGGTGCTCAAACTCAAATAGTGAAGCCACAGATGTATTTGAGTT TGAGCACCATTGGCTGCCTACTGCCTCGGA
KDM3B	115	TGCTGTTGACAGTGAGCGCGCTGTTAATGTGATGGTGTATTAGTGAAGCCACAGATGTAATACACCA TCACATTAACAGCATGCCTACTGCCTCGGA
KDM4A	116	TGCTGTTGACAGTGAGCGCGGACTGCTGTTTATGCTCATTTAGTGAAGCCACAGATGTAAATGAGCA TAAACAGCAGTCCTTGCCTACTGCCTCGGA
KDM4A	118	TGCTGTTGACAGTGAGCGCGGCCTCCCACCCTATCCAAATTAGTGAAGCCACAGATGTAATTTGGAT AGGGTGGGAGGCCATGCCTACTGCCTCGGA

KDM4B	119	TGCTGTTGACAGTGAGCGAGCGCTGACACTGTATTCTTATTAGTGAAGCCACAGATGTAATAAGAAT ACAGTGTCAGCGCCTGCCTACTGCCTCGGA
KDM4B	120	TGCTGTTGACAGTGAGCGACGCCCACCTTTGCAGAATAAATAGTGAAGCCACAGATGTATTTATTCT GCAAAGGTGGGCGCTGCCTACTGCCTCGGA
KDM4C	122	TGCTGTTGACAGTGAGCGCGGTGAAGATTTCAATGGATATTAGTGAAGCCACAGATGTAATATCCAT TGAAATCTTCACCATGCCTACTGCCTCGGA
KDM4C	124	TGCTGTTGACAGTGAGCGACCAGATAGCAGCAATGAAGAATAGTGAAGCCACAGATGTATTCTTCAT TGCTGCTATCTGGCTGCCTACTGCCTCGGA
KDM4D	125	TGCTGTTGACAGTGAGCGCGGTCAGTAGAGTTCCAGAATATAGTGAAGCCACAGATGTATATTCTGG AACTCTACTGACCTTGCCTACTGCCTCGGA
KDM4D	127	TGCTGTTGACAGTGAGCGCGGTCTTGTTGAGGTTAGCGTATAGTGAAGCCACAGATGTATACGCTAA CCTCAACAAGACCTTGCCTACTGCCTCGGA
KDM5A	128	TGCTGTTGACAGTGAGCGACCTGATCTTCTGCATCAGTTATAGTGAAGCCACAGATGTATAACTGAT GCAGAAGATCAGGCTGCCTACTGCCTCGGA
KDM5A	129	TGCTGTTGACAGTGAGCGCGGACCGCATAGAAGAAGTAAATAGTGAAGCCACAGATGTATTTACTTC TTCTATGCGGTCCATGCCTACTGCCTCGGA
KDM5A	130	TGCTGTTGACAGTGAGCGACGGACGTTTCTTAAGAAGAATTAGTGAAGCCACAGATGTAATTCTTCT TAAGAAACGTCCGCTGCCTACTGCCTCGGA
KDM5B	131	TGCTGTTGACAGTGAGCGCGCAGAGGCCATGAATATTAAATAGTGAAGCCACAGATGTATTTAATAT TCATGGCCTCTGCTTGCCTACTGCCTCGGA
KDM5B	132	TGCTGTTGACAGTGAGCGCGGTTTCAGTGGCTGGAATTAATAGTGAAGCCACAGATGTATTAATTCC AGCCACTGAAACCATGCCTACTGCCTCGGA
KDM5B	133	TGCTGTTGACAGTGAGCGCCGGTGCTATTTCTATTCCTTATAGTGAAGCCACAGATGTATAAGGAAT AGAAATAGCACCGTTGCCTACTGCCTCGGA
KDM5C	134	TGCTGTTGACAGTGAGCGCGCCCAGTTTATTGAGTCATATTAGTGAAGCCACAGATGTAATATGACT CAATAAACTGGGCATGCCTACTGCCTCGGA
KDM5C	135	TGCTGTTGACAGTGAGCGAGGCCTTTCTGGACCAGATGAATAGTGAAGCCACAGATGTATTCATCTG GTCCAGAAAGGCCCTGCCTACTGCCTCGGA
KDM5C	136	TGCTGTTGACAGTGAGCGAGCATTGTTTATCCCTATGAAATAGTGAAGCCACAGATGTATTTCATAG GGATAAACAATGCGTGCCTACTGCCTCGGA
KDM6A	137	TGCTGTTGACAGTGAGCGACGCGCAAATAGAAATAATTTATAGTGAAGCCACAGATGTATAAATTAT TTCTATTTGCGCGGTGCCTACTGCCTCGGA
KDM6A	138	TGCTGTTGACAGTGAGCGCCGGAAGGTGCTATTCAAGTATTAGTGAAGCCACAGATGTAATACTTGA ATAGCACCTTCCGATGCCTACTGCCTCGGA
KDM6A	139	TGCTGTTGACAGTGAGCGCCCACCTACACCTAGTATTTATTAGTGAAGCCACAGATGTAATAAATAC TAGGTGTAGGTGGATGCCTACTGCCTCGGA
KDM6B	140	TGCTGTTGACAGTGAGCGAGGAGACCTCGTGTGGATTAATTAGTGAAGCCACAGATGTAATTAATCC ACACGAGGTCTCCGTGCCTACTGCCTCGGA
KDM6B	141	TGCTGTTGACAGTGAGCGCCGCGGCTCGTGTATGTACATATAGTGAAGCCACAGATGTATATGTACA TACACGAGCCGCGTTGCCTACTGCCTCGGA
KDM6B	142	TGCTGTTGACAGTGAGCGCCCTGTTCGTGACAAGTGAGAATAGTGAAGCCACAGATGTATTCTCACT TGTCACGAACAGGATGCCTACTGCCTCGGA
UTY	155	TGCTGTTGACAGTGAGCGCCCTGTGACAAAGTGAATAATATAGTGAAGCCACAGATGTATATTATTC ACTTTGTCACAGGTTGCCTACTGCCTCGGA
UTY	156	TGCTGTTGACAGTGAGCGAGCCTTGCTGGAGCTCTTAAATTAGTGAAGCCACAGATGTAATTTAAGA GCTCCAGCAAGGCCTGCCTACTGCCTCGGA
KDM1B	157	TGCTGTTGACAGTGAGCGCCGATGCGGTATGAAACCAAATTAGTGAAGCCACAGATGTAATTTGGTT TCATACCGCATCGATGCCTACTGCCTCGGA
KDM1B	158	TGCTGTTGACAGTGAGCGAGCCGAGTCTGGGATGATAAATTAGTGAAGCCACAGATGTAATTTATCA TCCCAGACTCGGCCTGCCTACTGCCTCGGA
KDM1B	159	TGCTGTTGACAGTGAGCGCCCAGTGCAGTGTATTGATTATTAGTGAAGCCACAGATGTAATAATCAA TACACTGCACTGGATGCCTACTGCCTCGGA
KDM3C	160	TGCTGTTGACAGTGAGCGCGGATACAGAGTGAGAGTATATTAGTGAAGCCACAGATGTAATATACTC TCACTCTGTATCCATGCCTACTGCCTCGGA
KDM3C	161	TGCTGTTGACAGTGAGCGCCCACAGTTTCTGATCATAATTTAGTGAAGCCACAGATGTAAATTATGA TCAGAAACTGTGGATGCCTACTGCCTCGGA

KDM3C	162	TGCTGTTGACAGTGAGCGCGCCCATCACCTGAAGTTGTTATAGTGAAGCCACAGATGTATAACAACT TCAGGTGATGGGCTTGCCTACTGCCTCGGA
KDM5D	163	TGCTGTTGACAGTGAGCGACCAGTTTATTGACTCATATATTAGTGAAGCCACAGATGTAATATATGA GTCAATAAACTGGGTGCCTACTGCCTCGGA
KDM5D	164	TGCTGTTGACAGTGAGCGCGGAGCTGATATTCATTCCAAATAGTGAAGCCACAGATGTATTTGGAAT GAATATCAGCTCCATGCCTACTGCCTCGGA
KDM5D	165	TGCTGTTGACAGTGAGCGCGCCATAATTCGTGAGACAGAATAGTGAAGCCACAGATGTATTCTGTCT CACGAATTATGGCTTGCCTACTGCCTCGGA
PHF8	169	TGCTGTTGACAGTGAGCGAGGAGAAAGTCCTCAATGTCATTAGTGAAGCCACAGATGTAATGACATT GAGGACTTTCTCCCTGCCTACTGCCTCGGA
PHF8	170	TGCTGTTGACAGTGAGCGCGCAGCTCAAAGCCTATGAGATTAGTGAAGCCACAGATGTAATCTCATA GGCTTTGAGCTGCATGCCTACTGCCTCGGA
PHF8	171	TGCTGTTGACAGTGAGCGCCGAGAGATTGGGAAAGGAGAATAGTGAAGCCACAGATGTATTCTCCTT TCCCAATCTCTCGTTGCCTACTGCCTCGGA
PHF2	172	TGCTGTTGACAGTGAGCGAGCGATGAGTATGAGTACGTATTAGTGAAGCCACAGATGTAATACGTAC TCATACTCATCGCGTGCCTACTGCCTCGGA
PHF2	173	TGCTGTTGACAGTGAGCGAGGAAACTACTCCTTTAAGATTTAGTGAAGCCACAGATGTAAATCTTAA AGGAGTAGTTTCCCTGCCTACTGCCTCGGA
PHF2	174	TGCTGTTGACAGTGAGCGAAAGATGAATCTTCAACTTTAATAGTGAAGCCACAGATGTATTAAAGTT GAAGATTCATCTTCTGCCTACTGCCTCGGA
KDM8	175	TGCTGTTGACAGTGAGCGACCAGGCTCTATGCTTTCTGTATAGTGAAGCCACAGATGTATACAGAAA GCATAGAGCCTGGCTGCCTACTGCCTCGGA
KDM8	176	TGCTGTTGACAGTGAGCGCGGCTCTATGCTTTCTGTAATTTAGTGAAGCCACAGATGTAAATTACAG AAAGCATAGAGCCTTGCCTACTGCCTCGGA
NO66	177	TGCTGTTGACAGTGAGCGAGGCCCAGCATTCAGATTCTAATAGTGAAGCCACAGATGTATTAGAATC TGAATGCTGGGCCCTGCCTACTGCCTCGGA
NO66	178	TGCTGTTGACAGTGAGCGACGTGTGTATCATCTGGAAGAATAGTGAAGCCACAGATGTATTCTTCCA GATGATACACACGGTGCCTACTGCCTCGGA
NO66	179	TGCTGTTGACAGTGAGCGCGGCAACCACGTTGTATGATAATAGTGAAGCCACAGATGTATTATCATA CAACGTGGTTGCCATGCCTACTGCCTCGGA
MINA53	180	TGCTGTTGACAGTGAGCGCGCACCTACCAGAACAATTCATTAGTGAAGCCACAGATGTAATGAATTG TTCTGGTAGGTGCTTGCCTACTGCCTCGGA
MINA53	181	TGCTGTTGACAGTGAGCGAGGCTTGTATTTGATACTGCAATAGTGAAGCCACAGATGTATTGCAGTA TCAAATACAAGCCCTGCCTACTGCCTCGGA
MINA53	182	TGCTGTTGACAGTGAGCGAGCACGCAACACTATGGACAAATAGTGAAGCCACAGATGTATTTGTCCA TAGTGTTGCGTGCCTGCCTACTGCCTCGGA
shFF	control	TGCTGTTGACAGTGAGCGCCCGCCTGAAGTCTCTGATTAATAGTGAAGCCACAGATGTATTAATCAG AGACTTCAGGCGGTTGCCTACTGCCTCGGA
shAR	control	TGCTGTTGACAGTGAGCGACCAGCAGAAATGATTGCACTATAGTGAAGCCACAGATGTATAGTGCA ATCATTTCTGCTGGCTGCCTACTGCCTCGGA

3.2.2 shRNA cloning

For shRNA cloning, 4 µg of shFF plasmid in pMSCV-puro backbone (Addgene #24828) was cleaved by 10 units of EcoRI (NEB, Cat.No. R3101S) and 10 units of XhoI (NEB, Cat.No. R0146S) for two hours in 37°C to remove Firefly Luciferase-targeting shRNA sequence. Digestion was confirmed by agarose gel electrophoresis. Digested backbone was extracted from 2% agarose gel prepared in TAE (Tris-Acetate-EDTA) buffer using NucleoSpin gel and PCR clean-up kit (Macherey-Nagel), and dephosphorylated by Antarctic phosphatase (NEB, Cat.No. M0289S). Oligos for shRNA were PCR-amplified

to generate compatible ends with EcoRI/XhoI digestion. For PCR reaction, 100 µM shRNA oligos were mixed with 10 µL of 5X Phusion buffer, 10 µL of 5M betaine, 2.5 µL of 100% DMSO, 1 µL of 2.5 mM dNTP mixture, 0.5 µL of 250 µM of PCR primers and 0.5 µL of Phusion polymerase. Volume was adjusted to 50 µL with sterile nuclease free water. PCR reactions were performed in the following conditions: initial denaturation at 94℃ for 5 mins, denaturing at 94℃ for 30 sec, annealing at 49℃ for 30 sec, extension at 72℃ for 30 sec. Final extension was performed at 72℃ for 2 mins. The cycle was repeated 30 times. The forward primer sequence was GATGGCTGCTCGAGAAGGTATATTGCTGTTGACAGTGAGCG, and the reverse primer was GTCTAGAGGAATTCCGAGGCAGTAGGC. The reaction was cleaned up by using NucleoSpin gel and PCR clean-up kit (Macherey-Nagel) following the manufacturer's instructions. Digested backbone and amplified shRNA sequence were mixed in 3:1 ratio and ligated by T4 DNA ligase (NEB, Cat. No. M0202S) at room temperature for an hour or at 16℃ overnight. Ligation mixture was transformed into Stbl3 *E.coli* strain and spread onto 100µg/mL ampicillin containing agar plates. Agar plates were incubated overnight in a bacterial incubator at 37 ℃. Next day, surviving colonies were picked for validation, incubated overnight in 5mL of Luria broth supplemented with 100 µg/mL ampicillin, followed by plasmid extraction by NucleoSpin Plasmid (Macherey-Nagel). The inserted sequence was validated by Sanger sequencing.

3.2.3 shRNA library packaging

For viral packaging with any plasmid with lentiviral or retroviral backbone, early passage HEK293T cells were used. HEK293T cells were cultured in DMEM media supplemented with 10% FBS and 1% Penicillin/Streptomycin in a humidified incubator at 37℃ and 5%CO_2. The day before transfection, cells were seeded in complete media (10% FBS with 1% Penicillin/Streptomycin) onto 10 cm dishes as 2.5x10^6 cells/dish. Packaging plasmid pUMVC (Addgene #8449) and envelop plasmid pCMV-VSV-G (Addgene #8454) were used for retroviral packaging. Plasmids were mixed well in 10:9:1 ratio (plasmid of interest: packaging plasmid: envelope plasmid) for a total of 5 µg DNA in 200 µL of Opti-MEM (Gibco, Cat.No. 31985062). Fugene 6 (Promega, Cat.No. E2692) was diluted in Opti-MEM (Gibco, Cat.No. 31985062) at a 1:10 ratio in 200 µL total volume. Plasmid mixture was added to Fugene 6 dilution, mixed well, and incubated for 20-30 minutes at room temperature. After incubation, HEK293T cells were transfected

by adding the mixture in a dropwise manner. About 16 hours after transfection, Fugene 6-containing media was replaced with fresh complete media. Viral supernatant was collected at 48 hours and 72 hours after transfection. Combined viral supernatants were filtered through 0.45µm syringe filters. Viral particles were precipitated with a final concentration of 10% (w/v) PEG-6000 (Sigma; Cat.No. P4338) for at least 16 hrs at 4°C. Following overnight incubation, the mixture was centrifuged at 2500 rpm for 25 mins and then 1250 rpm for 5 mins. Supernatant was carefully decontaminated after each centrifugation. White precipitate containing viral particles was resuspended in 500 µL ice-cold PBS. Viral suspension was aliquoted and kept at -80°C until usage.

3.2.4 shRNA screen

Before screening, a viral titration was determined for each cell line after every packaging using knockdown efficiency as the readout. Based on this, the relative amount of viral volume was determined for > 60% knockdown in the screen. Cells were seeded onto 6 multiwell plates at 0.15-0.2x10^6 cells/well 24 hours prior to the transduction. At the day of transduction, the media was replaced with fresh media supplemented with 8µg/mL protamine sulfate (Sigma, Cat. No. P4020). Each well was transduced by an shRNA viral suspension. After 48 hours, media is replaced with puromycin-containing media. Transduced cells are selected with puromycin for 72 hours with the concentrations provided in **Table 3.2**. At the end of puromycin selection, cells were counted with trypan blue and 100,000-150,000 cells were seeded onto 6 multiwell plates in duplicate for each shRNA condition for crystal violet staining. Remaining cells were collected or maintained until the end of the experiment for RT-qPCR to confirm knockdown efficiency. Cells were cultivated for 8 days and then stained with crystal violet. Each screening process was repeated at least three times.

3.2.5 Crystal violet staining and analysis

For crystal violet staining, 0.5% (w/v) crystal violet solution was prepared with 25% methanol solution. The media on the cells was aspirated and washed with PBS gently. Sufficient crystal violet solution was added to cover the surface area of each well. Cells were incubated with the stain at room temperature for 15-20 mins in an orbital shaker. The stain was collected and the cells were thoroughly washed with running tap water until the dye stopped to come off. The plates were then left to dry overnight in an aerated area.

Images of plates were taken and the confluency was analyzed by ImageJ using manual threshold. Each data point was normalized to their shFF control.

3.2.6 RNA extraction and RT-qPCR

Cell pellets were preserved in -80℃ until RNA extraction. RNA extraction was performed using the NucleoSpin RNA extraction kit (Macherey-Nagel, Cat no: 740955) following manufacturer's instructions. The concentrations of total RNA were determined by NanoDrop measurements. Either 500-1000 ng of total RNA was converted to cDNA by M-MLV reverse transcriptase (Thermo Fisher, cat no: 28025013) following manufacturer's instructions. Final volume was adjusted to a final concentration of 10 ng/μL of total RNA. For RT-qPCR reactions, a 10 μL of reaction volume was prepared in sterile nuclease free water with 10 ng of cDNA mixture, 0.25 μL of each 10 μM forward and reverse primers and 5 μL of 2X SYBR Green I master mixture (Roche, Cat no: 04707516001). RT-qPCR primers for KDMs are listed in **Table 3.4**.

Table 3.4 RT-qPCR primers for lysine demethylases and androgen receptor

Target	Forward primer	Reverse primer
AR	CCTGGCTTCCGCAACTTACAC	GGACTTGTGCATTGCGGTACTCA
KDM1A	ACACCCCGCAAGAAAGAGC	GACCCAGGCACGACAGTAG
KDM1B	TGTGTGAACAAGTATCTGCTCGCT	GCCATCTGTAGTGGTAACCTGC
KDM2A	GGGGTGGCTTGAGAGATCCT	TCCCCACACACATTTTGACATC
KDM2B	CAACGACGAGCTTCCAAACTG	CTTGTAGGCTTTCCCGGTCTT
KDM3A	TTAGCTGAACGAAAGTCACCTG	ATCTCCCAGAAAGCGAACAGA
KDM3B	AGATAAACCGCAACATTCGCT	CTGCACCACCAGAGTCCTG
KDM3C	CCAAAATTGCCTGGAAAAGA	ACATCACTCTCTGGGCTGCT
KDM4A	ATCCCAGTGCTAGGATAATGACC	TCTTTTGGAGGAACAACCTTGG
KDM4B	GAGGAGCTAGAGGCCAAGC	CTTCCAGGTCGGACCCTTC
KDM4C	AGCCTCTGACATGCGATTTGA	GGGTCGGCCACATATTCATTC
KDM4D	CTGCAACCTGAACGCTATGAC	TGCTCTCCTGGGTAACTGGAC
KDM5A	CCGTCTTTGAGCCGAGTTG	GGACTCTTGGAGTGAAACGAAA
KDM5B	CCATAGCCGAGCAGACTGG	GGATACGTGGCGTAAAATGAAGT
KDM5C	GTGGACAACTTGAGGTTTACCC	CGCCGTTCTACATTGGGAATCT
KDM5D	AGCAGAGCATTTGGAGGAGG	TCCCCTGCACACTGGTTTGT

KDM6A	TTCCTCGGAAGGTGCTATTCA	GAGGCTGGTTGCAGGATTCA
KDM6B	CTACCCCCTTCACATGGCAG	CTCTGACTCGTACAGTTGCCC
UTY	TTAGCCTGACAGTCGAGGAAA	GTAGGGTCTTCGTTCTGGCG
PHF2	GCAAACGACTGCTGAAGAGG	ACTCCAGTGAGGGGTAAACG
PHF8	GCCTTCTCCACTGAGGAGCAGGTA	CTCCTCATCCTGCCTTCCAGCTCT
KDM8	CTGTCCCAGTGGAAGTTGGT	GTAGTCGGGGATGCTGATGT
MINA53	CCCATTATGATGATGTCGA	TGTTCTGGTAGGTGCTGAT
NO66	CTGGAAACAAGGCAGTAGTGATT	GTACACTGAAGCCTGAAGGTGAT
B-ACTIN	CATGTACGTTGCTATCCAGGC	CTCCTTAATGTCACGCACGAT

3.2.7 MTS assay

For MTS assays, 2000 transduced cells were seeded onto flat-bottom clear 96 multiwell plates in 6 replicates. At the time of reading, 20 µL of MTS solution (prepared from Promega CellTiter 96® AQueous MTS Reagent Powder following manufacturer's instruction) was added to cells and incubated for 2-4 hrs in a dark, humidified incubator at 37°C and 5% CO_2. The plate was briefly shaken and read on plate reader at 490 nm.

3.3 EPIKOL library and CRISPR-Cas9 screens

3.3.1 EPIKOL library

The EPIgenetic Knock-Out Library (EPIKOL) was designed and generated in a collaborative effort of three KUTTAM labs supervised by Dr. Nathan Lack, Dr. Tugba Bagci-Onder and Dr. Tamer Onder. This library contains 7870 sgRNAs that target 719 epigenetic modifiers, 60 positive control genes in addition to 80 non-targeting control sgRNAs. To generate an epigenetic focused library, a curated list for epigenetic modifiers was first obtained from the EpiFactors database [351]. The positive control genes include both context-specific (n=25) and core-essential (n=35) genes. Context-specific genes include nuclear receptors, ABC transporters, apoptosis-related and metastasis-related genes. Core-essential genes were mostly associated with core transcription and translation machinery and had been essential in the dropout screens of 62 different cell lines described in the Genome CRISPR database [352]. Each gene in the library is targeted by 10 unique sgRNAs that were chosen from previous genome-wide CRISPR libraries [329,333]. In the case of overlapping sgRNA sequences, new sgRNAs were designed using online CRISPR designing tools CCTop [353] and E-CRISP [354]. The sgRNA

coverage of the cloned library is confirmed by high-throughput sequencing. The gRNA oligonucleotide library was cloned by Dr. Alişan Kayabölen into both the lentiCRISPRv2 (Addgene #52961) and LentiGuide-puro (Addgene #52963) backbones.

3.3.2 Viral Packaging

All viral packaging was done with early passage HEK293T cells cultured in DMEM media supplemented with 10% FBS and 1% Penicillin/Streptomycin in a humidified incubator at 37℃ and 5% CO_2. Cells ($5x10^6$ cells/10cm dish) were seeded in complete media (10%FBS, no antibiotics) 24 hours prior to the transfection. On the day of transfection, the media was replaced with DMEM media supplemented with 2% FBS (no antibiotics), 2-4 hours prior to the transfection. Packaging plasmid pCMV-d8.2-dVPR (Addgene #8455) and envelop plasmid pCMV-VSV-G (Addgene #8454) were used for lentiviral packaging. Plasmids were mixed in 10:9:1 ratio (EPIKOL library: packaging plasmid: envelope plasmid) and 12µg was diluted in 800 µL of 150mM NaCl solution. Transporter 5 (Polyscience Inc., Cat. No. 26008) was added in 1:3 (DNA:Reagent) ratio. The mixture was briefly vortexed and incubated for 20-30 mins before adding drop-wise onto cells. Media was changed 8 hrs after transfection. Viral supernatant was collected at 48 hrs and 72 hrs post-transfection. Viral supernatant was filtered through a 0.45µm syringe filter or SteriFlips (Millipore; Cat. No. SE1M003M00) and then precipitated with a final concentration of sterile 10% (w/v) PEG-6000 (Sigma; Cat. No. P4338) for at least 16 hrs in a 4℃ fridge. White precipitate was cold-centrifuged twice at 2500 rpm and 1250 rpm. Pellet was resuspended in sterile PBS solution and aliquoted on ice for single usage. All concentrated lentiviral aliquots were kept in an -80℃ freezer.

3.3.3 Viral titration and MOI calculation

To calculate the viral titre, cells were seeded in either 6 multiwell or 12 multiwell plates at $0.2x10^6$ cells/well or $0.1x10^6$ cells/well, respectively. Next day, each well was transduced with a different amount of virus. Two wells were left non-transduced to serve as viability control and antibiotic selection control. Cells were selected with antibiotics as previously described in *Section 3.1.2*. At the end of selection, cells in each well were counted by trypan blue exclusion. Multiplicity of infection (MOI) was calculated from the Poisson equation [355] using the following formula:

$$P(n) = \frac{m^n \times e^{-m}}{n!}$$

For n>0; $P(n > 0) = 1 - P(n = 0)$

$$P(n > 0) = 1 - \frac{m^0 \times e^{-m}}{0!} = 1 - e^{-m}$$

$$\mathrm{m} = -\ln(1 - P(n > 0))$$

n= particle of virus

m= MOI

P(n > 0) = The transduced population as decimal number, calculated experimentally.

3.3.4 Cas9-expressing stable cell line generation

LentiCas9-blast (Addgene #52962) lentiviruses were packaged as described in *Section 3.3.2* and titrated as described in *Section 3.3.3*. Cells were seeded onto 6 multiwell plates at $2x10^5$ cells/well and then transduced at a MOI=5. Cells were selected with Blasticidin S HCl two days after transduction as previously described (*Section3.1.2*). Surviving cells were propagated for at least three passages in blasticidin-containing media. This process was repeated for all cell lines used in the EPIKOL screen.

3.3.5 CRISPR screens and high-throughput sequencing

For the screen, we used EPIKOL library in lentiGuide-puro (Addgene #52963) backbone as it gave higher viral titre. Cas9-expressing stable PCa cell lines were seeded onto three 15 cm plates as $4.5x10^6$ cells per plate. Cells were transduced with the EPIKOL library at MOI=0.3 with 500x coverage. Two days after transduction, cells were selected with puromycin for three days. At the end of selection $4x10^6$ cells were collected for sequencing (T=0) and $13.5x10^6$ cells were maintained further for up to 15 doubling time. Cells were trypsinized and seeded at a 1500x library representation every 2-3 cell division. At the 15^{th} doubling time, $4x10^6$ cells were collected for sequencing. Cells were kept in selective media at half of the concentration that is used for antibiotic selection to eliminate any possible growth of cells which don't carry desired plasmids. Collected cell pellets were kept in -80°C until genomic DNA isolation. Genomic DNA was isolated by PureLink Genomic DNA mini kit (Invitrogen, Cat. No. K1820) following the manufacturer's instructions. Genomic DNA concentrations were measured by NanoDrop. Each dropout screen was repeated three times.

Library preparation was done with a two-stage amplification to attach Illumina adapters and indexes to the first PCR products. For library preparation, 4 µg of genomic DNA was amplified by using Kapa HiFi HotStart ReadyMix (Roche, Cat.No. KK2602). For external PCR step, 8 reactions were prepared using 0.5 µg of genomic DNA with 12.5 µL of Kapa HiFi HotStart ReadyMix, 2.5 µL of external forward primer (10uM), 2.5 µL of external reverse primer (10uM) listed in **Table 3.5** and nuclease free water up to 25 µL. External PCR products for each sample were pooled to be used in internal PCR. For internal PCR, 2 reactions were prepared in 50 µL reaction volumes with 0.5 µL of pooled external PCR product, 25 µL of Kapa HiFi HotStart ReadyMix, 2.5 µL of mixed forward staggered primer pool (10uM), 2.5 µL of indexed reverse primer (10uM) listed in **Table 3.5** and 19.5 µL of nuclease free water. PCR reactions were performed in the following conditions: initial denaturation at 95℃ for 3 mins, denaturing at 95℃ for 25 sec, annealing at 65℃ for 20 sec, extension at 72℃ for 15 sec. Final extension was performed at 72℃ for 3 mins. The number of PCR cycles were 25x for external PCR and 15x for internal PCR. Separate to genomic DNA amplification, 1ng of plasmid was used in every library preparation to serve as positive control. After second amplification, all PCR products were run on the 1.5% TBE (Tris-borate-EDTA) gel for 70 mins at 100 volts. The expected bands were gel-isolated. Sample concentrations were measured by Qubit and run on 4200 TapeStation High Sensitivity D1000 for DNA to confirm their size and purity. Following QC validation, samples were sent to the Genewiz sequencing facility in the USA to be sequenced in HiSeq4000 platform with 2x150 base pair sequencing mode with single index.

Table 3.5 List of LentiGuide backbone compatible primers used in library preparation for sequencing

Primer Name	Sequence	Index
EpiV2External_ Forward	AATGGACTATCATATGCTTACCGTAACTTGAAAGTATTTCG	
EpiV2External_ Reverse	CTTTAGTTTGTATGTCTGTTGCTATTATGTCTACTATTCTTTCC	
Forward_stag1	AATGATACGGCGACCACCGAGATCTACACTCTTTCCCTACACGACG CTCTTCCGATCTATCTTGTGGAAAGGACGAAACACCG	
Forward_stag2	AATGATACGGCGACCACCGAGATCTACACTCTTTCCCTACACGACG CTCTTCCGATCTCTTCTTGTGGAAAGGACGAAACACCG	
Forward_stag3	AATGATACGGCGACCACCGAGATCTACACTCTTTCCCTACACGACG CTCTTCCGATCTGACTCTTGTGGAAAGGACGAAACACCG	

Forward_stag4	AATGATACGGCGACCACCGAGATCTACACTCTTTCCCTACACGACG CTCTTCCGATCTTCGATCTTGTGGAAAGGACGAAACACCG	
Forward_stag5	AATGATACGGCGACCACCGAGATCTACACTCTTTCCCTACACGACG CTCTTCCGATCTATCGCTCTTGTGGAAAGGACGAAACACCG	
Forward_stag6	AATGATACGGCGACCACCGAGATCTACACTCTTTCCCTACACGACG CTCTTCCGATCTGTCAGATCTTGTGGAAAGGACGAAACACCG	
Forward_stag7	AATGATACGGCGACCACCGAGATCTACACTCTTTCCCTACACGACG CTCTTCCGATCTTGCATCGTCTTGTGGAAAGGACGAAACACCG	
Forward_stag8	AATGATACGGCGACCACCGAGATCTACACTCTTTCCCTACACGACG CTCTTCCGATCTCTACGTGATCTTGTGGAAAGGACGAAACACCG	
Forward_stag9	AATGATACGGCGACCACCGAGATCTACACTCTTTCCCTACACGACG CTCTTCCGATCTACTCGTGATTCTTGTGGAAAGGACGAAACACCG	
rev_index1	CAAGCAGAAGACGGCATACGAGATCGTGATGTGACTGGAGTTCAG ACGTGTGCTCTTCCGATCTTCTACTATTCTTTCCCCTGCACTGT	CGTGAT
rev_index2	CAAGCAGAAGACGGCATACGAGATACATCGGTGACTGGAGTTCAG ACGTGTGCTCTTCCGATCTTCTACTATTCTTTCCCCTGCACTGT	ACATCG
rev_index3	CAAGCAGAAGACGGCATACGAGATGCCTAAGTGACTGGAGTTCAG ACGTGTGCTCTTCCGATCTTCTACTATTCTTTCCCCTGCACTGT	GCCTAA
rev_index4	CAAGCAGAAGACGGCATACGAGATTGGTCAGTGACTGGAGTTCAG ACGTGTGCTCTTCCGATCTTCTACTATTCTTTCCCCTGCACTGT	TGGTCA
rev_index5	CAAGCAGAAGACGGCATACGAGATCACTGTGTGACTGGAGTTCAG ACGTGTGCTCTTCCGATCTTCTACTATTCTTTCCCCTGCACTGT	CACTGT
rev_index6	CAAGCAGAAGACGGCATACGAGATATTGGCGTGACTGGAGTTCAG ACGTGTGCTCTTCCGATCTTCTACTATTCTTTCCCCTGCACTGT	ATTGGC
rev_index7	CAAGCAGAAGACGGCATACGAGATGATCTGGTGACTGGAGTTCAG ACGTGTGCTCTTCCGATCTTCTACTATTCTTTCCCCTGCACTGT	GATCTG
rev_index8	CAAGCAGAAGACGGCATACGAGATTCAAGTGTGACTGGAGTTCAG ACGTGTGCTCTTCCGATCTTCTACTATTCTTTCCCCTGCACTGT	TCAAGT
rev_index9	CAAGCAGAAGACGGCATACGAGATCTGATCGTGACTGGAGTTCAG ACGTGTGCTCTTCCGATCTTCTACTATTCTTTCCCCTGCACTGT	CTGATC
rev_index10	CAAGCAGAAGACGGCATACGAGATAAGCTAGTGACTGGAGTTCAG ACGTGTGCTCTTCCGATCTTCTACTATTCTTTCCCCTGCACTGT	AAGCTA
rev_index11	CAAGCAGAAGACGGCATACGAGATGTAGCCGTGACTGGAGTTCAG ACGTGTGCTCTTCCGATCTTCTACTATTCTTTCCCCTGCACTGT	GTAGCC
rev_index12	CAAGCAGAAGACGGCATACGAGATTACAAGGTGACTGGAGTTCAG ACGTGTGCTCTTCCGATCTTCTACTATTCTTTCCCCTGCACTGT	TACAAG
rev_index13	CAAGCAGAAGACGGCATACGAGATTTGACTGTGACTGGAGTTCAG ACGTGTGCTCTTCCGATCTTCTACTATTCTTTCCCCTGCACTGT	TTGACT
rev_index14	CAAGCAGAAGACGGCATACGAGATGGAACTGTGACTGGAGTTCAG ACGTGTGCTCTTCCGATCTTCTACTATTCTTTCCCCTGCACTGT	GGAACT
rev_index15	CAAGCAGAAGACGGCATACGAGATTGACATGTGACTGGAGTTCAG ACGTGTGCTCTTCCGATCTTCTACTATTCTTTCCCCTGCACTGT	TGACAT

rev_index16	CAAGCAGAAGACGGCATACGAGATGGACGGGTGACTGGAGTTCAG ACGTGTGCTCTTCCGATCTTCTACTATTCTTTCCCCTGCACTGT	GGACGG
rev_index17	CAAGCAGAAGACGGCATACGAGATCTCTACGTGACTGGAGTTCAG ACGTGTGCTCTTCCGATCTTCTACTATTCTTTCCCCTGCACTGT	CTCTAC
rev_index18	CAAGCAGAAGACGGCATACGAGATGCGGACGTGACTGGAGTTCAG ACGTGTGCTCTTCCGATCTTCTACTATTCTTTCCCCTGCACTGT	GCGGAC
rev_index19	CAAGCAGAAGACGGCATACGAGATTTTCACGTGACTGGAGTTCAG ACGTGTGCTCTTCCGATCTTCTACTATTCTTTCCCCTGCACTGT	TTTCAC
rev_index20	CAAGCAGAAGACGGCATACGAGATGGCCACGTGACTGGAGTTCAG ACGTGTGCTCTTCCGATCTTCTACTATTCTTTCCCCTGCACTGT	GGCCAC
rev_index21	CAAGCAGAAGACGGCATACGAGATCGAAACGTGACTGGAGTTCAG ACGTGTGCTCTTCCGATCTTCTACTATTCTTTCCCCTGCACTGT	CGAAAC
rev_index22	CAAGCAGAAGACGGCATACGAGATCGTACGGTGACTGGAGTTCAG ACGTGTGCTCTTCCGATCTTCTACTATTCTTTCCCCTGCACTGT	CGTACG
rev_index23	CAAGCAGAAGACGGCATACGAGATCCACTCGTGACTGGAGTTCAG ACGTGTGCTCTTCCGATCTTCTACTATTCTTTCCCCTGCACTGT	CCACTC
rev_index24	CAAGCAGAAGACGGCATACGAGATGCTACCGTGACTGGAGTTCAG ACGTGTGCTCTTCCGATCTTCTACTATTCTTTCCCCTGCACTGT	GCTACC
rev_index25	CAAGCAGAAGACGGCATACGAGATATCAGTGTGACTGGAGTTCAG ACGTGTGCTCTTCCGATCTTCTACTATTCTTTCCCCTGCACTGT	ATCAGT
rev_index26	CAAGCAGAAGACGGCATACGAGATGCTCATGTGACTGGAGTTCAG ACGTGTGCTCTTCCGATCTTCTACTATTCTTTCCCCTGCACTGT	GCTCAT
rev_index27	CAAGCAGAAGACGGCATACGAGATAGGAATGTGACTGGAGTTCAG ACGTGTGCTCTTCCGATCTTCTACTATTCTTTCCCCTGCACTGT	AGGAAT
rev_index28	CAAGCAGAAGACGGCATACGAGATCTTTTGGTGACTGGAGTTCAG ACGTGTGCTCTTCCGATCTTCTACTATTCTTTCCCCTGCACTGT	CTTTTG
rev_index29	CAAGCAGAAGACGGCATACGAGATTAGTTGGTGACTGGAGTTCAG ACGTGTGCTCTTCCGATCTTCTACTATTCTTTCCCCTGCACTGT	TAGTTG
rev_index30	CAAGCAGAAGACGGCATACGAGATCCGGTGGTGACTGGAGTTCAG ACGTGTGCTCTTCCGATCTTCTACTATTCTTTCCCCTGCACTGT	CCGGTG
rev_index31	CAAGCAGAAGACGGCATACGAGATATCGTGGTGACTGGAGTTCAG ACGTGTGCTCTTCCGATCTTCTACTATTCTTTCCCCTGCACTGT	ATCGTG
rev_index32	CAAGCAGAAGACGGCATACGAGATTGAGTGGTGACTGGAGTTCAG ACGTGTGCTCTTCCGATCTTCTACTATTCTTTCCCCTGCACTGT	TGAGTG
rev_index33	CAAGCAGAAGACGGCATACGAGATCGCCTGGTGACTGGAGTTCAG ACGTGTGCTCTTCCGATCTTCTACTATTCTTTCCCCTGCACTGT	CGCCTG
rev_index34	CAAGCAGAAGACGGCATACGAGATGCCATGGTGACTGGAGTTCAG ACGTGTGCTCTTCCGATCTTCTACTATTCTTTCCCCTGCACTGT	GCCATG
rev_index35	CAAGCAGAAGACGGCATACGAGATAAAATGGTGACTGGAGTTCAG ACGTGTGCTCTTCCGATCTTCTACTATTCTTTCCCCTGCACTGT	AAAATG
rev_index36	CAAGCAGAAGACGGCATACGAGATTGTTGGGTGACTGGAGTTCAG ACGTGTGCTCTTCCGATCTTCTACTATTCTTTCCCCTGCACTGT	TGTTGG

rev_index37	CAAGCAGAAGACGGCATACGAGATATTCCGGTGACTGGAGTTCAG ACGTGTGCTCTTCCGATCTTCTACTATTCTTTCCCCTGCACTGT	ATTCCG
rev_index38	CAAGCAGAAGACGGCATACGAGATAGCTAGGTGACTGGAGTTCAG ACGTGTGCTCTTCCGATCTTCTACTATTCTTTCCCCTGCACTGT	AGCTAG

3.3.6 MAGeCK analysis

MAGeCK algorithm [356] (version 0.5.9.2) was used through all steps of the analysis including sgRNA count quantification and identification of significantly depleted genes. For each sample, R1 fastq files were processed by MAGeCK's count function to provide sgRNA level counts. Biological replicates were presented as individual input files during sgRNA counting. All samples were combined and median normalised by `–norm-method "median"` argument of MAGeCK's count. Identification of essential genes was calculated by MAGeCK's test function. For each comparison, replicates were pooled as "-t Arep1,Arep2,Arep3" and "-c Brep1,Brep2,Brep3" for conditionA and conditionB respectively. In addition, negative control sgRNA were supplied with "--control-sgrna" function. Median normalised combined tables were used for visualisation. R (version 2021.09.0) and ggplot2 package (version 3.3.5) were used for boxplot and density plots. Data analysis with MAGeCK was done by Tunç Morova.

3.3.7 sgRNA and shRNA cloning

A minimum of 2 sgRNAs showing a strong phenotype for selected "hit" genes were cloned into pLentiCRISPR2.v2 (Addgene #52961) and pLKO5 (Addgene #57822) plasmids. For this process, forward oligo flanking with 5'-CACCG and reverse oligo flanking with CAAA-3' were ordered as listed in **Table 3.6**. These oligos were annealed and phosphorylated by using 1 µL of each oligos (100 µM stock concentration), 1 µL of 10X T4 ligase buffer (NEB), and 0.5 µL of T4 PNK (NEB M0201S) diluted in sterile nuclease free water brought up to 20 µL reaction volume. Thermocycler conditions were set to 37℃ for 30 mins, 95℃ for 5 mins ramping down to 25℃ at 5℃/min. Annealed oligos were diluted at 1:200 in sterile nuclease free water for ligation step.

5 µg of plasmid DNA were digested by BsmBI enzyme (NEB R0580S) for 3 hours at 37℃ in 20 µL reaction volume. The digested backbone was run on a 1% TBE agarose gel at 100V for 1 hour. The digested band was cut and extracted from the gel using Monarch DNA Gel Extraction kit (NEB T1020S). 50 ng of digested plasmid was mixed

with 1 µL of diluted oligo duplex, 2 µL 10X T4 ligase Buffer (NEB) and 1 µL T4 DNA ligase (NEB M0202S) adjusted to 11 µL reaction volume with sterile water. The mixture was incubated at room temperature for 1 hour and transformed into Stbl3 *E.coli* strain. The cloning was confirmed with Sanger sequencing.

Table 3.6 Oligo sequences for sgRNA cloning.

Type #	Target Gene	Forward Oligo	Reverse Oligo
	NonTargeting	caccGTACCATACCGCGTACCCTT	aaacAAGGGTACGCGGTATGGTAC
sgRNA1	RPS11	caccGGGCTTCAAGACACCCAAGG	aaacCCTTGGGTGTCTTGAAGCCC
sgRNA2	RPS11	caccgTGTAGTGCAGATAGTCTCGG	aaacCCGAGACTATCTGCACTACAc
sgRNA1	BAP1	caccgCACGGACGTATCATCCACCA	aaacTGGTGGATGATACGTCCGTGc
sgRNA2	BAP1	caccGAACCGTCAGACAGTACTAG	aaacCTAGTACTGTCTGACGGTTC
sgRNA3	BAP1	caccGTCCATCAAGACTAGCAGCG	aaacCGCTGCTAGTCTTGATGGAC
sgRNA1	MRGBP	caccgCAGCGCCTGCATGTCGTACA	aaacTGTACGACATGCAGGCGCTGc
sgRNA2	MRGBP	caccGGCGCTCACCGACGGGCTTG	aaacCAAGCCCGTCGGTGAGCGCC
sgRNA3	MRGBP	caccgTGTCCCGAATACAAATCATG	aaacCATGATTTGTATTCGGGACAc
sgRNA1	NIPBL	caccGCTTGTCCATAGCCTCAACC	aaacGGTTGAGGCTATGGACAAGC
sgRNA2	NIPBL	caccgTACGCCCCACAAAGCCCTGC	aaacGCAGGGCTTTGTGGGGCGTAc
sgRNA3	NIPBL	caccgTTAGCCTGTGCACCATGTGT	aaacACACATGGTGCACAGGCTAAc
sgRNA1	CSNK2A1	caccgAGACATTGTAAAAGACCCTG	aaacCAGGGTCTTTTACAATGTCTc
sgRNA2	CSNK2A1	caccgCTAGTTGGTGAGGATAGCCA	aaacTGGCTATCCTCACCAACTAGc
sgRNA3	CSNK2A1	caccGATTGATCATGAGCACAGAA	aaacTTCTGTGCTCATGATCAATC
sgRNA1	PAXIP1	caccGTGATTCTGTCCGTTCAGTG	aaacCACTGAACGGACAGAATCACc
sgRNA2	PAXIP1	caccgTCTTCATAAATAATCAGACG	aaacCGTCTGATTATTTATGAAGAc
sgRNA3	PAXIP1	caccgTTACTACTGACCTTTACAAC	aaacGTTGTAAAGGTCAGTAGTAAc
sgRNA1	PCGF2	caccgAACGGCTCCAATGAGGACCG	aaacCGGTCCTCATTGGAGCCGTTc
sgRNA2	PCGF2	caccGGACCTGCACGTCACACATG	aaacCATGTGTGACGTGCAGGTCC
sgRNA1	SETDB1	caccgAAGGAAAGAGTCTACTGTCG	aaacCGACAGTAGACTCTTTCCTTc
sgRNA2	SETDB1	caccgAGATGTGAGTGGATCTATCG	aaacCGATAGATCCACTCACATCTc
sgRNA3	SETDB1	caccGTTATCTATAAGACACCTTG	aaacCAAGGTGTCTTATAGATAAC
sgRNA1	SIN3B	caccGTACTTCCCCACTGCAGCGA	aaacTCGCTGCAGTGGGGAAGTAC
sgRNA2	SIN3B	caccgTCTTCTAGCATCGATACTCC	aaacGGAGTATCGATGCTAGAAGAc
sgRNA1	SIRT6	caccgCACTTGCCCTTGTCCGCGTA	aaacTACGCGGACAAGGGCAAGTGc
sgRNA2	SIRT6	caccgCTTCCACAAACATGTTCCCG	aaacCGGGAACATGTTTGTGGAAGc
sgRNA3	SIRT6	caccGTACGTCCGAGACACAGTCG	aaacCGACTGTGTCTCGGACGTAC
sgRNA1	SMARCC2	caccgATTGTAGCAACTGTACAACC	aaacGGTTGTACAGTTGCTACAATc
sgRNA2	SMARCC2	caccgTATGCCTATTACCTGCACCA	aaacTGGTGCAGGTAATAGGCATAc
sgRNA1	DPF2	caccgAGAGGCGAGCATTGTAATTG	aaacCAATTACAATGCTCGCCTCTc

sgRNA2	DPF2	caccGAAGATACTCCCAAGCGTCG	aaacCGACGCTTGGGAGTATCTTC

Genetic Perturbation Platform web portal provided by Broad Institute was utilized to design shRNAs (https://portals.broadinstitute.org/gpp/public/). shRNA oligos were ordered, annealed and phosphorylated as described above (Sequences are provided in **Table 3.7**). 10 µg of pLKO1-puro (Addgene #8453) was digested by EcoRI-HF (NEB R3101S) and AgeI-HF (NEB R3552S) at 37℃ for 2 hours. The digested backbone was run on a 0.8% TBE agarose gel and gel extracted using Monarch DNA Gel Extraction kit (NEB T1020S). 50 ng of digested plasmid was mixed with 1 µL of diluted oligo duplex, 2 µL 10X T4 ligase Buffer (NEB) and 1 µL T4 DNA ligase (NEB M0202S) adjusted to 11 µL reaction volume with sterile water. The mixture was incubated at room temperature for 1 hour and transformed into Stbl3 *E.coli* strain. The cloning was confirmed with Sanger sequencing.

Table 3.7 Oligo sequences for shRNA cloning

shRNA#	Target gene	Forward oligo	Reverse oligo
	shGFP	CCGGACAACAGCCACAACGTCTATACTCGAGTATAGACGTTGTGGCTGTTGTTTTTTG	AATTCAAAAAACAACAGCCACAACGTCTATACTCGAGTATAGACGTTGTGGCTGTTGT
shRNA1	SMARCC2	CCGGGCCTGTCTCGACCTAACATTTCTCGAGAAATGTTAGGTCGAGACAGGCTTTTTG	AATTCAAAAAGCCTGTCTCGACCTAACATTTCTCGAGAAATGTTAGGTCGAGACAGGC
shRNA2	SMARCC2	CCGGTCACTAAACTGCCGATCAAATCTCGAGATTTGATCGGCAGTTTAGTGATTTTTG	AATTCAAAAATCACTAAACTGCCGATCAAATCTCGAGATTTGATCGGCAGTTTAGTGA
shRNA1	DPF2	CCGGCGACTTTCCTTCCCATCTATTCTCGAGAATAGATGGGAAGGAAAGTCGTTTTTG	AATTCAAAAACGACTTTCCTTCCCATCTATTCTCGAGAATAGATGGGAAGGAAAGTCG
shRNA2	DPF2	CCGGCGAGTGCAAATGTTGCAATATCTCGAGATATTGCAACATTTGCACTCGTTTTTG	AATTCAAAAACGAGTGCAAATGTTGCAATATCTCGAGATATTGCAACATTTGCACTCG

3.3.8 eGFP competition assay

A minimum of 2 sgRNAs per gene candidate were cloned into the GFP expressing pLKO5 plasmid (Addgene #57822). Plasmids were packaged and infected into Cas9-expressing stable cell lines in MOI= 0.5. Initial eGFP expression was determined by flow cytometry using BD FACSCanto II and every 3-4 days following the previous measurement. Data is normalized to eGFP percentage of initial day of corresponding construct and non-targeting control. RPS11 (ribosomal gene) was used as positive control for the experiment. Each experiment repeated at least three times. sgRNA sequences are provided in **Table 3.6**.

3.3.9 Validation assays

For SMARCC2 and DFP2 genes, two sgRNAs per gene were cloned into LentiCRISPRv2 (Addgene #52961) and two shRNAs per gene were cloned into pLKO1-puro (Addgene #8453) (Sequences are provided in **Table 3.6** and **Table 3.7**). Cells were transduced with packaged lentiviruses containing these constructs and selected with puromycin for three days. Selected cells were counted and seeded onto either 6 multiwell or 96 multiwell plates. Cell viability was measured with CellTiter Glo assay in 96 multiwell plates for 10 days in a gRNA/Cas9 knockout experiments and for seven days for shRNA knockdown experiments. The readings were normalized to non-targeting controls. Viability was also quantified by crystal violet staining as previously described in *Section 3.2.5.*

3.3.10 Western Blotting

$5x10^6$ cells collected for western blot. Cell pellets were washed with PBS before freezing and stored in -80°C till lysis. 500 µL of ice-cold RIPA lysis buffer supplemented with 1X protease inhibitor cocktail added on cell pellets and mixed gently. The mixture was kept on ice for 30 mins, centrifuged at maximum speed for 30 mins at 4°C in benchtop centrifuge. The supernatant was transferred to new Eppendorf tube and kept at 4°C. The protein concentration was determined using BCA Protein Assay (Pierce, Cat.No. 23227). The samples were cooked with 6X loading dye at 95°C for 15mins, loaded on 8% SDS-PAGE gel and run until the dye reached to the edges. Proteins were transferred to PVDF membrane by Bio-Rad semi-dry transfer system in high molecular weight settings. The membrane was blocked with 5% milk diluted in 1X TBS-T for 1 hour. After washed with 1X TBS-T, membrane was incubated with primary antibodies diluted in 5% (w/v) BSA in 1X TBS-T overnight in cold room. Next day, primary antibodies were collected and the membrane was washed with 1X TBS-T twice. Secondary antibodies diluted in blocking solution was incubated for 1 hour in room temperature. Membrane was washed three times with 1X TBS-T in 5 mins intervals. For signal development, membrane is incubated with ECL Western Blotting substrate (Pierce, Cat.No.32109) for 1 min and imaged in LI-COR Odyssey imaging system. GAPDH (Santa Cruz, sc-25778), SMARCC2 (Cell Signaling, Cat.No.12760S) and AR (Santa Cruz, sc-7305) antibodies were used as primary antibodies. Goat anti-mouse IgG-HRP (Santa Cruz, sc-2055) and goat anti-rabbit IgG-HRP (Santa Cruz, sc-2054) were used as secondary antibodies.

3.3.11 RNA-sequencing

MR49F cells were transduced with sgRNAs in LentiCRISPRv2 plasmid and selected with puromycin for 3 days. Cells were harvested for RNA isolation at day 11 after transduction. Three biological replicates were prepared. Total RNA was extracted using NucleoSpin RNA kit (Macherey-Nagel, REF 740984) following manufacturer's instructions. Library preparation, quality check and sequencing were done in BGI facilities in Hong Kong. Samples were sequenced in DNBseq platform for transcriptomics analysis with 20M paired-end reads per sample. FASTQ files were checked for the quality by FastQC (v0.11.9). Paired-end reads were aligned to hg38 human RefSeq reference set of transcripts using STAR aligner (PMID: 23104886) with following options (--outSAMtype BAM SortedByCoordinate --outSAMunmapped Within --outSAMattributes Standard). Differentially expressed genes were called by DESeq2 [357] using a cut-off at +/-1 for log fold change (LFC) with false discovery rate (FDR) < 0.05. To find enriched pathways, Gene Set Enrichement Analysis (GSEA)[358] was performed by using publicly available hallmark and curated (c2) gene sets. The data was processed and plotted by Umut Berkay Altıntaş.

3.3.12 Chromatin immunoprecipitation and sequencing

BRG1 and SMARCC2 ChIP-seq was done using a double cross-linking strategy to stabilize the SWI/SNF complex. The cells were first fixed at room temperature with 2mM DSG (Thermo Scientific, Cat# 20593) for 45 min prior to 1% formaldehyde fixation for 10 min. The cells sequentially lysed with LB1 (50 mM HEPES-KOH (pH 7.6), 140 mM NaCl, 1 mM EDTA, 10% (vol/vol) glycerol, 0.5% (vol/vol) NP-40/Igepal CA-630 and 0.25% (vol/vol) Triton X-100), LB2 (10 mM Tris-HCl (pH 8.0), 200 mM NaCl, 1 mM EDTA and 0.5 mM EGTA) to enrich for nucleus. The nucleus was further lysed in LB3 and sonicated for 10 mins (30 sec 'On' and 30 sec 'Off' cycles) using Bioruptor (Diagenode). The IP was performed overnight at 4°C with 4 µg of BRG1 (Abcam, ab110641) or SMARCC2 (Bethyl Lab A301-039A) conjugated protein G magnetic beads (Thermo Scientific). The DNA was then purified using the Monarch DNA cleanup kit (NEB) after overnight de-crosslinking at 65°C. The library for high throughput sequencing was prepared using the Ultra II DNA library kit (NEB) according to the manufacturer's instructions. The ChIP library was further sequenced on a Illumina

NovoSeq platform with a minimum of 30M paired-end reads per sample. ChIP-seq was performed by Dr. Shreyas Lingadahalli.

FASTQ files were checked with FASTq (v0.11.9) for the quality. Paired-end reads were concatenated and aligned to hg38 human genome using BWA[359]. Unique paired-end reads with MAPQ > 30 are collected by samtools (-F3076 -f2). Peaks were called by MACS3[360] with default options (-g hs -q 0.01) and peaks with -logFDR > 5 are considered for further analysis. Bigwig signals over the genome were generated by genomecov function in BEDtools [361]. For GIGGLE analysis, Toolkit for Cistrome data browser (http://dbtoolkit.cistrome.org) was used [362,363]. Gene annotation analysis was performed using annotatePeaks.pl script of HOMER (v4.11) on hg38 [364]. Peaks were called from reference genome hg38 and scanned for known motifs using Hocomoco Human v11 with fimo utility of MEME suite [365]. The motif rank was calculated based on the differences of log10 transformed q-values for each transcription factor. These analyses were performed and plotted by Umut Berkay Altıntaş.

Chapter 4 Investigation of essential lysine demethylases in PCa

4.1 Aim of the study

Previous studies by our lab [257] and others [118,171,251,260,263,265,267,275,278] have demonstrated that lysine demethylases are involved in CRPC progression. This has been proposed to be due to either regulation of AR transcriptional activity and protein stability [118,171,254,265] or other oncogenic pathways that promote CRPC [260,263,366]. In particular, KDM1A (LSD1) is extremely well validated and has been shown to be critical to cell growth of both PCa and CRPC cells [367]. Given this promise, several clinical trials have started for the KDM1A inhibitors in late-stage PCa (ClinicalTrials.gov Identifier: NCT03895684, NCT04628988). Yet, while there has been considerable success developing KDM inhibitors it is unclear how reproducible much of this work is due to their pleotropic activity. Therefore, before initiating a small molecule development program, I wanted to validate the role of KDMs in late-stage prostate cancer.

4.2 Results

4.2.1 Initial optimizations

To conduct a focused KDM screen, I chose to use a shRNA library due to both the availability of many of these reagents in our lab and relatively rapid screening protocol. However, rather than using a pooled screen, this work was done in an arrayed format as it would eliminate the need for low MOI requirement which might reduce the knockdown efficiency. Our shRNA library (n= 64) contained either 2 shRNAs (n= 6 genes) or 3 shRNAs (n= 17 genes) that targeted 23 KDM family members with one positive control (AR-targeting shRNA, shAR) and one non-targeting control (Firefly Luciferase-targeting shRNA, shFF)(**Table 3.3)**. Of these, 37 shRNAs targeting 14 distinct KDMs were taken as a subset from a larger epigenetic shRNA library generously provided by Dr. Tamer Önder. Literature review identified 9 additional KDMs that were not present in our initial library. Therefore, to complete the KDM library, I ordered oligos for additional validated shRNA sequences (n=27 shRNAs) from the Genetic Perturbation Platform (https://portals.broadinstitute.org/gpp/public/) and cloned them into MSCV-pm backbone by restriction enzyme cloning. The sequence of cloned plasmids was validated by Sanger sequencing. The knockdown efficiency of each shRNA was then tested in LNCaP cells after antibiotic selection selection (**Figure 4.1a)**. shRNAs targeting KDM8 and KDM5D

induced >80% knockdown efficiency, whereas shRNAs targeting PHF8, PHF2, NO66, KDM1B, MINA53 (except sh3) and KDM3C showed 60-80% knockdown efficiency. UTY-targeting shRNAs yield only 40% decrease in mRNA level.

With the completed library, I then optimized the screening protocol to characterize how each KDM gene impacted proliferation. Unfortunately, my experiments using the colorimetric metabolic assay MTS (3-(4,5-dimethylthiazol-2-yl)-5-(3-carboxymethoxyphenyl)-2-(4-sulfophenyl)-2H-tetrazolium) as a proliferation readout gave inconsistent results especially in the growth curve of non-targeting and untreated control. Therefore, I compared different viability assays to find both a robust and practical method that would give consistent and reproducible results. Focusing on using only shRNA targeting either KDM1A, a well validated essential KDM, or AR, we transduced LNCaP cells with an optimized retroviral amount giving >80% knockdown (**Figure 4.1b,d**). After antibiotic selection, cells were seeded for different viability assays: colorimetric metabolic assay (MTS), electrical impedance assay (Xcelligence) or cell enumeration assays including crystal violet staining and trypan blue exclusion. Crystal violet, trypan blue exclusion and Xcelligence measurements gave similar results whereas inconsistencies were observed in MTS assay (**Figure 4.1e,f,g,h**). While trypan blue was reproducible, the low-throughput limited its utility for our focused screen. Considering its low cost, ease of use and reproducibility, I decided to use crystal violet staining to quantify cell proliferation in our KDM assay. With this protocol, I then determined both the optimal time point and cell density to make the proliferation measurements (**Figure 4.1h**). We were looking for a condition where the cells would not become overconfluent by the end of experiment in the non-targeting control group (shFF). During optimization, I also observed that the shRNA-target mRNA level increased towards the end of the growth curve (**Figure 4.1c**), potentially due to impartial antibiotic selection or overpopulation of the cells with less-robust knockdown. To maintain the selective pressure, the cells were therefore maintained in antibiotic containing media throughout the experiment.

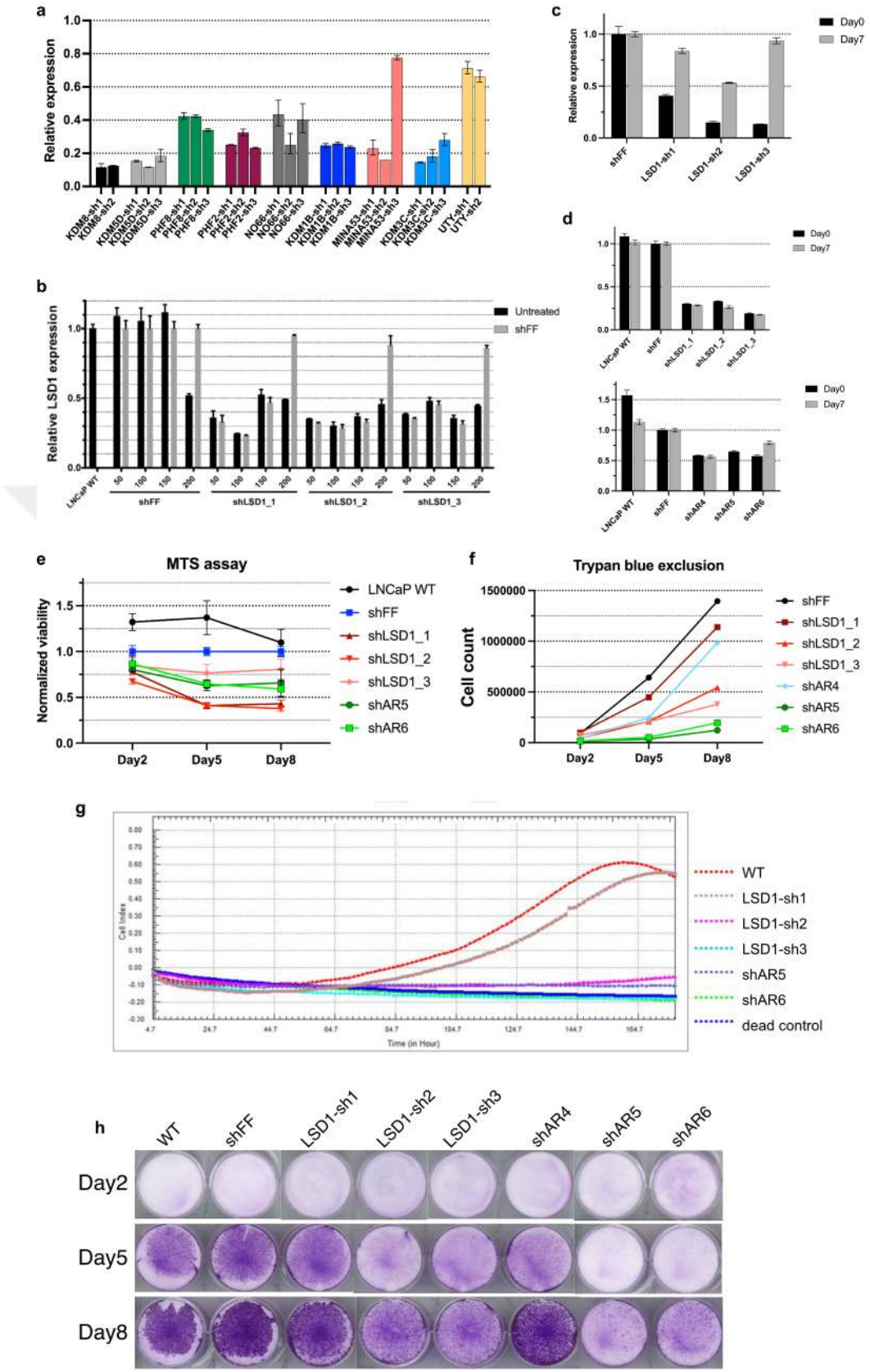

Figure 4.1 Condition optimizations for shRNA screen in LNCaP cells. (a) Knockdown efficiency of newly cloned KDMs. (b)Determining optimal viral volume by testing different volumes of viral suspension for non-toxic efficient knockdown (c) Comparison in knockdown efficiencies between day 0 and day 7 after puromycin selection. (d) Relative mRNA expression for optimization experiments. (e-f-g-h) Comparison of viability assays. (e) MTS assay (f) Trypan blue exclusion (g) Xcelligence (h) Crystal violet staining.

To generate viruses with relatively similar multiplicity of infection, all retrovirus expressing shRNAs were packaged at the same time. Importantly, the resulting retroviruses were precipitated with PEG and then resuspended in PBS to concentrate the viruses and avoid any non-specific activity caused by the different culture media. From this, the knockdown efficiency of several shRNAs were tested with different viral amounts to determine an optimal retroviral volume for each cell line (**Figure 4.2**).

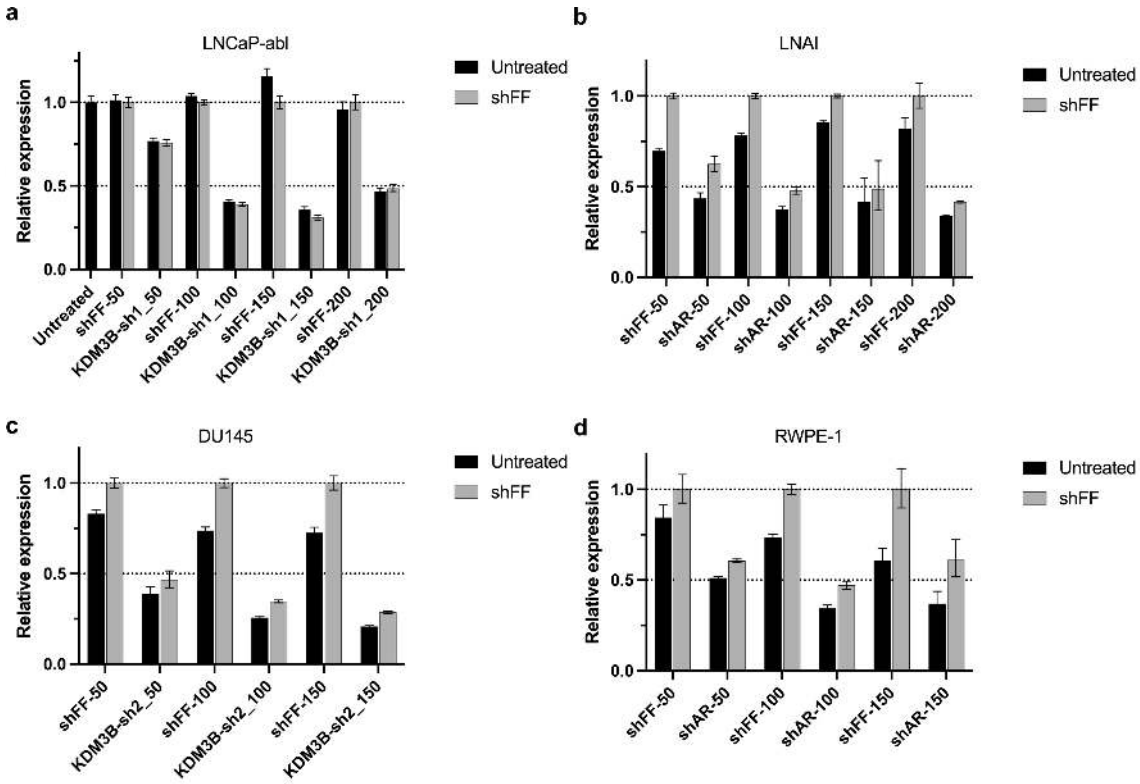

Figure 4.2 RT-qPCR results for viral volume optimization in each cell line.

4.2.2 Screen results

With the optimized screening conditions, I conducted the KDM-focused shRNA screen on five different cell lines that represent different stages of PCa progression: androgen-dependent LNCaP, androgen-independent LNCaP-abl and LNAI cells, AR-null DU145, and immortalized non-neoplastic prostate epithelial cell line RWPE-1 (**Table 4.1)**. In this experimental protocol, the cells were transduced in an arrayed format and selected by antibiotic selection for 72 hrs. Cells were then counted and seeded onto 6 multiwell plates in duplicates. After 8 days growth, cells were stained with crystal violet solution and proliferation was quantified with ImageJ. The entire screen was repeated with three

biological replicas for each cell line. The relative proliferation was calculated by normalizing to the negative control (shFF).

Table 4.1 Cell line used in shRNA screen and certain characteristics

Cell line	Origin	Androgen sensitivity	Initial cell density
LNCaP	Human PCa cells derived from lymph node metastasis [345]	Sensitive	$0.1x10^6$
LNCaP-abl	LNCaP cells propagated in androgen free media for 10 months in cell culture [346]	Insensitive	$0.1x10^6$
LNAI	LNCaP cells propagated in castrated mice for several months	Insensitive	$0.1x10^6$
DU145	Human PCa cells derived from brain metastatic site [349]	Insensitive	$0.05x10^6$
RWPE-1	Immortalized human prostate epithelial cells by human papilloma virus 18 (HPV-18) transfection [350]	Sensitive	$0.05x10^6$

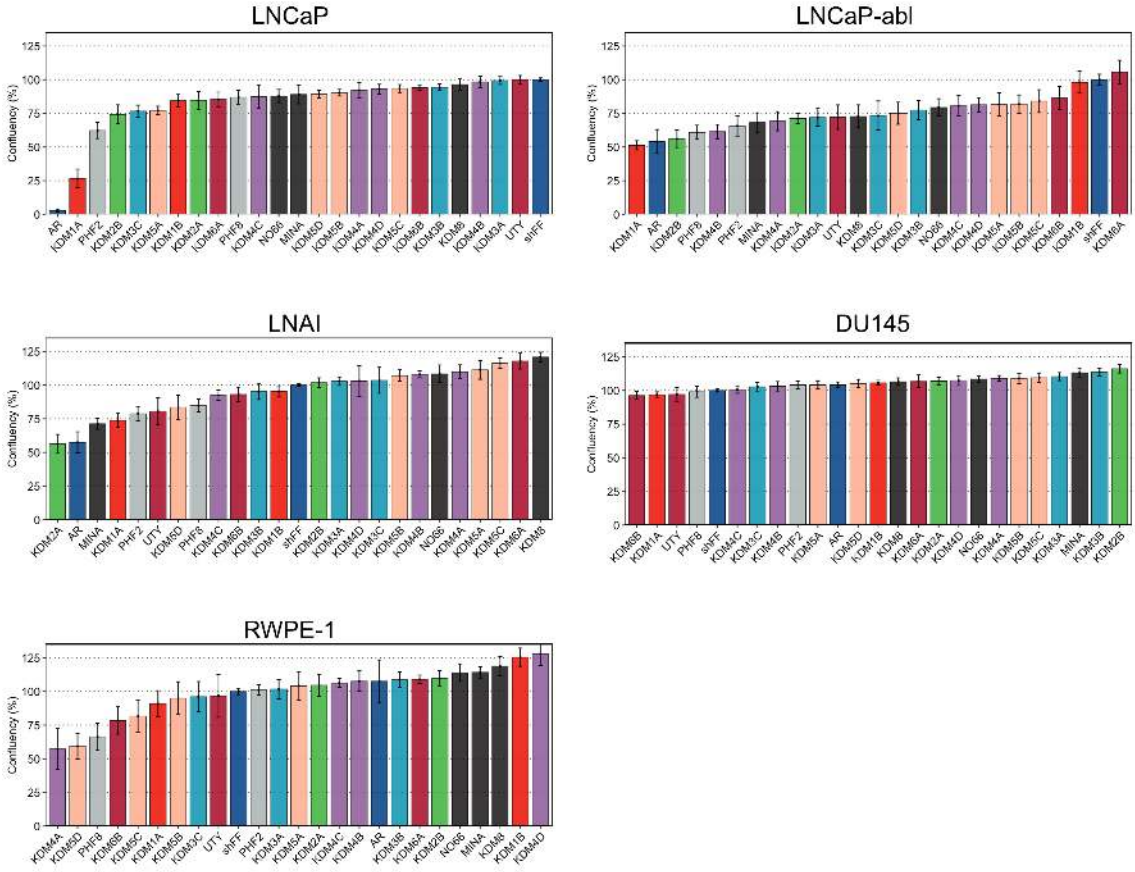

Figure 4.3 Gene based results of KDM-focused shRNA screen in multiple cell lines. The ImageJ-estimated confluency from crystal violet staining is normalized to their shFF control. The mean of normalized confluency is calculated for each sample and plotted with the standard error of the mean.

As expected, we observed marked decrease in proliferation following AR knockdown in AR-expressing cell lines LNCaP, LNCaP-abl and LNAI while there was no change in growth of the AR-null/low cells DU145 and RWPE1 (**Figure 4.3**). Similar to the published work [171,246,251], LSD1 knockdown severely reduced the cell proliferation of LNCaP and LNCaP-abl cells (**Figure 4.3**).

We observed marked differences in KDM sensitivity in each cell line. DU145 cells were largely insensitive to KDM knockdown, whereas LNCaP-abl cells were highly sensitive to loss of *KDM* expression (**Figure 4.3**). Yet broadly, knockdown of these KDM enzymes had a very moderate effect on PCa proliferation. Except for AR and KDM1A, knockdown of any KDM gene did not yield a proliferation decrease >50% in any cell lines (**Figure 4.3**). We observed a mild decrease (>25%) in confluency following the knockdown of PHF2 (LNCaP); MINA and KDM2A (LNAI); KDM4A, KDM5D and PHF8 (RWPE-1) (**Figure 4.4a**). LNCaP-abl were more broadly affected than other cells by shRNA treatment following the knockdown of KDM2A, KDM2B, KDM3A, KDM3C, KDM4A, KDM4B, KDM5D, UTY, PHF2, PHF8, MINA and KDM8. Next, we examined the

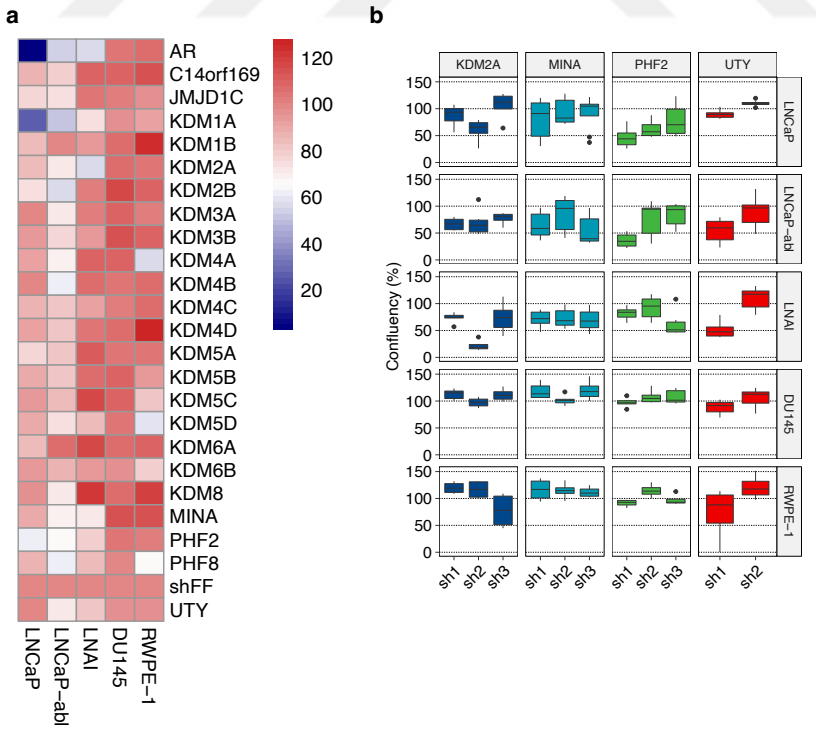

Figure 4.4 Confluency comparison across the cell lines. (a) Heatmap of gene-based confluency for all cell lines tested. (b) Boxplot of individual shRNA results for promising KDMs identified from the screen.

individual performance of shRNAs for promising KDM groups (**Figure 4.4b).** However, we observed high variability within each gene. Based on these findings we decided not to characterize any specific KDM gene.

4.3 Discussion

Lysine demethylases have been suggested to be important for PCa development and progression. Multiple studies have demonstrated that different KDMs interact with AR and are required for transcriptional activity [118,171,244,254,260,263,265,275,276]. Several of these have been shown to be crucial for cell viability [171,254,260] or highly overexpressed in prostate cancer patients [269,275,278]. To expand on this published work, we tested the effect of all known KDM on viability in different models of PCa progression. Before initiating this large study, we optimized viral amount, duration of the experiment, proliferation assay and seeding density. The cells were maintained in selective media supplemented with antibiotics to prevent any possible overpopulation of cells without shRNA expression. The screens were performed as three biological replicates across five distinct cell lines. We observed robust, consistent staining with marked decrease in positive control (shAR) and normal growth in non-targeting shFF samples. However, despite the good signal to noise with our controls and strong reproducibility, our screen did not provide strong evidence to pursue a KDM for further drug optimization. Excluding KDM1A, knockdown of any *KDM* gene had limited impact on PCa proliferation in any model. These results were markedly different than published work. One possibility could be due to the sensitivity of the proliferation assay. Crystal violet staining can capture a dramatic change in confluency and is very robust against false positives. However, assays based on metabolic activity may be more sensitive to smaller changes in proliferation. It is also possible that androgen treatment or hypoxic conditions may reveal proliferation differences when coupled with KDM targeting, a condition that we did not test. Yet, as we'll discuss in the following chapter, our CRISPR-Cas9 screen largely supported these shRNA results suggesting a broader biological phenotype rather than an experimental error. While speculative, there may be compensation mechanisms between different KDM proteins as they recognize and demethylate similar targets. As a consequence, eliminating one of the members may not be enough to observe a phenotype. We considered pooling shRNAs targeting a certain KDM family; however, the variability in knockdown levels for each shRNA complicated

the experimental design. Using a pool of sgRNAs targeting several genes in a KDM family could characterize this potential compensation mechanism however this would have limited utility in pharmacological development. Finally, we also need to consider that the expression level in clinical samples or being an AR-interactor may not necessarily be translated into an essential role for cell survival. When each gene was tested, there may be a positive selection bias that could encourage the authors to select for those RNAi with off-target effects on proliferation. Such reproducibility problems have been extensively demonstrated in oncology research [368–370].

Chapter 5 Epigenome-wide CRISPR-Cas9 screen in PCa

5.1 Aim of the study

ENZA improves progression-free and overall survival in both CRPC and hormone-sensitive PCa [54,70,74,344]. Yet while initially effective, resistance to ENZA eventually develops in almost all patients. This can occur through several different mechanisms (*Section 1.2.3*) including epigenetic modifications that support lineage plasticity and transdifferentiation during disease progression [235,284,371]. Understanding how ENZA-resistance occurs is essential to treating lethal late-stage PCa. While several epigenetic modifying enzymes have demonstrated an important role in ENZA-resistance, only a handful of these genes have been tested. Therefore, in this chapter we systematically screened all epigenetic modifiers in multiple ENZA-resistant models to identify potential therapeutic targets.

In this chapter Tunc Morova did the initial mapping and quantification of CRISPR NGS, Shreyas Lingadahalli performed ChIP-seq, Berkay Altintas analyzed ChIP-seq, clinical ATACseq and RNA-seq, and Betul Ersoy helped with RT-qPCR experiments.

5.2 Results

5.2.1 Epigenetic knockout library design

To test the essentiality of epigenetic modifiers in PCa we, in collaboration with the Önder and Bağcı-Önder laboratory, generated a custom Epigenetic Knock-Out Library (EPIKOL). The first version of the library (EPIKOL.v1) contained manually selected epigenetic modifiers (n=251) with each sgRNAs targeting the protein domains (n=1780 sgRNAs, 5 sgRNAs/domain). Targeting protein domains instead of 5' exons of genes was proposed to induce more loss-of-function mutations caused by indels, thereby increases the effectiveness of negative selection [372]. Individual gRNA were designed using CCTop online tool [353]. This library was tested on LNCaP cells in a time dependent experiment. Unexpectedly the preliminary analysis showed a bimodal distribution of gRNA read counts without a normal distribution in all time points. This distribution suggests that bias was introduced in the screening process, either during cell culture or PCR amplification step. Further, the library lacked many internal controls limiting our ability to speculate if the problem occurred in viral packaging, transduction, or cell

maintenance steps. Finally, since the initial publication, there have been conflicting evidence of the importance of targeting the functional domain of a protein [340]. To overcome these limitations, we redesigned our EPIKOL library (EPIKOL.v2) with an increasing number of epigenetic modifiers, more sgRNAs specific to each gene and a large number of positive controls to better interpret our screens. For the second version of the library (**Figure 5.1a**), a list of all chromatin-related proteins (n=719) was obtained from the EpiFactor database [351]. Positive controls were selected from core essential genes (n=35) identified from publicly available drop-out screen results from 62 different cell lines [352]. The majority of these essential genes were required for transcription and translation. We also included context-specific control genes (n=25) such as nuclear receptors, ABC transporters, apoptosis-related and metastasis-related genes. Each gene

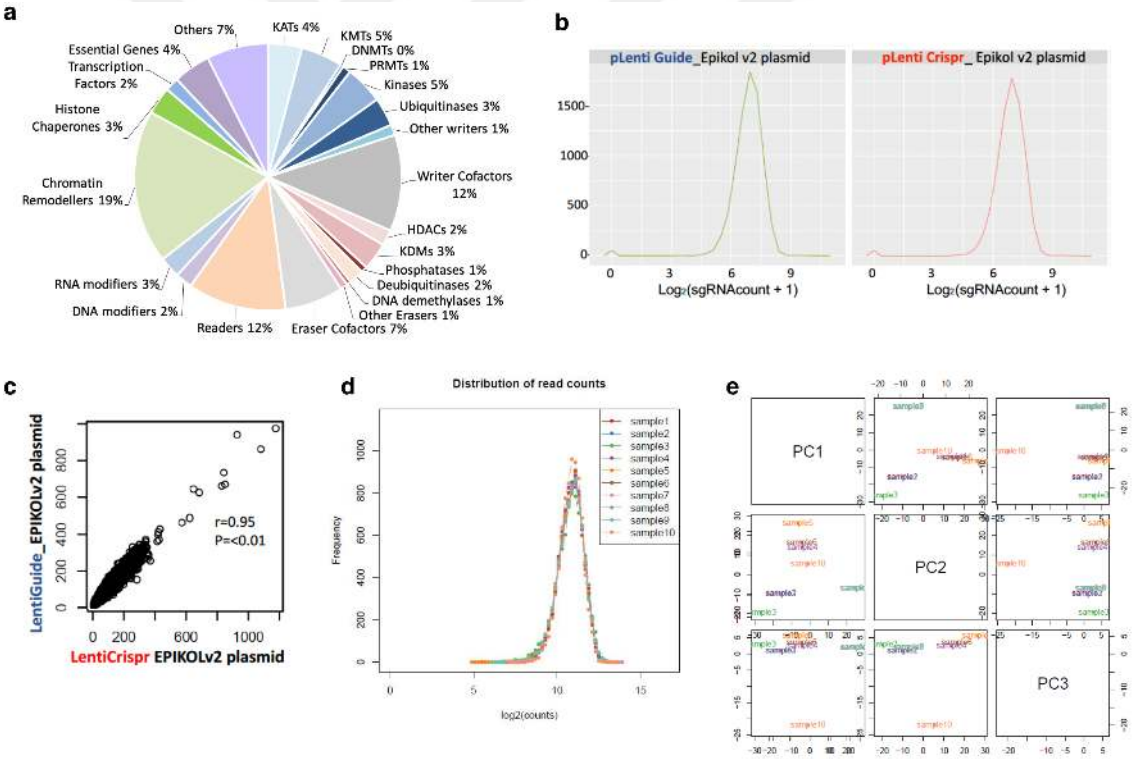

Figure 5.1 EPIKOL library and PCR optimizations. (a) The distribution of histone modifiers in the library. (b) The validation of library cloning by high-throughput sequencing and (c) its correlation in two different lentiviral backbones. (d-e) PCR cycle optimizations using EPIKOL in LentiGuide backbone. (d) Read count distribution of sgRNAs. (e) Principal component analysis of PCR samples. Sample 1-9 were isolated from transduced LNCaP cells without Cas9 expression. Sample 1-3: External PCR 20x cycles, internal PCR 10,15, 20x cycles respectively. Sample 4-6: External PCR 25x cycles, internal PCR 10,15, 20x cycles respectively. Sample 7-9: External PCR 30x cycles, internal PCR 10,15, 20x cycles respectively. Sample 10: plasmid control. Figure (a,b,c) taken from [341].

was targeted by 10 sgRNAs previously designed from validated genome-wide libraries [329,333]. For those sgRNAs that were either duplicated in these libraries or were missing, additional sgRNAs were designed using online CRISPR designing tools CCTop [353] and E-CRISP [354]. Nontargeting sgRNAs (n=80 sgRNAs) were included to act as negative controls. The final version of the EPIKOL v2 contained 7870 sgRNAs in total [343]. These sgRNAs were synthesized as a pooled oligonucleotides and cloned into lentiCRISPRv2 (Addgene #52961) and lentiGuide-Puro (Addgene #52963) lentiviral backbones by Dr. Alişan Kayabölen. The sgRNA coverage and the diversity of the library was confirmed by NGS (**Figure 5.1b, c**).

5.2.2 Optimization of PCR amplification from genomic DNA

Given our preliminary optimization, we next tested the efficiency and potential bias of PCR amplification from genomic DNA. For this, wild-type LNCaP cells were transduced at MOI= 0.3 with a 250x coverage of the EPIKOL v2 library in LentiGuide backbone. As these cells do not contain Cas9 protein, no genome editing will occur. As a result, all sgRNAs in the library should be fully represented in the transduced population. Cell pellets were collected after antibiotic selection and genomic DNA was isolated. To optimize the PCR conditions, we first performed quantitative PCR using varying amounts of genomic DNA. We observed that the signal intensified after 30 cycles and greater amplification is observed with 250 ng genomic DNA in 25 µL total reaction volume with 1 µM final primer concentration. In the internal PCR for adapter ligation, we PCR-amplified genomic DNAs and used it as the template for the second PCR step at a 1:100 dilution. The signal intensified after the 5th cycle, reaching a plateau after 25 cycles. To avoid under- or over- amplification, we therefore decided to test 20, 25, 30 cycles for external PCR; and 10, 15, 20 cycles for internal PCR using 250 ng genomic DNA per 25 µL reaction volume as the template. Untransduced library plasmid was used as our diversity control. The PCR products were run on 1.5% TBE agarose gel, gel-extracted and sent for sequencing with a minimum of $14x10^6$ reads per library. Our sequencing results showed a normal distribution for all conditions tested with the samples clustering based on their external PCR cycle number in a principal component analysis (PCA) (**Figure 5.1d, e**). Overall, we did not observe any bias introduced in the transduction, PCR amplification or high-throughput sequencing. From these results we chose to use 25x external and 15x internal PCR cycles.

5.2.3 Screen performance assessment

After PCR optimization, we performed an unbiased CRISPR-Cas9 proliferation screen in nine different PCa cell lines: androgen-sensitive LNCaP, androgen-insensitive LNCaP-abl, two ENZA-resistant cell lines MR49F and LNCaP-enzaR, AR-variant expressing 22Rv1, docetaxel-resistant 22Rv1-DoceR, cabazitaxel-resistant 22Rv1-CabaR, AR-null DU145, and immortalized non-neoplastic prostate epithelial cell line RWPE-1 (**Table 5.1**). The MR49F cell line was generated by serial propagation of LNCaP cells in castrated mice and isolated from a tumor grown in ENZA-treated mice. LNCaP-enzaR, 22Rv1-DoceR, 22Rv1-CabaR were generated and shared by Dr. Ceyda Açılan-Ayhan. LNCaP-enzaR cell line was generated by chronically treating LNCaP cells with increasing doses of ENZA. 22Rv1-DoceR and 22Rv1-CabaR cell lines were generated by chronically treating 22Rv1 cells with increasing doses of docetaxel and cabazitaxel.

Table 5.1 Cell lines tested in epigenome-wide CRISPR screen

Cell line	Origin	Characteristics	Doubling time
LNCaP	Human PCa cells derived from lymph node metastasis [345]	Advanced PCa model	34 hrs
LNCaP-abl	LNCaP cells propagated in androgen free media for 10 months in cell culture [346]	CRPC model, androgen insensitive	34 hrs
MR49F	LNCaP cells propagated in castrated mice and then reinjected into castrated and ENZA-treated mice [347]	ENZA-resistant	34 hrs
LNCaP-enzaR	LNCaP cells propagated in ENZA-containing media for several months in cell culture	ENZA-resistant	42 hrs
22Rv1	CWR22 xenograft propagated in castrated mice [348]	AR variant expression	40 hrs
22Rv1-DoceR	22Rv1 cells propagated in docetaxel-containing media for several months in cell culture	Docetaxel-resistant	47 hrs
22Rv1-CabaR	22Rv1 cells propagated in cabazitaxel-containing media for several months in cell culture	Cabazitaxel-resistant	46 hrs
DU145	Human PCa cells derived from brain metastatic site [349]	No AR expression	36 hrs
RWPE-1	Immortalized human prostate epithelial cells by human papilloma virus 18 (HPV-18) transfection [350]	Normal-like prostate epithelial cells, low AR expression	58 hrs

The EPIKOLv2 sgRNA library in the LentiGuide backbone was transduced into stable Cas9-expressing PCa cell lines at low multiplicity of infection (MOI=0.3) with a median coverage of 500x cells per sgRNA (**Figure 5.2a**). Following puromycin selection, cells were harvested at fixed doubling times (0, 5x, 10x and 15x for LNCaP, LNCaP-abl, 22Rv1, DU145 and RWPE-1; 0 and 15x for others) to minimize differences in growth rates between cell populations. Genomic DNA was isolated from these cells, and integrated sgRNA barcodes were then PCR-amplified from genomic DNA. All experiments were done in three biological replicas. Following deep sequencing of these samples, we conducted an initial quality check to understand the overall performance of the screen. First, we looked into the distribution of read counts. Except some samples in 22Rv1-CabaR and LNCaP-enzaR, we observed a normal distribution of sgRNA abundance at the initial time point with a slight shift in both arms at later time points as expected (**Figure 5.2b**). Principal component analysis revealed the initial collection samples from all cell lines clustered the with plasmid control and then separated in a time dependent manner (**Figure 5.2c**). Both sgRNA distribution and PCA analysis revealed a separation from other samples for the first biological replicate of LNCaP-enzaR, and the first and third biological replicates of 22Rv1-CabaR. Due to this variability these samples were excluded from further analysis. Next, we checked the performance of internal control groups at initial and latest collection points. Core-essential genes were depleted in all cell lines, whereas non-targeting controls remained unchanged compared to initial levels (**Figure 5.2d**). Further supporting these screening results, we observed that AR is selectively essential for the proliferation of AR-dependent cell lines (LNCaP, LNCaP-abl, MR49F, LNCaP-enzaR, 22Rv1, 22Rv1-DoceR, 22Rv1-CabaR) and does not affect AR-independent cell lines (RWPE-1 and DU145) (**Figure 5.2e**). These results suggest that our CRISPR dropout screens were successful.

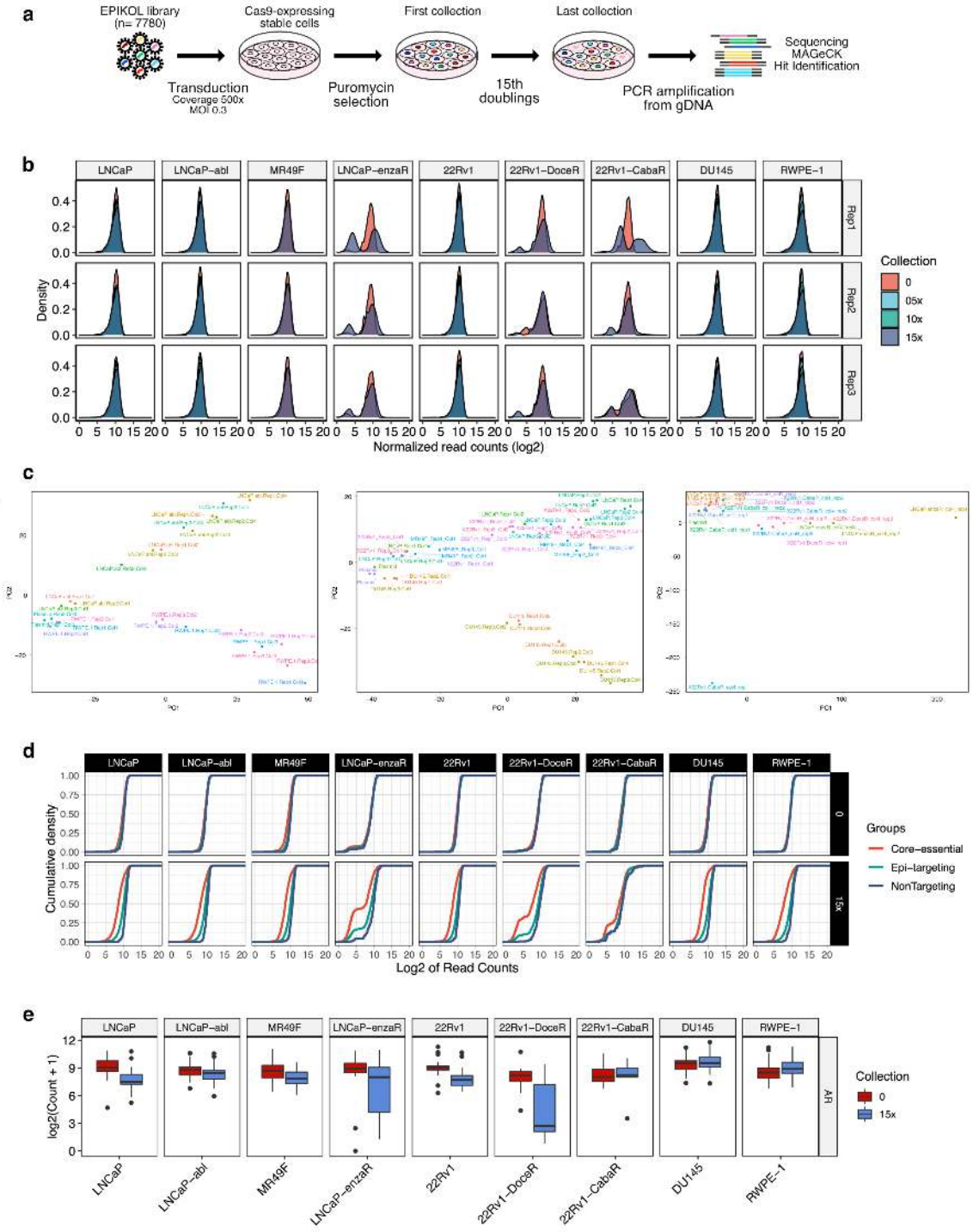

Figure 5.2 Screen design and performance assessment. (a) Schematic of screen design. Cells were transduced with low MOI (0.3) and 500x coverage. Selected cells were collected at 0 and 15x doubling time. Samples were PCR-amplified and sent to NGS (b) The distribution of normalized read counts of sgRNAs grouped by their collection time. NGS results were mapped to the sgRNA sequences and MAGeCK provided median-based normalized read counts per sgRNA. (c) PCA analysis of screen results based on read counts. Samples were clustered based on their cell identity and collection time. Initial collections were located closed to untransduced library control. (d) The cumulative distribution of read counts at initial and latest collection point for positive control, epi-targeting sgRNAs, and nontargeting controls. (e) The read counts of AR per cell line at initial and latest collections.

5.2.4 Screen Results

To understand the statistical deviation from the initial population, we performed MAGeCK [356] analysis which normalizes the count data and calculates log2 fold change for every sgRNA. The performance of each sgRNA is compared with the overall library population and each sgRNA performance is aggregated to a gene-based analysis which provides statistical power in the form of Robust-Rank aggregation (RRA) score. From this, we set two criteria to determine candidate "hit" genes from the screen: (1) the RRA score should be less than 0.05 (significantly decreased proliferation), (2) at least 5 independent sgRNAs should be depleted targeting a specific gene. Based on these criteria, we identified 403 genes significantly depleted in any screened cell line (**Figure 5.3a**). From this, 128 genes were depleted in all four wildtype cell lines (LNCaP, 22Rv1, DU145, RWPE-1) suggesting a lineage-specific role. 149 epigenetic modifiers were found to be essential in at least one of CRPC cell line screened. AR and FOXA1 were significantly depleted only in AR-expressing cell lines supporting its critical role in AR-dependent PCa, whereas BRD4 was depleted in all cancer cell lines including AR-null DU145. The comparison between LNCaP (AR-expressing) and DU145 (AR-null) revealed LNCaP-specific dependencies in 29 genes which include known AR-interactors such as NCOA1, EP300, LSD1 and FOXA1 (**Figure 5.3b**). Further, 30 epigenetic modifiers selectively depleted in 22Rv1 cells (ARv7 expressing) compared to LNCaP (no ARv7 expression) including ARID1B, BRD9 and CDK7 (**Figure 5.3b**). We identified 32 genes depleted in either 22Rv1 derivatives (22Rv1, 22Rv1-DoceR and 22Rv1-CabaR) including FOXA1, AR and BRCA2, and 12 taxane-resistance specific depletions such as ABCB1 and SMARCD1 (**Figure 5.3b**). The comparison between LNCaP and its derivatives will be discussed in the next section.

For initial validation of the CRISPR screen, we chose NIPBL, MRGBP, BAP1, SIRT6, PAXIP1, SETDB1 and CSNK2A1 and FOXA1 as they significantly decreased proliferation in multiple PCa cell lines. We transduced LNCaP-abl cells with sgRNAs co-expressed with GFP at low MOI and characterized the change in GFP-positive population by flow cytometry for 20 days. RPS11 was used as positive control due to its role in protein coding. Cell proliferation decreased in knockout cells compared to wildtype cells for common PCa-essential MRGBP, NIPBL, BAP1 and FOXA1, and also for LNCaP-

derived CRPC-essential SIRT6, PAXIP1, SETDB1 and CSNK2A1 (**Figure 5.3c**), emphasizing the credibility of our screen results.

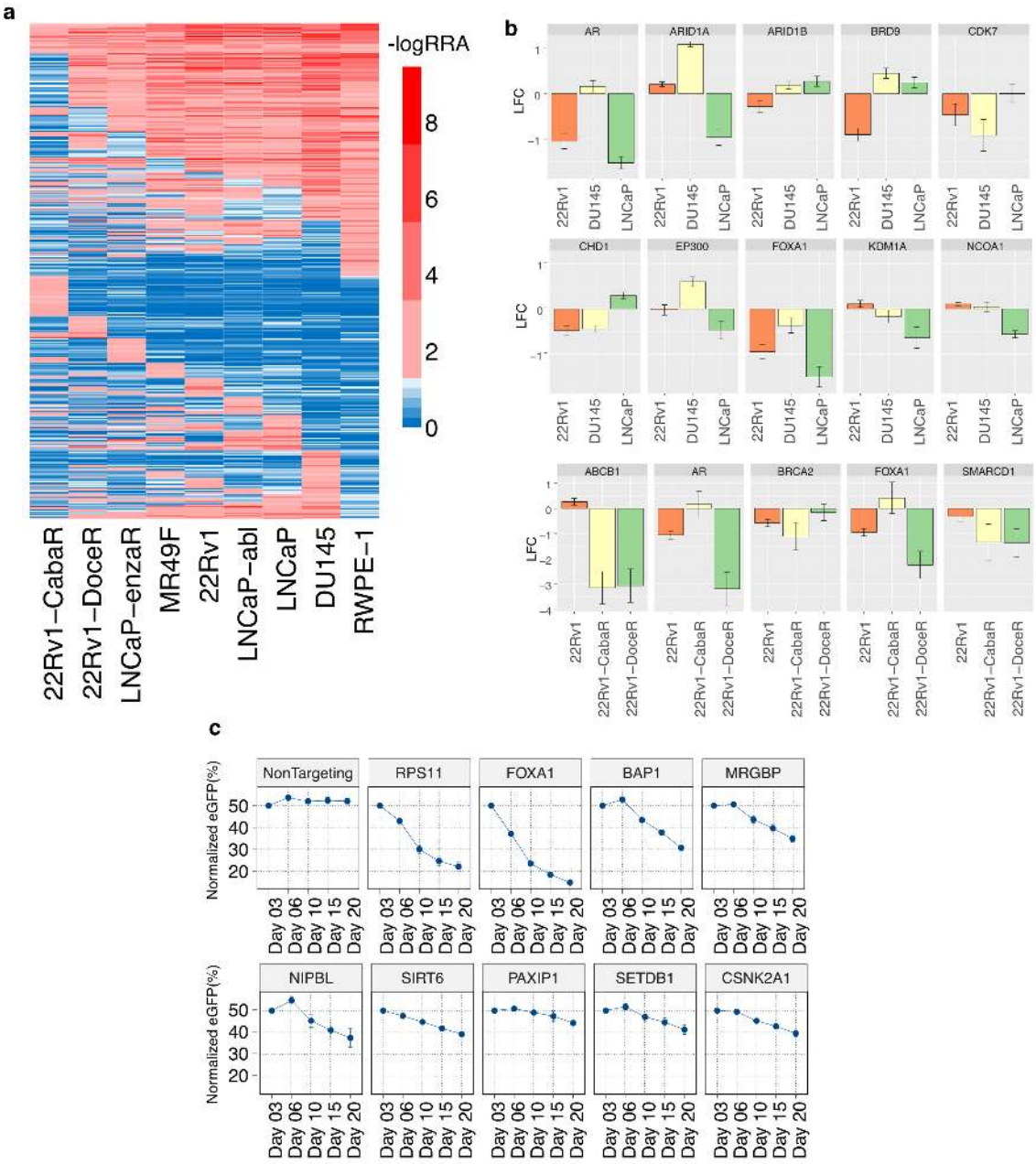

Figure 5.3 CRISPR screen results and validation of few genes. (a) Heatmap of screen results in nine cell lines. 'Hit' genes were identified for each cell line with RRA< 0.05 and efficient sgRNA>4, and the pool of these genes was plotted by their -logRRA scores. For further comparisons, any gene affecting normal like control (RWPE-1) is removed from the analysis. (b) Log2 Fold Change of individual genes in CRISPR screen identified by pairwise comparison between LNCaP (AR+/ARv7-) and either DU145 (AR-) or 22Rv1 (AR+/ARv7+), and between 22Rv1 and its taxane-resistant derivatives. The mean of log2FoldChange is plotted with standard error of the mean. (c) Validation by eGFP competition assay in LNCaP-abl cells for 20 days. eGFP signal is traced by flow cytometry in every 4-5days. The mean of normalized eGFP percentage is plotted with standard error of the mean. Non-targeting control and RPS11-targeting sgRNAs serve as negative control and positive control.

Given our previous study with KDM genes, we investigated the role of these genes in PCa proliferation. CRISPR screen identified KDM1A, KDM2A, KDM4B and KDM8 in LNCaP and KDM1A, KDM2A and KDM8 in RWPE-1 as essential (**Figure 5.4**). KDM8 was essential in almost all cell lines except LNCaP-abl, LNCaP-enzaR and 22Rv1-CabaR. Except KDM1A, shRNA screen failed to capture other KDMs identified as essential by CRISPR-Cas9 screen. Although CRISPR screen identified more essential KDMs than shRNA screen, the identified ones such as KDM2A and KDM8 also affected normal-like prostate epithelial cells, suggesting a lineage-dependent role. Eliminating the ones affecting normal-like control (RWPE-1), CRISPR screen identifies KDM4B in LNCaP, and KDM3B in LNCaP-abl. In addition, similar to our shRNA screen results, KDM1A (also known as LSD1) knockouts significantly depleted from the population in LNCaP and LNCaP-abl. KDM1A inhibitors have been already tested in clinical trials, and KDM3B was previously identified as essential in LNCaP-abl [257]. No KDM-dependency was found in DU145 consistent with shRNA screen results. The results from the CRISPR screen supported our observations in the shRNA screen.

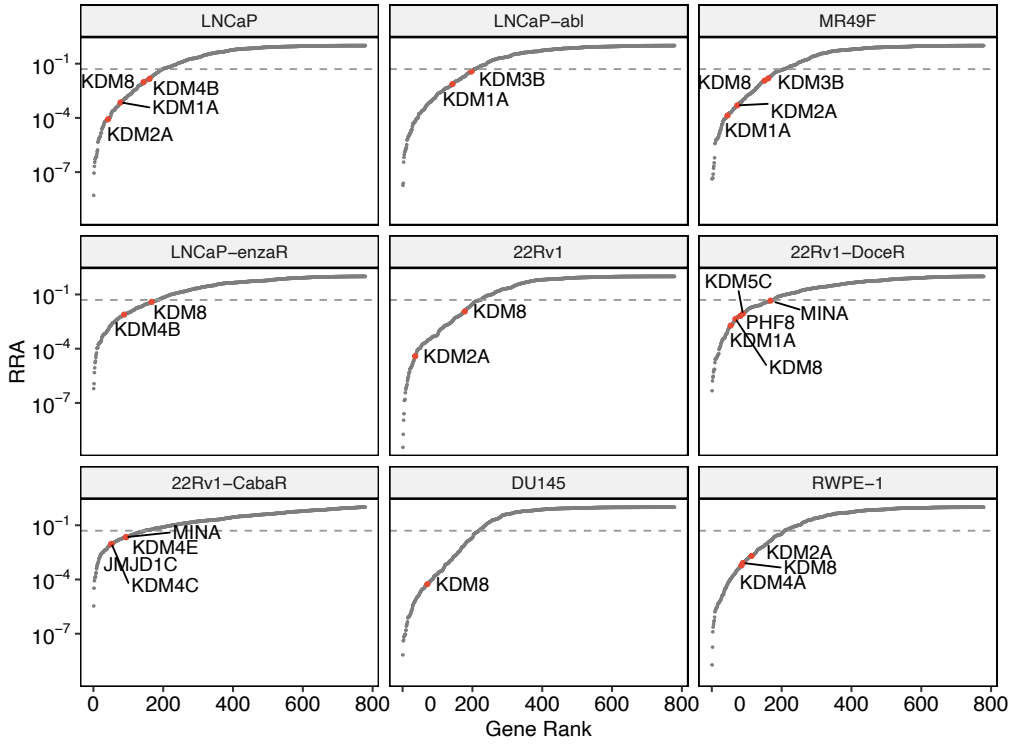

Figure 5.4 Lysine demethylase scores in CRISPR screen in multiple cell lines. KDMs with RRA<0.05 and with at least 5 effective sgRNA were plotted in red color and labeled. The dashed line shows RRA = 0.05 threshold.

5.3 Investigation of epigenetic modifiers involved in ENZA resistance

To identify epigenetic drivers of ENZA resistance in CRPC, we compared the MAGeCK results of LNCaP-abl, MR49F, LNCaP-enzaR, the parental cell line LNCaP and the normal-like control cell line RWPE-1 cells. We chose to study PCa cell lines derived from the same parental LNCaP model to provide a relatively homogenous genetic background that would allow us to focus on those epigenetic dependencies in different stages of PCa. With this scoring threshold, we identified numerous AR co-regulators including LSD1, EZH2, BRD4, and MLL that have been shown to impair the proliferation of LNCaP derivatives (**Figure 5.5a-c**) [120,171,236,373]. As previously demonstrated [76,77], AR was required for LNCaP, LNCaP-abl, LNCaP-enzaR, and MR49F but not for RWPE-1 (AR-low/null cell line) (**Figure 5.2e**). To focus on PCa-associated epigenetic dependencies, we excluded those genes that were essential to either the non-neoplastic prostate epithelial cell line RWPE-1 or those that broadly affect cell growth and are defined as "common essential" in DepMap (https://depmap.org/portal/). From this, we found 76 epigenetic modifiers that were essential in at least one cell line (**Figure 5.5c**). Given the common genetic background we observed a marked overlap in epigenetic dependencies, with many of these genes being essential in both LNCaP and at least one of the CRPC cell lines (29/76) (**Figure 5.5c**).

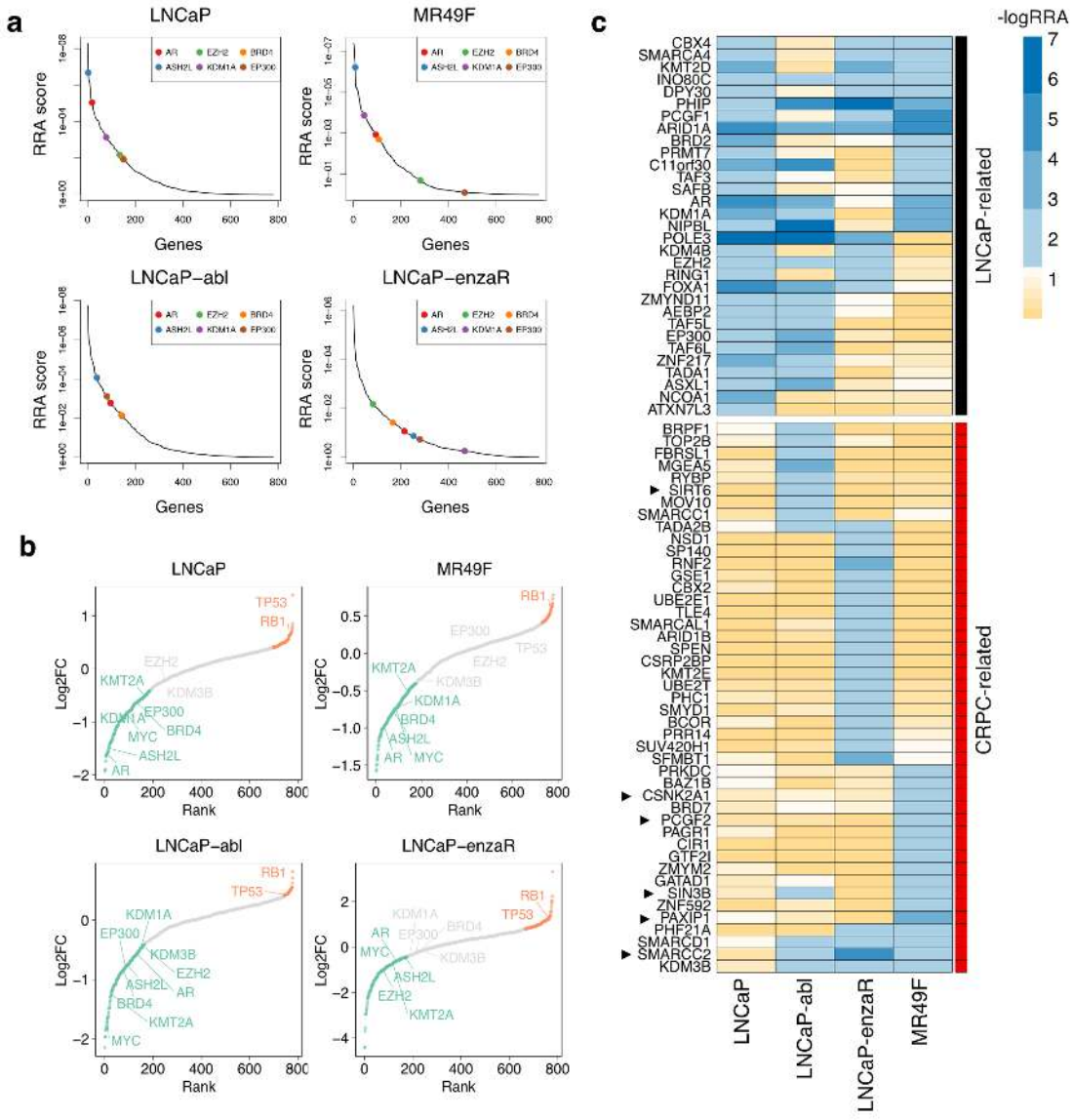

Figure 5.5 Identification of epigenetic dependencies in ENZA resistance. (a) MAGeCK analysis of read counts plotted as RRA score vs Gene rank for dropout screen. Genes known to be important for PCa are labeled. (b) Log2 Fold chance and gene ranking of PCa-associated genes based on MAGeCK results. Dropped out genes are in green color and positively selected genes are in orange color. (c) Heatmap of -logRRA scores of the candidate genes in negative selection. Genes having a broad effect on other cell lines in DepMap and RWPE-1 are removed from the list. Top panel shows LNCaP-related epigenetic dependencies, bottom panel shows CRPC-related epigenetic dependencies. Arrowheads indicate the candidates for validation. Color scale represents -logRRA score, white color shows RRA= 0.05 threshold.

5.3.1 Identified candidates are validated as essential only for ENZA-resistant cells

To better understand the role of epigenetic modifying enzymes in ENZA-resistance, we focused on those genes that were specifically essential in CRPC cell lines. From this, we identified several epigenetic modifying enzymes (SMARCC2, PAXIP1, SIN3B, CSNK2A1, SETDB1, and SIRT6) that showed a greater impact on the proliferation of either LNCaP-abl, MR49F, or LNCaP-enzaR cells than the parental LNCaP cells (**Figure 5.5c**). To validate the results from our CRISPR screen, we tested the effect of each gene on cell proliferation using an eGFP competition assay (**Figure 5.6a**). In this, we transduced both Cas9-expressing LNCaP and MR49F cells with sgRNA-eGFP constructs targeting the hit genes at a MOI=0.5. We then quantified the relative proliferation rate of wildtype (non-fluorescent) and knockout cells (eGFP+) by flow cytometry. Consistent with our pooled CRISPR screen, MR49F cells treated with sgRNAs showed a significant

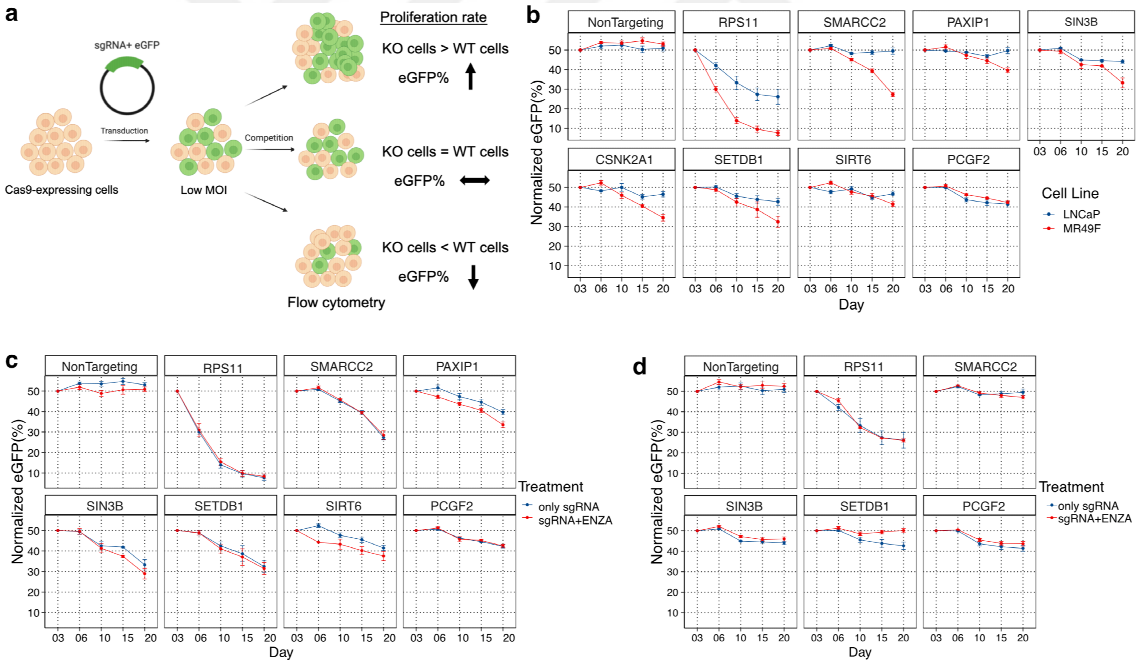

Figure 5.6 eGFP competition assay for "hit" validation in LNCaP and MR49F cells. (a)Schematic of eGFP competition assay. Cas9 expressing cells were transduced with MOI 0.5 and eGFP signal is monitored by flow cytometry for 20 days. The expected outcomes and their indications are listed in the figure. (b,c,d) eGFP competition assays in (b) LNCaP and MR49F cells in regular growth media, and in (c) MR49F cells and (d) LNCaP cells treated with either only sgRNA or sgRNA and ENZA. The eGFP percentage is normalized to non-targeting control for each day, and to the initial reading of each sgRNA. The experiments were performed in three biological replicates and the mean of normalized eGFP percentage is plotted with the standard error of the mean.

decrease in proliferation while LNCaP cells showed no significant change upon gene knockout (**Figure 5.6b**). Next, we asked whether gene knockouts could drive epigenetic-mediated resensitization. To test this, we repeated the eGFP competition assay for all genes both with and without ENZA in MR49F cells. For all genes, ENZA treatment did not impact the proliferation of resistant cells (**Figure 5.6c**) suggesting that these epigenetic modifying enzymes do not re-sensitize cells to ENZA but instead provide a gained indispensable function during the development of resistance. We also tested LNCaP cells for a possible synergistic effect of ENZA when combined with any gene knockouts. However, ENZA growth inhibitory effect remained the same regardless of gene knockouts in LNCaP cells (**Figure 5.6d**), further supporting that the epigenetic dependency in ENZA resistance is acquired during the disease progression.

5.3.2 The loss of cBAF components SMARCC2 and DPF2 decreases proliferation in ENZA-resistant cells.

From the validated genes, we observed the greatest difference in proliferation following the knockout of SMARCC2 which reduced eGFP population by 40% in MR49F cells and had no significant effect on LNCaP cell proliferation. To confirm these results, we performed additional validation with orthogonal assays. First, we knocked out SMARCC2 in both ENZA-sensitive and -resistant cell lines with multiple sgRNAs in different backbone than that of eGFP competition assay and performed crystal violet staining (**Figure 5.7a**). Similar to our initial validation, we observed a significant decrease in MR49F and LNCaP-enzaR growth while ENZA-sensitive LNCaP cells remained unaffected (**Figure 5.7b**). These results were supported with an orthogonal proliferation measurement using CellTiter-Glo assays (**Figure 5.7c**). In addition, we demonstrated that SMARCC2 knockdown by two independent shRNA confirmed the decreased proliferation in MR49F cells while having a minimal effect on LNCaP cell growth (**Figure 5.7d**). SMARCC2 is a core component of the ATP-dependent SWI/SNF chromatin remodeling complex. This multiprotein chromatin remodeling complex regulates chromatin accessibility has been found to have an increasingly important role in PCa (***Section 1.3.5)***. Depending on the subunit composition, the SWI/SNF complex can form canonical (cBAF), polybromo-associated (PBAF), or non-canonical (ncBAF) complexes with distinct functional activities. To determine if there were distinct BAF dependencies, we re-examined our CRISPR screen data (**Figure 5.7e**). While many

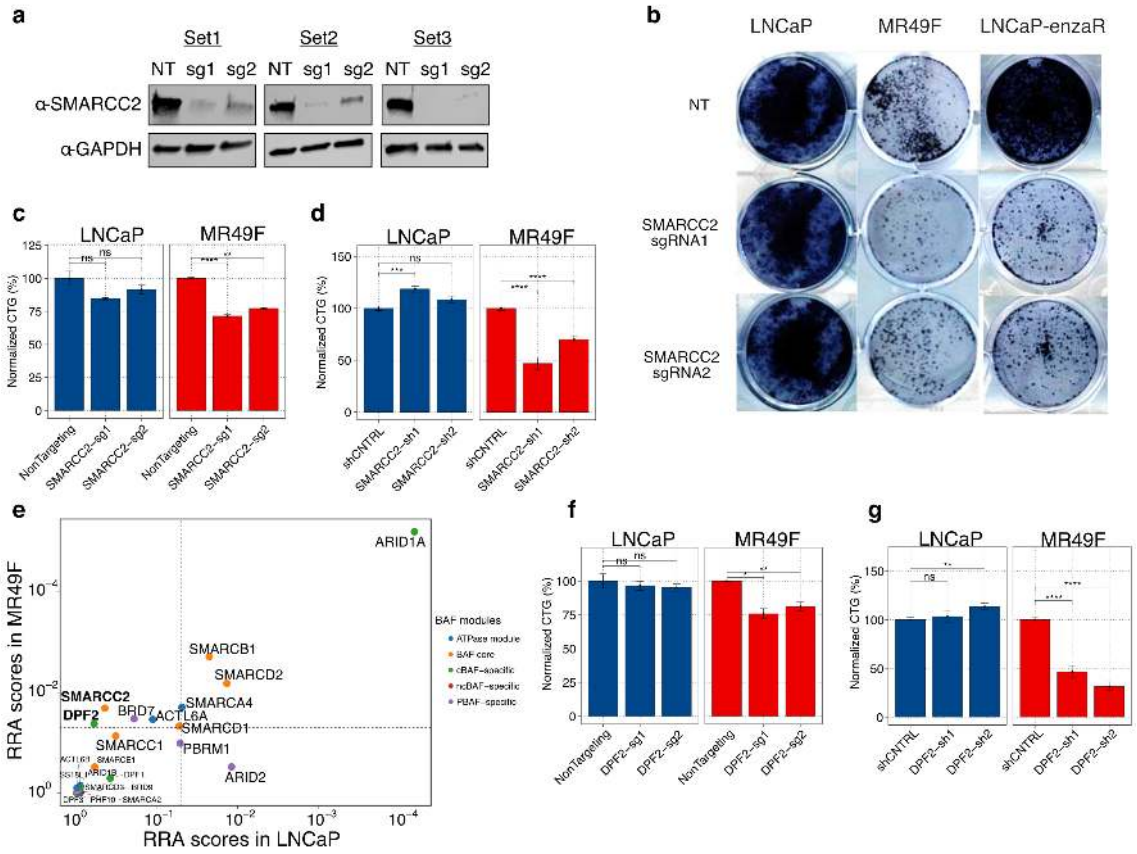

Figure 5.7 SMARCC2 and cBAF-specific DPF2 validations. (a) Western blot showing SMARCC2 depletion in protein level. (b-c) SMARCC2 validation by (b) Crytal violet staining and (c) CellTiter Glo in knockout cells. (d) SMARCC2 validation using shRNA. (e) CRISPR screen performance of other SWI/SNF components in LNCaP vs MR49F. (f-g) DPF2 validation using CellTiter Glo upon (f) sgRNA and (g) shRNA treatments. Data in (c-d-f-g) is the mean of three biological replicates plotted with standard error of the mean. Student's t-test, p-value < 0.05 *, <0.01 **, <0.001 ***, <0.0001 ****.

common subunits were essential in both LNCaP and MR49F cells, we observed that DPF2 was depleted exclusively in MR49F cells. Although SMARCC2 is shared in both cBAF and PBAF complexes, DPF2 is only found in cBAF complex [196]. When we tested the essentiality in both MR49F and LNCaP cells, we observed that DPF2 loss selectively reduced the viability of only MR49F cells following either shRNA knockdown or CRISPR knockout (**Figure 5.7f-g**). Overall, these results suggest that the ENZA-resistant PCa have cBAF-specific dependencies.

5.3.3 SMARCC2 and BRG1 expand their binding sites in enzalutamide resistance.

As loss of SMARCC2 did not cause re-sensitization to ENZA, we proposed that the cBAF complex promoted significant remodeling of chromatin accessibility during progression

to ENZA resistance. To explore this, we conducted chromatin immunoprecipitation sequencing (ChIP-seq) of both SMARCC2 and the ATPase subunit BRG1 (also known as SMARCA4) in MR49F and LNCaP cells. Strikingly, we noted a marked expansion of SMARCC2 binding sites in MR49F (n=40191) as compared to LNCaP (n=18557) (**Figure 5.8a**). While the majority of LNCaP-binding sites were also found in MR49F cells, over 25,000 SMARCC2 binding sites were unique to only ENZA-resistant MR49F cells (**Figure 5.8a**). A similar trend was observed for BRG1 binding sites (**Figure 5.8a**). SMARCC2 cistrome showed approximately 75% overlap with BRG1 cistrome in both cell lines (**Figure 5.8a**) suggesting the recruitment of the whole SWI/SNF complex (BAF sites).

To better understand the role of SMARCC2, we categorized SMARCC2 binding regions in MR49F as retained BAF sites (n=10757), gained BAF sites (n=19028) and gained SMARCC2 sites (n=8682) (**Figure 5.8b, c**). Retained BAF (rBAF) sites refers to the binding regions that are co-occupied by SMARCC2 and BRG1 in both LNCaP and MR49F, whereas gained BAF (gBAF) sites are only found in MR49F, ENZA-specific. Gained SMARCC2 (gSMA) sites refers to the sites lacking BRG1 binding and only captured in MR49F cells. Overall, SMARCC2 binding sites are mostly located in intronic and intergenic regions, especially gSMA sites (**Figure 5.8d**). There are only slight differences in genomic annotations between rBAF and gBAF; intronic regions are slightly more occupied by rBAF while intergenic regions are slightly more occupied by gBAF. We noticed a difference for the promoter binding in gSMA versus rBAF and gBAF sites; promoter regions consist of only 4.8% of gSMA sites while it is about 10% of both gBAF and rBAF sites (**Figure 5.8d**).

Using GIGGLE [374], we identified different set of transcription factors binding sites sharing similarities with rBAF, gBAF and gSMA sites **(Figure 5.8e**). We observed low GIGGLE scores in gSMA binding sites, implying that those regions are less likely to be occupied by transcription factors with available ChIP-seq data. In contrast, rBAF sites tend to be bound by AR and its cofactors FOXA1, PIAS1, GATA2, GRLH2 and HOXB13. Additionally, SWI/SNF components BRG1 and ARID1A, and nuclear receptors GR and ESR1 frequently overlap with these rBAF sites. gBAF sites tend to be occupied by transcription regulatory proteins including NELFA and NELFE, PAF1, TBP,

SRSF3, CDK7, CDK9, TTTF2 and XRN2. Interestingly, we observed three ETS transcription factors FLI1, ERG and SPI1 preferably enriched in gBAF regions which is also supported by motif analysis, in addition to growth-promoting transcription factors MYC and MAPK1 (**Figure 5.8e,f**).

Next, we compared the accessibility of these rBAF, gBAF and gSMA regions in clinical primary PCa samples (n=23) [375] and patient-derived CRPC xenograft models (n=6)[376]. We observed that gSMA sites has low accessibility (**Figure 5.8g**) implying transcriptionally silenced regions. Both rBAF and gBAF sites are accessible in primary PCa cases and remain accessible in CRPC samples (**Figure 5.8g**), which might be functionally necessary in both stages of PCa.

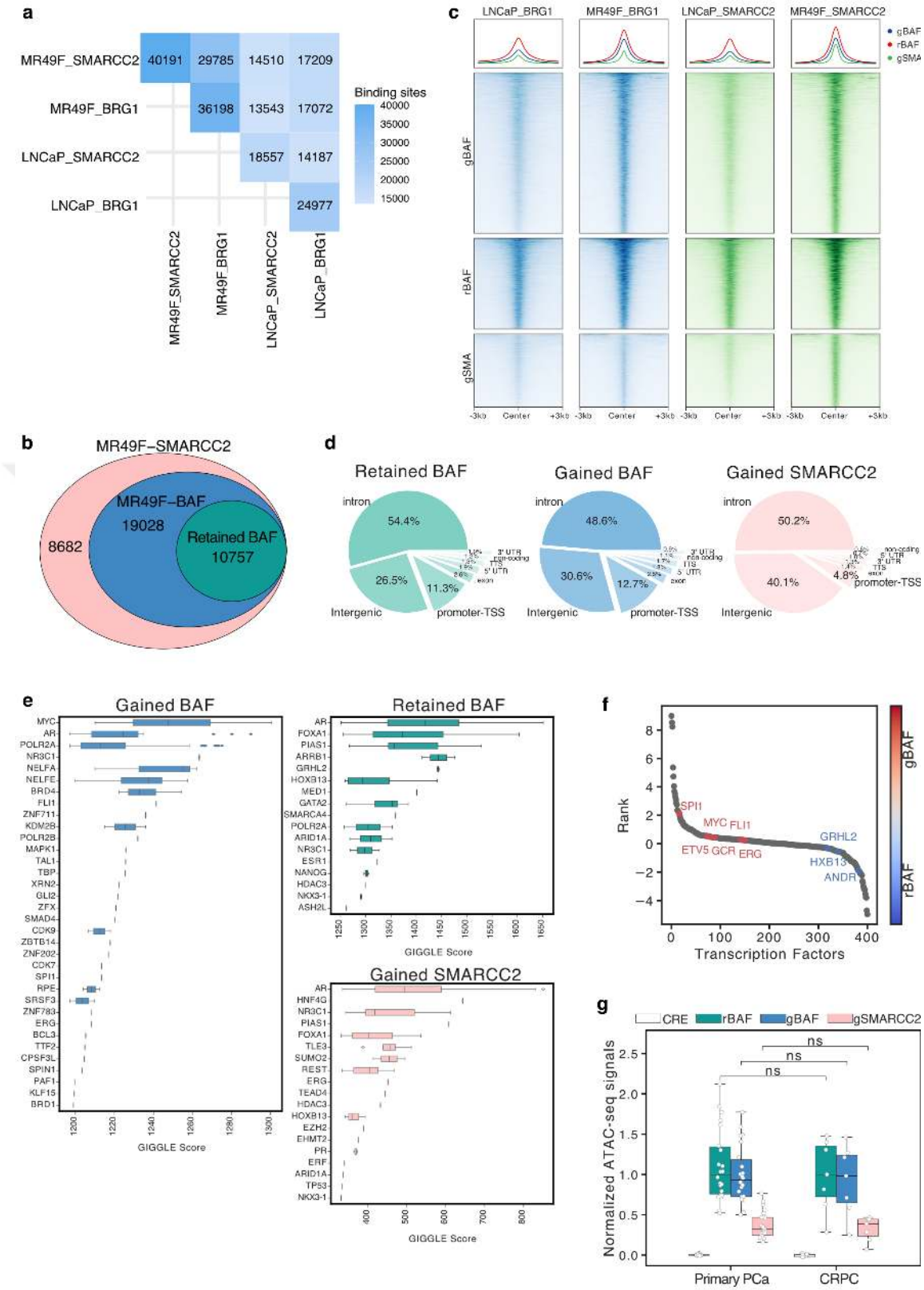

Figure 5.8 SMARCC2 and BRG1 chromatin binding in ENZA resistance. (a) Correlation matrix showing SMARCC2 and BRG1 binding in LNCaP and MR49F. (b) Categories of SMARCC2 binding in MR49F cells. BAF regions refers to the regions co-occupied by SMARCC2 and BRG1. Retained BAF (rBAF) represents BAF regions captured both in LNCaP and MR49F cells. MR49F BAF sites contain rBAF and gained BAF (gBAF). gBAF are only found in MR49F cells (ENZA-specific).

Figure 5.8 Figure caption continued. MR49F SMARCC2 binding sites consist of rBAF, gBAF and gained SMARCC2 (gSMA). gSMA represents the regions with no BRG1 binding and only found in MR49F cells. (c) Heatmap of SMARCC2 binding categories in LNCaP and MR49F for SMARCC2 and BRG1 binding. (d) Genomic annotations of rBAF, gBAF, gSMA regions. (e) GIGGLE analysis in rBAF, gBAF and gSMA. (f) Transcription factor motif analysis comparison in rBAF vs gBAF. (g) Chromatin accessibility for rBAF, gBAF and gSMA in clinical primary PCa samples and patient-derived CRPC xenograft models.

5.3.4 SMARCC2 differentially regulates gene expression in ENZA-resistant cells

We next explored the role of SMARCC2 on transcriptional regulation in ENZA resistance. We performed RNA-seq of MR49F cells that were treated with two different SMARCC2-targeting sgRNAs (**Figure 5.7a**). We observed strong correlation across both biological replicas (n=3) and individual sgRNAs (**Figure 5.9c**). However, given the impact on proliferation the changes to the transcriptome were very subtle. SMARCC2 loss downregulated only 49 genes and upregulated 91 genes in both sgRNAs (LFC +/- 1, p-adj<0.01) (**Figure 5.9b,c**). Gene set enrichment analysis (GSEA)[52] on hallmark pathways revealed differential expression in major pathways including E2F targets, G2/M checkpoint, IL6-JAK-STAT3 pathway and glycolysis (**Figure 5.9f**). Gene based analysis showed that multiple proteins in transmembrane transport of anions and small molecules were downregulated. We also noted downregulation of certain pro-survival genes including EGF and CAMK1D. Interestingly, several canonical androgen response genes KLK2, KLK3, TMPRSS2 and NKX3.1 were found to be upregulated upon SMARCC2 loss (**Figure 5.9f**). Next, we compared the transcriptional profile of ENZA resistant cell in AR knockout condition (LFC +/- 1, p-adj<0.01) (**Figure 5.9b**). Most of SMARCC2 signature genes (66/130) are also differentially expressed by AR (**Figure 5.9d, e**). SMARCC2 loss mildly affects AR and AR-targeted gene expression suggesting that it might positively regulate AR-dependent transcription but not essential for it (**Figure 5.9e**). The expression levels of other SWI/SNF components were not affected by SMARCC2 loss except BCL11B which is downregulated (**Figure 5.9g**). Upon AR depletion, specifying units SMARCD3 and DPF3 are upregulated (**Figure 5.9g**).

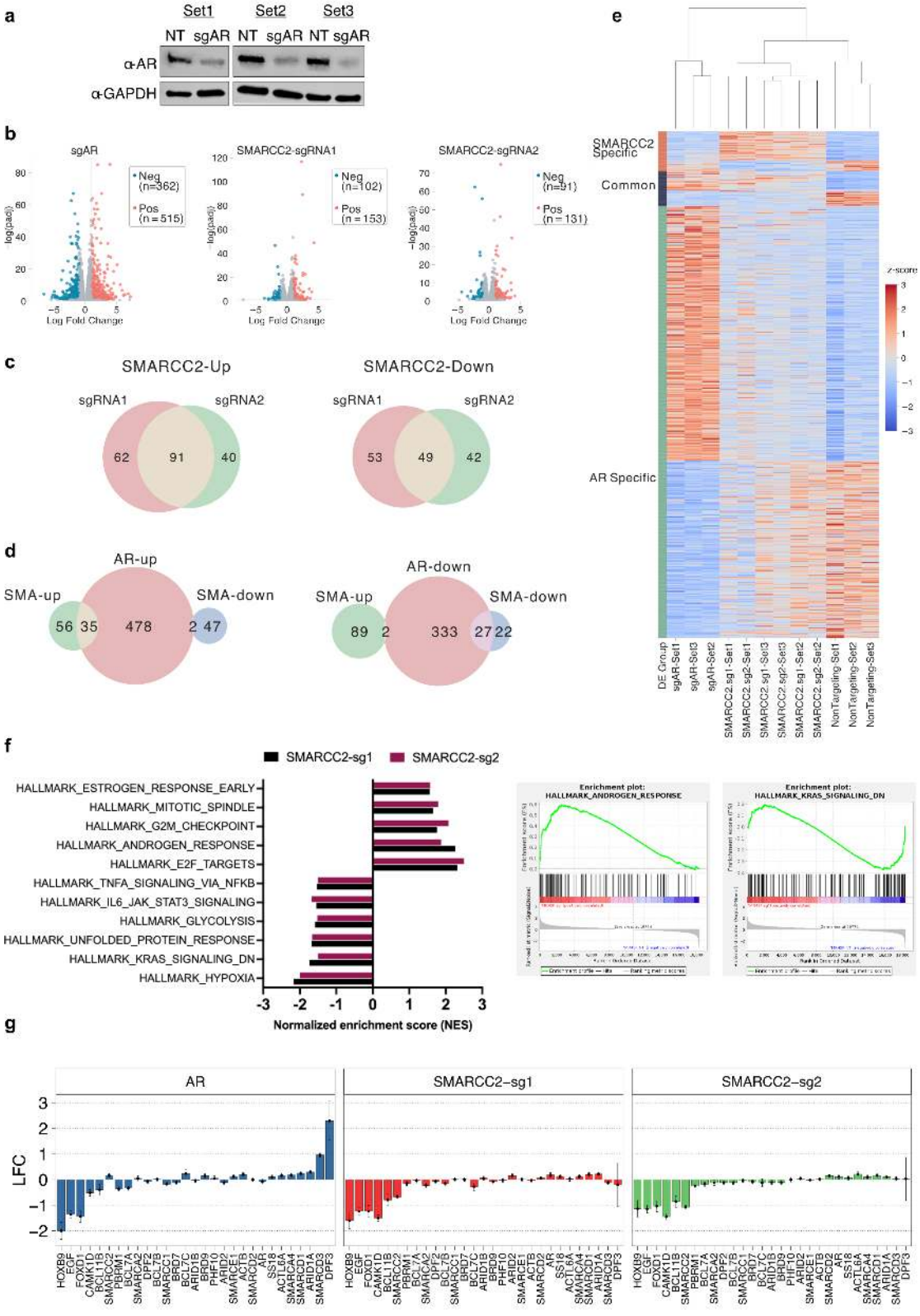

Figure 5.9 Differential gene expression upon SMARCC2 and AR depletion in MR49F cells. (a) Western blot of AR knockout in MR49F cells. (b) Volcano plot of differential gene expression upon SMARCC2 and AR loss. (c) The comparison of the effect of two different SMARCC2-targeting sgRNA on differentially regulated genes. (d) The comparison between AR-regulated and SMARCC2-regulated genes. (e) Heatmap of transcript counts per sgRNA treatment. Three biological replicates were collected for RNA-seq experiments. Differentially regulated genes are defined as p-adj<0.05 and |LFC| >1. (f) GSEA analysis on hallmark genesets for SMARCC2 regulated genes. (g) Examples of SMARCC2 regulated genes and the expression of SWI/SNF subunits in different sgRNA treatments.

Next, we compared SMARCC2 binding sites to differentially regulated genes to understand whether the transcriptomic changes are a direct outcome of chromatin binding. We found 74 upregulated and 36 downregulated genes near SMARCC2 binding sites (+/- 100kb)**(Figure 5.10**). Interestingly, we observed that the majority of these differentially expressed genes has at least one gBAF binding site. However, none of the differentially regulated genes had only rBAF or gSMA sites; rBAF and gSMA tend to be present in gBAF-bound regions. These observations suggest a three-dimensional regulatory role for BRG1-dependent SMARCC2 binding in ENZA resistance.

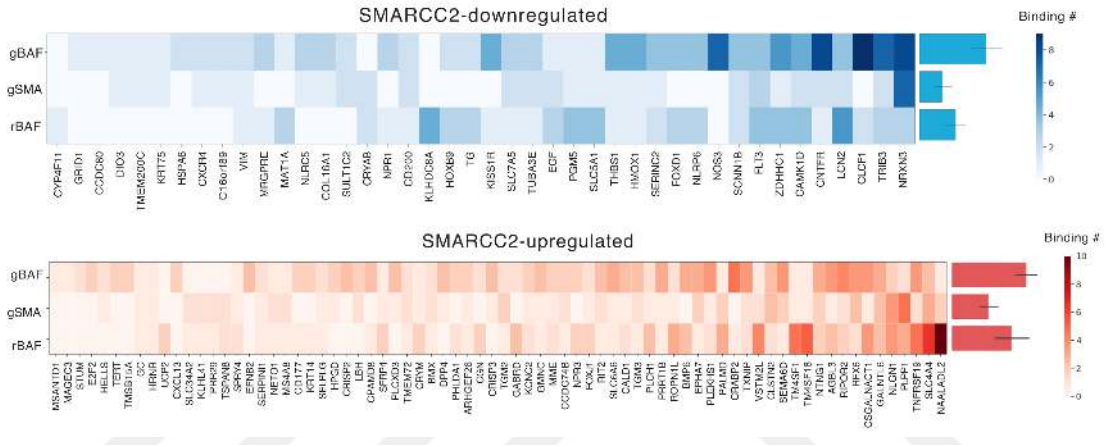

Figure 5.10 The distribution of rBAF, gBAF and gSMA regions in proximity of differentially regulated genes. Color scale indicates the number of binding events within +/- 100kb to the gene transcription start site. Blue: downregulated genes identified in RNA-seq experiments. Red: upregulated genes identified in RNA-seq experiments.

5.4 Discussion

Epigenetic factors have emerged as a promising drug target for the treatment late stage PCa. Multiple studies revealed an essential role of epigenetic factors as AR coregulator or lineage differentiation to a neuroendocrine stage [205,207]. However, there are only a few epigenetic factors that show promising preclinical evidence for CRPC treatment. This is partially due to the lack of systematic testing of all epigenetic modifiers. For this reason, we aimed to generate an epigenetic focused CRISPR library to systematically test every epigenetic modifier for viability.

In this focused CRISPR screen, we demonstrated that SMARCC2, a core component of the SWI/SNF complex, is selectively essential in ENZA-resistant cell lines. The ATP-dependent SWI/SNF chromatin remodeling complex is a large evolutionarily conserved

multiprotein complex that can have distinct protein combinations which impacts the biological role [190]. Functional studies have revealed three main categories of mammalian SWI/SNF complexes: cBAF, PBAF, and ncBAF. Starting from the initial SMARCC1 or SMARCC2 nucleation dimer, every module in the complex has at least one specific subunit that determines its category [194]. SMARCC2 acts as a core subunit for the initial steps of SWI/SNF core assembly in cBAF and PBAF, but not found in ncBAF [194]. Our EPIKOL screen data revealed no PBAF-specific or ncBAF-specific components that were essential in ENZA-resistant models, while the cBAF-specific component DPF2 was only essential for ENZA-resistant cells. Overall, these findings demonstrate that cBAF is strongly selective in ENZA-resistant models suggesting that this may be a common adaptation mechanism.

Recent studies have revealed that eliminating a single subunit is typically insufficient to disrupt the complex formation [194,202] due to their modular structures and combinatorial compositions. Certain subunits compete for incorporation, and this behavior correlates to their synthetic lethal relationship as shown with SMARCC1-SMARCC2 and SMARCA4-SMARCA2 pairs [202]. In PCa, BRG1 has been shown to be synthetic lethal in both cell lines with TMRPSS2-ERG fusion [289] and PTEN-loss [288] which is consistent with our CRISPR data. Several other SWI/SNF complex subunits have been identified as AR interactors [213–215] and were shown to be broadly essential in both previous work [284,377,378] and our CRISPR screen. Recent studies showed that SMARCC2 depletion does not prevent either the formation or the activity of the BAF complex suggesting that normal cells may contain a compensatory mechanism [202]. Considering that its structurally-related counterpart SMARCC1 was not negatively selected in our EPIKOL screen and the mRNA level did not change by SMARCC2 knockout, our data suggests that SMARCC2 cannot be compensated by SMARCC1 in these models.

We observed that the SWI/SNF complex binding sites were considerably expanded in the ENZA-resistant model. The majority of BAF sites in ENZA-sensitive LNCaP were also conserved in ENZA-resistant MR49F; we referred to them as retained BAF sites. These sites are found to be accessible in both primary and CRPC clinical samples and more likely to be co-occupied by AR and its cofactors. However, our data suggests that their

binding is not sufficient to alter the gene expression in ENZA-resistant model, possibly related to the collection time point as observed by other work [119]. Differentially expressed genes are commonly found within +/-100 kb of at least one gBAF binding site which may or may not be accompanied by rBAF or gSMA sites, suggesting an essential role for ENZA-specific SMARCC2 and BRG1 co-binding. Interestingly, gBAF sites are enriched for oncogenic transcription factors MYC, GR, and MAPK1, ETS transcription factors ERG, FLI1 and SPI1, and multiple proteins in the regulation of the transcriptional elongation and termination. Although we were not able to see an overall difference in the accessibility of gBAF binding sites in primary versus CRPC patients, the genes that are bound by gBAF and differentially regulated were inaccessible in primary PCa samples and become accessible in CRPC samples in individual cases. These observations suggest a three-dimensional regulatory role rather than a simple direct regulation for SMARCC2 in ENZA resistance.

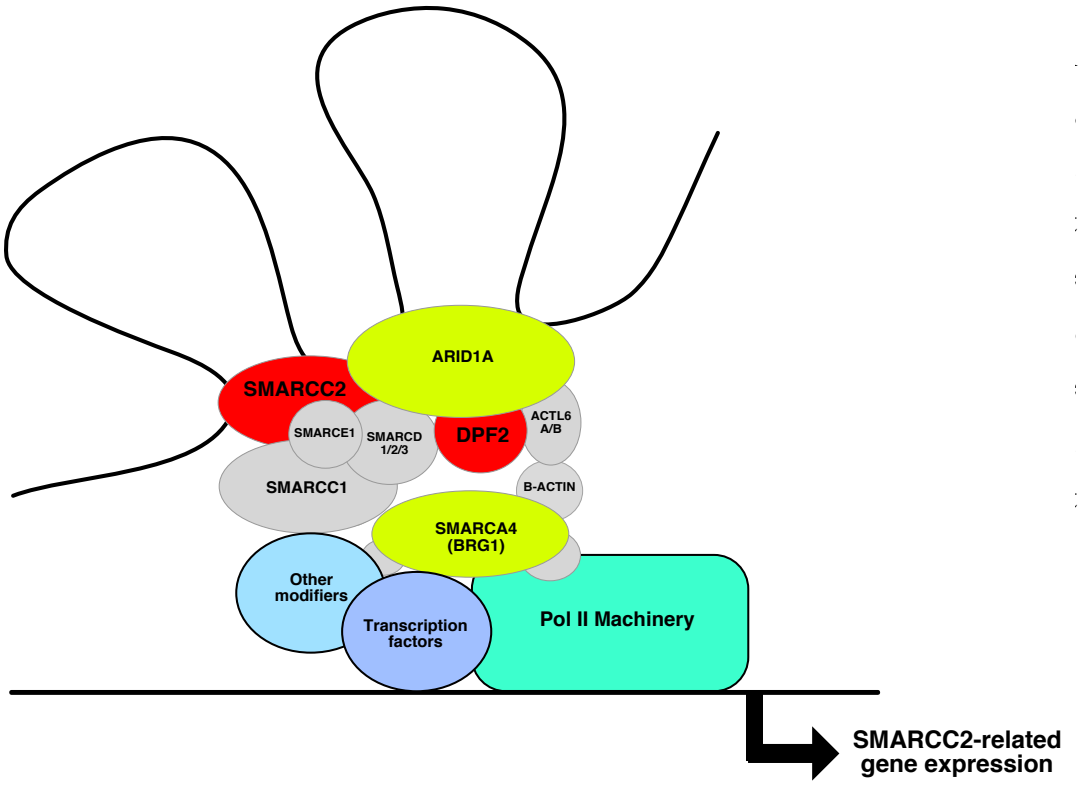

Figure 5.11 Illustration of potential three-dimensional regulatory role of SMARCC2-dependent SWI/SNF complex. Our data suggests that SMARCC2 gained an indispensable role in ENZA resistance. SMARCC2-dependent SWI/SNF complex binds new regions in ENZA-resistant model, which showed similarity with oncogenic transcription factors such as MYC and ERG as well as transcription-associated factors. These ENZA-specific binding sites were found in close proximity to SMARCC2-regulated genes. SWI/SNF subunits are colored in red (ENZA-dependent), green (common-dependent), gray (other subunits).

Chapter 6 SUMMARY AND CONCLUSION

Despite advances in the field, PCa remains one of the most common cancer-related cause of death. Although most primary PCa cases are successfully treated, recurrent or metastatic disease is typically lethal. Androgen deprivation therapy is the mainstream treatment for these aggressive cancers. Either by adaptive mechanisms or simply by overgrowth of a subclone, the tumor eventually becomes androgen-independent in castrated conditions, and further transforms to drug resistant under selective pressure with increased disease aggressiveness. During this transition the cancer gains distinct epigenetic alterations including DNA methylation pattern, chromatin accessibility and histone mark alterations. These epigenetic alterations are believed to play a critical role in disease progression. We therefore hypothesized that specific epigenetic modifiers have an essential role in CRPC cell proliferation and survival. To identify critical epigenetic vulnerabilities in CRPC, I conducted an arrayed KDM-focused shRNA screen and an epigenome-wide CRISPR screen in multiple different PCa cell lines representing different stages of the disease.

While the KDM-focused shRNA screen was able to recapitulate the published results for KDM1A, we did not find additional KDM-dependent vulnerability in any of the cell lines tested nor could we repeat several published studies. This is unlikely due to a technical or experimental error as these results were supported by the subsequent CRISPR screen results. As discussed previously, due their structural similarities and similar substrates on histones, KDMs might compensate for the loss of a single KDM. Targeting a KDM subfamily could potentially induce greater phenotype due to their possible synthetic lethal dependencies.

To explore the role of epigenetic modifying enzymes in PCa progression, we therefore designed an epigenetic-focused CRISPR library. With this we focused on the epigenetic vulnerabilities in ENZA-resistant PCa. Despite our two ENZA-resistant cell lines being derived by different methods, in different labs and at different times, they both required SMARCC2 for cell proliferation. Interestingly, based on our screen results, SMARCC2 is also essential in the 22Rv1 cell line that is AR-dependent and intrinsically ENZA-resistant, but not in the DU145 cell line that is AR-null and intrinsically ENZA-resistant.

We showed that SMARCC2 is selectively essential in ENZA-resistant models but not in the parental cell line by orthogonal validation assays. From the CRISPR screen we did not observe any PBAF or non-canonical BAF dependency. In contrast, DPF2, a canonical BAF-specific subunit, was essential in MR49F and validated to be selectively essential in ENZA-resistant cells. Interestingly, during the transition to ENZA-resistance SMARCC2 and BRG1 expanded their binding site by almost two-fold. This led to the potential binding of alternative transcription factors such as MYC, GR and ETS factors.

Chapter 7 FUTURE EXPERIMENTS

Overall, our data suggests that SMARCC2 expands its regulatory role in ENZA-resistance which is partially overlapping with AR function. Although we haven't validated the epigenetic dependency of other SWI/SNF subunits, DPF2 dependency suggests an important role for cBAF in ENZA resistance. We need to explore more about the SMARCC2-dependent DNA binding, protein interaction and composition of SWI/SNF complex to understand the mechanism behind its ENZA-specific dependency. BRG1 chromatin binding profile with and without SMARCC2 would distinguish SMARCC2-dependent binding sites and uncover whether SMARCC2 depletion abrogates complex formation in ENZA-resistant model as SMARCC1 cannot compensate SMARCC2 depletion. It would be also interesting to see the topological regulation with and without ENZA presence. For the composition, the published works on SWI/SNF complex composition utilize density sedimentation for SWI/SNF complex. It would be interesting to test the fractionation of the complex upon SMARCC2 depletion. Alternatively, identifying endogenous BRG1 interactors based on the SMARCC2 presence would give more information on SMARCC2-dependent complex composition and SMARCC2-dependent interactors.

In addition to SWI/SNF composition, post-translational modifications in SMARCC2 might be differentially regulated in ENZA resistance. After the confirmation of different interactors in ENZA-sensitive versus ENZA-resistant stage, potential PTM sites could be mutated and its effect on cell survival or on interaction with a known protein could be tested.

Although we could observe the commonality on epigenetic dependencies in 4 different cells (LNCaP, LNCaP-abl, LNCaP-enzaR, MR49F), it would be interesting to perform the CRISPR screen *in vivo* in male mice injected with EPIKOL-transduced LNCaP cells. When tumor is formed, the mice would be castrated after getting samples for reference point. After certain time, samples should be collected to identify epigenetic dependencies in castrate condition and the mice should be treated with ENZA. The ENZA-resistant tumor should be collected as a final point. The results would be more powerful as the samples originated from the same source, and *in vivo* experiments can recapitulate the tumor environment better than cell culture. Epigenetic modifiers both with tumor-suppressor and oncogenic role could be identified, providing an evolutionary track in each step. The limitations would be the number of mice, the tumor size restricted by ethical rules, and the propagation of the tumor. Not to burden the animals with large tumor size, the tumor can be transferred into already castrated/ENZA treated mice. Also, it would require large number of cells initially injected into the mice, a successful engraftment and a good number of control arms (untreated mice). Further expansion of this type of experiment is to switch to a CROP-seq vector, which would allow us to analyze transcriptomic changes and observe heterogenous populations based on gene perturbations in single cell resolution.

Chapter 8 APPENDIX

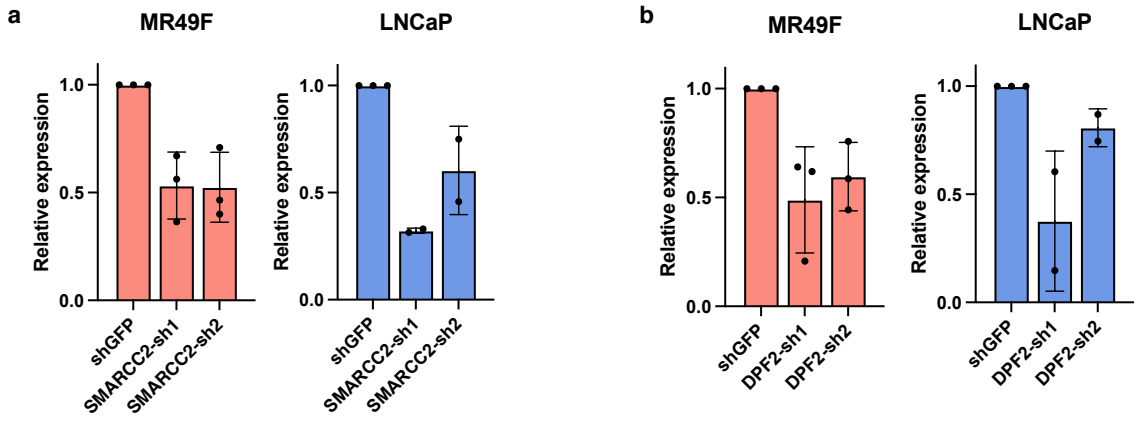

Figure 8.1 RT-qPCR results of SMARCC2 and DPF2-targeting shRNA treatment. Supporting information for Figure 5.7. MR49F and LNCaP cells were treated with two different shRNAs targeting either (a)SMARCC2 and (b)DPF2. Cells were collected after puromycin treatment.

BIBLIOGRAPHY

1. Wein AJ, Kavoussi LR, Campbell MF, editors. Campbell-Walsh Urology: Tenth edition. 10th ed. Philadelphia, PA: Elsevier Saunders; 2012.

2. Toivanen R, Shen MM. Prostate organogenesis: tissue induction, hormonal regulation and cell type specification. Development. 2017;144: 1382–1398.

3. Verze P, Cai T, Lorenzetti S. The role of the prostate in male fertility, health and disease. Nat Rev Urol. 7/2016;13: 379–386.

4. McNeal JE. The zonal anatomy of the prostate. Prostate. 1981;2: 35–49.

5. Aaron L, Franco OE, Hayward SW. Review of Prostate Anatomy and Embryology and the Etiology of Benign Prostatic Hyperplasia. Urol Clin North Am. 2016;43: 279–288.

6. Taplin ME, Ho S-M. The Endocrinology of Prostate Cancer. J Clin Endocrinol Metab. 2001;86: 3467–3477.

7. Kluth LA, Shariat SF, Kratzik C, Tagawa S, Sonpavde G, Rieken M, et al. The hypothalamic–pituitary–gonadal axis and prostate cancer: implications for androgen deprivation therapy. World J Urol. 6/2014;32: 669–676.

8. Nargund VH. Effects of psychological stress on male fertility. Nat Rev Urol. 7/2015;12: 373–382.

9. Tan MHE, Li J, Xu HE, Melcher K, Yong E-L. Androgen receptor: structure, role in prostate cancer and drug discovery. Acta Pharmacol Sin. 2015;36: 3–23.

10. Weikum ER, Liu X, Ortlund EA. The nuclear receptor superfamily: A structural perspective. Protein Sci. 2018;27: 1876–1892.

11. Helsen C, Kerkhofs S, Clinckemalie L, Spans L, Laurent M, Boonen S, et al. Structural basis for nuclear hormone receptor DNA binding. Mol Cell Endocrinol. 01/2012;348: 411–417.

12. Chaturvedi AP, Dehm SM. Androgen Receptor Dependence. Adv Exp Med Biol. 2019;1210: 333–350.

13. Jenster G, van der Korput HAGM, Trapman J, Brinkmann AO. Identification of Two Transcription Activation Units in the N-terminal Domain of the Human Androgen Receptor

(∗). J Biol Chem. 1995;270: 7341–7346.

14. Callewaert L, Van Tilborgh N, Claessens F. Interplay between Two Hormone-Independent Activation Domains in the Androgen Receptor. Cancer Res. 2006;66: 543–553.

15. Lu J, Van der Steen T, Tindall DJ. Are androgen receptor variants a substitute for the full-length receptor? Nat Rev Urol. 3/2015;12: 137–144.

16. Lu C, Brown LC, Antonarakis ES, Armstrong AJ, Luo J. Androgen receptor variant-driven prostate cancer II: advances in laboratory investigations. Prostate Cancer Prostatic Dis. 2020;23: 381–397.

17. Gelmann EP. Molecular Biology of the Androgen Receptor. J Clin Oncol. 07/2002;20: 3001–3015.

18. Davies P, Watt K, Kelly SM, Clark C, Price NC, McEwan IJ. Consequences of poly-glutamine repeat length for the conformation and folding of the androgen receptor amino-terminal domain. J Mol Endocrinol. 2008;41: 301–314.

19. Claessens F, Denayer S, Van Tilborgh N, Kerkhofs S, Helsen C, Haelens A. Diverse roles of androgen receptor (AR) domains in AR-mediated signaling. Nucl Recept Signal. 01/2008;6: nrs.06008.

20. Claessens F, Joniau S, Helsen C. Comparing the rules of engagement of androgen and glucocorticoid receptors. Cell Mol Life Sci. 2017;74: 2217–2228.

21. Kulik M, Bothe M, Kibar G, Fuchs A, Schöne S, Prekovic S, et al. Androgen and glucocorticoid receptor direct distinct transcriptional programs by receptor-specific and shared DNA binding sites. Nucleic Acids Res. 2021;49: 3856–3875.

22. Sahu B, Laakso M, Pihlajamaa P, Ovaska K, Sinielnikov I, Hautaniemi S, et al. FoxA1 Specifies Unique Androgen and Glucocorticoid Receptor Binding Events in Prostate Cancer Cells. Cancer Res. 2013;73: 1570–1580.

23. Saporita AJ, Zhang Q, Navai N, Dincer Z, Hahn J, Cai X, et al. Identification and Characterization of a Ligand-regulated Nuclear Export Signal in Androgen Receptor. J Biol Chem. 2003;278: 41998–42005.

24. Cutress ML, Whitaker HC, Mills IG, Stewart M, Neal DE. Structural basis for the nuclear import of the human androgen receptor. J Cell Sci. 2008;121: 957–968.

25. Matias PM, Donner P, Coelho R, Thomaz M, Peixoto C, Macedo S, et al. Structural evidence for ligand specificity in the binding domain of the human androgen receptor. Implications for pathogenic gene mutations. J Biol Chem. 2000;275: 26164–26171.

26. Nadal M, Prekovic S, Gallastegui N, Helsen C, Abella M, Zielinska K, et al. Structure of the homodimeric androgen receptor ligand-binding domain. Nat Commun. 4/2017;8: 14388.

27. Pereira de Jésus-Tran K, Côté P-L, Cantin L, Blanchet J, Labrie F, Breton R. Comparison of crystal structures of human androgen receptor ligand-binding domain complexed with various agonists reveals molecular determinants responsible for binding affinity. Protein Sci. 2006;15: 987–999.

28. Gao W, Kim J, Dalton JT. Pharmacokinetics and pharmacodynamics of nonsteroidal androgen receptor ligands. Pharm Res. 2006;23: 1641–1658.

29. Bohl CE, Miller DD, Chen J, Bell CE, Dalton JT. Structural basis for accommodation of nonsteroidal ligands in the androgen receptor. J Biol Chem. 2005;280: 37747–37754.

30. Gim HJ, Park J, Jung ME, Houk KN. Conformational dynamics of androgen receptors bound to agonists and antagonists. Sci Rep. 2021;11: 15887.

31. Lack NA, Axerio-Cilies P, Tavassoli P, Han FQ, Chan KH, Feau C, et al. Targeting the binding function 3 (BF3) site of the human androgen receptor through virtual screening. J Med Chem. 2011;54: 8563–8573.

32. Axerio-Cilies P, Lack NA, Nayana MRS, Chan KH, Yeung A, Leblanc E, et al. Inhibitors of androgen receptor activation function-2 (AF2) site identified through virtual screening. J Med Chem. 2011;54: 6197–6205.

33. Tran C, Ouk S, Clegg NJ, Chen Y, Watson PA, Arora V, et al. Development of a Second-Generation Antiandrogen for Treatment of Advanced Prostate Cancer. Science. 2009;324: 787–790.

34. Yuan X, Cai C, Chen S, Chen S, Yu Z, Balk SP. Androgen receptor functions in castration-resistant prostate cancer and mechanisms of resistance to new agents targeting the androgen axis. Oncogene. 2014;33: 2815–2825.

35. He B, Gampe RT Jr, Kole AJ, Hnat AT, Stanley TB, An G, et al. Structural basis for androgen receptor interdomain and coactivator interactions suggests a transition in nuclear receptor activation function dominance. Mol Cell. 2004;16: 425–438.

36. He B, Kemppainen JA, Wilson EM. FXXLF and WXXLF sequences mediate the NH2-terminal interaction with the ligand binding domain of the androgen receptor. J Biol Chem. 2000;275: 22986–22994.

37. He B, Kemppainen JA, Voegel JJ, Gronemeyer H, Wilson EM. Activation Function 2 in the Human Androgen Receptor Ligand Binding Domain Mediates Interdomain Communication with the NH2-terminal Domain *. J Biol Chem. 1999;274: 37219–37225.

38. Siegel RL, Miller KD, Fuchs HE, Jemal A. Cancer Statistics, 2021. CA Cancer J Clin. 2021;71: 7–33.

39. Pernar CH, Ebot EM, Wilson KM, Mucci LA. The Epidemiology of Prostate Cancer. Cold Spring Harb Perspect Med. 12/2018;8: a030361.

40. Cancer of the prostate - cancer stat facts. [cited 15 Oct 2021]. Available: https://seer.cancer.gov/statfacts/html/prost.html

41. Mucci LA, Hjelmborg JB, Harris JR, Czene K, Havelick DJ, Scheike T, et al. Familial Risk and Heritability of Cancer Among Twins in Nordic Countries. JAMA. 01 2016;315: 68–76.

42. Farashi S, Kryza T, Clements J, Batra J. Post-GWAS in prostate cancer: from genetic association to biological contribution. Nat Rev Cancer. 1/2019;19: 46–59.

43. Al Olama AA, Kote-Jarai Z, Berndt SI, Conti DV, Schumacher F, Han Y, et al. A meta-analysis of 87,040 individuals identifies 23 new susceptibility loci for prostate cancer. Nat Genet. 10/2014;46: 1103–1109.

44. Mottet N, van den Bergh RCN, Briers E, Van den Broeck T, Cumberbatch MG, De Santis M, et al. EAU-EANM-ESTRO-ESUR-SIOG Guidelines on Prostate Cancer-2020 Update. Part 1: Screening, Diagnosis, and Local Treatment with Curative Intent. Eur Urol. 2021;79: 243–262.

45. Pullar B, Shah N. Prostate cancer. Surgery. 10/2016;34: 505–511.

46. Mottet N, Bellmunt J, Bolla M, Briers E, Cumberbatch MG, De Santis M, et al. EAU-ESTRO-SIOG Guidelines on Prostate Cancer. Part 1: Screening, Diagnosis, and Local Treatment with Curative Intent. Eur Urol. 04/2017;71: 618–629.

47. Braunhut BL, Punnen S, Kryvenko ON. Updates on Grading and Staging of Prostate Cancer. Surg Pathol Clin. 12/2018;11: 759–774.

48. Lowrance WT, Breau RH, Chou R, Chapin BF, Crispino T, Dreicer R, et al. Advanced Prostate Cancer: AUA/ASTRO/SUO Guideline PART I. J Urol. 2021;205: 14–21.

49. Spratt DE, Dai DLY, Den RB, Troncoso P, Yousefi K, Ross AE, et al. Performance of a Prostate Cancer Genomic Classifier in Predicting Metastasis in Men with Prostate-specific Antigen Persistence Postprostatectomy. Eur Urol. 2018;74: 107–114.

50. Preisser F, Chun FKH, Pompe RS, Heinze A, Salomon G, Graefen M, et al. Persistent Prostate-Specific Antigen After Radical Prostatectomy and Its Impact on Oncologic Outcomes. Eur Urol. 2019;76: 106–114.

51. Thompson IM. Flare Associated with LHRH-Agonist Therapy. Rev Urol. 2001;3 Suppl 3: S10-4.

52. Engel JB, Schally AV. Drug Insight: clinical use of agonists and antagonists of luteinizing-hormone-releasing hormone. Nat Clin Pract Endocrinol Metab. 2007;3: 157–167.

53. Schally AV, Comaru-Schally AM. Mode of Action of LHRH Analogs. BC Decker; 2003.

54. Armstrong AJ, Szmulewitz RZ, Petrylak DP, Holzbeierlein J, Villers A, Azad A, et al. ARCHES: A Randomized, Phase III Study of Androgen Deprivation Therapy With Enzalutamide or Placebo in Men With Metastatic Hormone-Sensitive Prostate Cancer. J Clin Orthod. 2019;37: 2974–2986.

55. Sweeney CJ, Chen Y-H, Carducci M, Liu G, Jarrard DF, Eisenberger M, et al. Chemohormonal Therapy in Metastatic Hormone-Sensitive Prostate Cancer. N Engl J Med. 2015;373: 737–746.

56. Gillessen S, Attard G, Beer TM, Beltran H, Bjartell A, Bossi A, et al. Management of Patients with Advanced Prostate Cancer: Report of the Advanced Prostate Cancer Consensus Conference 2019. Eur Urol. 2020;77: 508–547.

57. Steele CB, Li J, Huang B, Weir HK. Prostate cancer survival in the United States by race and stage (2001-2009): Findings from the CONCORD-2 study. Cancer. 2017;123 Suppl 24: 5160–5177.

58. SEER*Explorer: An interactive website for SEER cancer statistics [Internet]. Surveillance Research Program, National Cancer Institute. [cited 16 Apr 2020]. Available: https://seer.cancer.gov/explorer/

59. Cornford P, van den Bergh RCN, Briers E, Van den Broeck T, Cumberbatch MG, De Santis M, et al. EAU-EANM-ESTRO-ESUR-SIOG Guidelines on Prostate Cancer. Part II-2020 Update: Treatment of Relapsing and Metastatic Prostate Cancer. Eur Urol. 2021;79: 263–282.

60. Lowrance WT, Breau RH, Chou R, Chapin BF, Crispino T, Dreicer R, et al. Advanced Prostate Cancer: AUA/ASTRO/SUO Guideline PART II. J Urol. 2021;205: 22–29.

61. Abou D, Benabdallah N, Jiang W, Peng L, Zhang H, Villmer A, et al. Prostate cancer theranostics - an overview. Front Oncol. 2020;10: 884.

62. Schweizer MT, Antonarakis ES. Abiraterone and other novel androgen-directed strategies for the treatment of prostate cancer: a new era of hormonal therapies is born. Ther Adv Urol. 2012;4: 167–178.

63. de Bono JS, North S, Saad F, Flaig TW, Hainsworth JD, Fléchon A, et al. Abiraterone and Increased Survival in Metastatic Prostate Cancer. N Engl J Med. 2011; 11.

64. Ryan CJ, Smith MR, Fizazi K, Saad F, Mulders PFA, Sternberg CN, et al. Abiraterone acetate plus prednisone versus placebo plus prednisone in chemotherapy-naive men with metastatic castration-resistant prostate cancer (COU-AA-302): final overall survival analysis of a randomised, double-blind, placebo-controlled phase 3 study. Lancet Oncol. 2015;16: 152–160.

65. Schellhammer PF, Venner P, Haas GP, Small EJ, Nieh PT, Seabaugh DR, et al. Prostate specific antigen decreases after withdrawal of antiandrogen therapy with bicalutamide or flutamide in patients receiving combined androgen blockade. J Urol. 1997;157: 1731–1735.

66. Lorente D, Mateo J, Zafeiriou Z, Smith AD, Sandhu S, Ferraldeschi R, et al. Switching and withdrawing hormonal agents for castration-resistant prostate cancer. Nat Rev Urol. 1/2015;12: 37–47.

67. Soo A, O'Callaghan ME, Kopsaftis T, Vatandoust S, Moretti K, Kichenadasse G. PSA response to antiandrogen withdrawal: a systematic review and meta-analysis. Prostate Cancer Prostatic Dis. 2021;24: 826–836.

68. Smith MR, Saad F, Chowdhury S, Oudard S, Hadaschik BA, Graff JN, et al. Apalutamide Treatment and Metastasis-free Survival in Prostate Cancer. N Engl J Med. 2018;378: 1408–1418.

69. Fizazi K, Shore N, Tammela TL, Ulys A, Vjaters E, Polyakov S, et al. Darolutamide in Nonmetastatic, Castration-Resistant Prostate Cancer. N Engl J Med. 2019;380: 1235–1246.

70. Sternberg CN, Fizazi K, Saad F, Shore ND, De Giorgi U, Penson DF, et al. Enzalutamide and Survival in Nonmetastatic, Castration-Resistant Prostate Cancer. N Engl J Med. 2020;382: 2197–2206.

71. Penson DF, Armstrong AJ, Concepcion RS, Agarwal N, Olsson CA, Karsh LI, et al. Enzalutamide versus bicalutamide in patients with nonmetastatic castration-resistant prostate cancer: a prespecified subgroup analysis of the STRIVE trial. Prostate Cancer Prostatic Dis. 2021. doi:10.1038/s41391-021-00465-7

72. Heidenreich A, Chowdhury S, Klotz L, Siemens DR, Villers A, Ivanescu C, et al. Impact of Enzalutamide Compared with Bicalutamide on Quality of Life in Men with Metastatic Castration-resistant Prostate Cancer: Additional Analyses from the TERRAIN Randomised Clinical Trial. Eur Urol. 2017;71: 534–542.

73. Schultz NM, Shore ND, Chowdhury S, Klotz LH, Concepcion RS, Penson DF, et al. Number-needed-to-treat analysis of clinical progression in patients with metastatic castration-resistant prostate cancer in the STRIVE and TERRAIN trials. BMC Urol. 2018;18: 77.

74. Beer TM, Armstrong AJ, Rathkopf DE, Loriot Y, Sternberg CN, Higano CS, et al. Enzalutamide in Metastatic Prostate Cancer before Chemotherapy. N Engl J Med. 2014;371: 424–433.

75. Sekine Y, Nakayama H, Miyazawa Y, Arai S, Koike H, Matsui H, et al. Ratio of the expression levels of androgen receptor splice variant 7 to androgen receptor in castration refractory prostate cancer. Oncol Lett. 2021;22: 831.

76. He Y, Wei T, Ye Z, Orme JJ, Lin D, Sheng H, et al. A noncanonical AR addiction drives enzalutamide resistance in prostate cancer. Nat Commun. 2021;12: 1521.

77. Bishop JL, Thaper D, Vahid S, Davies A, Ketola K, Kuruma H, et al. The Master Neural Transcription Factor BRN2 Is an Androgen Receptor–Suppressed Driver of Neuroendocrine Differentiation in Prostate Cancer. Cancer Discov. 2017;7: 54–71.

78. Feldman BJ, Feldman D. The development of androgen-independent prostate cancer. Nat Rev Cancer. 10/2001;1: 34–45.

79. Zong Y, Goldstein AS. Adaptation or selection—mechanisms of castration-resistant prostate cancer. Nat Rev Urol. 2/2013;10: 90–98.

80. Karantanos T, Corn PG, Thompson TC. Prostate cancer progression after androgen deprivation therapy: mechanisms of castrate resistance and novel therapeutic approaches. Oncogene. 2013;32: 5501–5511.

81. Chandrasekar T, Yang JC, Gao AC, Evans CP. Mechanisms of resistance in castration-resistant prostate cancer. Transl Androl Urol. 2015;4: 16.

82. Katsogiannou M, Ziouziou H, Karaki S, Andrieu C, Henry de Villeneuve M, Rocchi P. The hallmarks of castration-resistant prostate cancers. Cancer Treat Rev. 07/2015;41: 588–597.

83. Kumar A, Coleman I, Morrissey C, Zhang X, True LD, Gulati R, et al. Substantial interindividual and limited intraindividual genomic diversity among tumors from men with metastatic prostate cancer. Nat Med. 4/2016;22: 369–378.

84. Viswanathan SR, Ha G, Hoff AM, Wala JA, Carrot-Zhang J, Whelan CW, et al. Structural Alterations Driving Castration-Resistant Prostate Cancer Revealed by Linked-Read Genome Sequencing. Cell. 07/2018;174: 433-447.e19.

85. Quigley DA, Dang HX, Zhao SG, Lloyd P, Aggarwal R, Alumkal JJ, et al. Genomic Hallmarks and Structural Variation in Metastatic Prostate Cancer. Cell. 2018;174: 758-769.e9.

86. Takeda DY, Spisák S, Seo J-H, Bell C, O'Connor E, Korthauer K, et al. A Somatically Acquired Enhancer of the Androgen Receptor Is a Noncoding Driver in Advanced Prostate Cancer. Cell. 07/2018;174: 422-432.e13.

87. Buchanan G, Yang M, Harris JM, Nahm HS, Han G, Moore N, et al. Mutations at the boundary of the hinge and ligand binding domain of the androgen receptor confer increased transactivation function. Mol Endocrinol. 2001;15: 46–56.

88. Hay CW, McEwan IJ. The impact of point mutations in the human androgen receptor: classification of mutations on the basis of transcriptional activity. PLoS One. 2012;7: e32514.

89. Mostaghel EA, Zhang A, Hernandez S, Marck BT, Zhang X, Tamae D, et al. Contribution of Adrenal Glands to Intratumor Androgens and Growth of Castration-Resistant Prostate Cancer. Clin Cancer Res. 2019;25: 426–439.

90. Lallous N, Volik SV, Awrey S, Leblanc E, Tse R, Murillo J, et al. Functional analysis of androgen receptor mutations that confer anti-androgen resistance identified in circulating cell-free DNA from prostate cancer patients. Genome Biol. 2016;17: 10.

91. Culig Z, Hobisch A, Cronauer MV. Androgen Receptor Activation in Prostatic Tumor Cell Lines by Insulin-like Growth Factor-I, Keratinocyte Growth Factor, and Epidermal Growth Factor. Cancer Res. 1994; 5474–5478.

92. Sun C, Shi Y, Xu LL, Nageswararao C, Davis LD, Segawa T, et al. Androgen receptor mutation (T877A) promotes prostate cancer cell growth and cell survival. Oncogene. 2006;25: 3905–3913.

93. Joseph JD, Lu N, Qian J, Sensintaffar J, Shao G, Brigham D, et al. A Clinically Relevant Androgen Receptor Mutation Confers Resistance to Second-Generation Antiandrogens Enzalutamide and ARN-509. Cancer Discov. 2013;3: 1020–1029.

94. Korpal M, Korn JM, Gao X, Rakiec DP, Ruddy DA, Doshi S, et al. An F876L Mutation in Androgen Receptor Confers Genetic and Phenotypic Resistance to MDV3100 (Enzalutamide). Cancer Discov. 2013;3: 1030–1043.

95. Guo Z, Yang X, Sun F, Jiang R, Linn DE, Chen H, et al. A novel androgen receptor splice variant is up-regulated during prostate cancer progression and promotes androgen depletion-resistant growth. Cancer Res. 2009;69: 2305–2313.

96. Hu R, Dunn TA, Wei S, Isharwal S, Veltri RW, Humphreys E, et al. Ligand-independent androgen receptor variants derived from splicing of cryptic exons signify hormone-refractory prostate cancer. Cancer Res. 2009;69: 16–22.

97. Li Y, Chan SC, Brand LJ, Hwang TH, Silverstein KAT, Dehm SM. Androgen receptor splice variants mediate enzalutamide resistance in castration-resistant prostate cancer cell lines. Cancer Res. 2013;73: 483–489.

98. Cao B, Qi Y, Zhang G, Xu D, Zhan Y, Alvarez X, et al. Androgen receptor splice variants activating the full-length receptor in mediating resistance to androgen-directed therapy. Oncotarget. 2014;5: 1646–1656.

99. Zhan Y, Zhang G, Wang X, Qi Y, Bai S, Li D, et al. Interplay between Cytoplasmic and Nuclear Androgen Receptor Splice Variants Mediates Castration Resistance. Mol Cancer Res. 2017;15: 59–68.

100. Zhu Y, Dalrymple SL, Coleman I, Zheng SL, Xu J, Hooper JE, et al. Role of androgen receptor splice variant-7 (AR-V7) in prostate cancer resistance to 2nd-generation androgen receptor signaling inhibitors. Oncogene. 2020;39: 6935–6949.

101. Antonarakis ES, Lu C, Wang H, Luber B, Nakazawa M, Roeser JC, et al. AR-V7 and resistance to enzalutamide and abiraterone in prostate cancer. N Engl J Med. 2014;371: 1028–1038.

102. Scher HI, Lu D, Schreiber NA, Louw J, Graf RP, Vargas HA, et al. Association of AR-V7 on Circulating Tumor Cells as a Treatment-Specific Biomarker With Outcomes and Survival in Castration-Resistant Prostate Cancer. JAMA Oncol. 2016;2: 1441–1449.

103. Sharp A, Welti JC, Lambros MBK, Dolling D, Rodrigues DN, Pope L, et al. Clinical Utility of Circulating Tumour Cell Androgen Receptor Splice Variant-7 Status in Metastatic Castration-resistant Prostate Cancer. Eur Urol. 2019;76: 676–685.

104. Sharp A, Coleman I, Yuan W, Sprenger C, Dolling D, Rodrigues DN, et al. Androgen receptor splice variant-7 expression emerges with castration resistance in prostate cancer. J Clin Invest. 2019;129: 192–208.

105. Xu D, Zhan Y, Qi Y, Cao B, Bai S, Xu W, et al. Androgen Receptor Splice Variants Dimerize to Transactivate Target Genes. Cancer Res. 2015;75: 3663–3671.

106. Roggero CM, Jin L, Cao S, Sonavane R, Kopplin NG, Ta HQ, et al. A detailed characterization of stepwise activation of the androgen receptor variant 7 in prostate cancer cells. Oncogene. 2021;40: 1106–1117.

107. Cato L, de Tribolet-Hardy J, Lee I, Rottenberg JT, Coleman I, Melchers D, et al. ARv7 Represses Tumor-Suppressor Genes in Castration-Resistant Prostate Cancer. Cancer Cell. 2019;35: 401-413.e6.

108. He Y, Lu J, Ye Z, Hao S, Wang L, Kohli M, et al. Androgen receptor splice variants bind to constitutively open chromatin and promote abiraterone-resistant growth of prostate cancer. Nucleic Acids Res. 2018;46: 1895–1911.

109. Chen Z, Wu D, Thomas-Ahner JM, Lu C, Zhao P, Zhang Q, et al. Diverse AR-V7 cistromes in castration-resistant prostate cancer are governed by HoxB13. Proc Natl Acad Sci U S A. 2018;115: 6810–6815.

110. Montgomery RB, Mostaghel EA, Vessella R, Hess DL, Kalhorn TF, Higano CS, et al.

Maintenance of intratumoral androgens in metastatic prostate cancer: a mechanism for castration-resistant tumor growth. Cancer Res. 2008;68: 4447–4454.

111. Cai C, Chen S, Ng P, Bubley GJ, Nelson PS, Mostaghel EA, et al. Intratumoral de novo steroid synthesis activates androgen receptor in castration-resistant prostate cancer and is upregulated by treatment with CYP17A1 inhibitors. Cancer Res. 2011;71: 6503–6513.

112. Robinson D, Van Allen EM, Wu Y-M, Schultz N, Lonigro RJ, Mosquera J-M, et al. Integrative Clinical Genomics of Advanced Prostate Cancer. Cell. 2015;161: 1215–1228.

113. PCF/SU2C International Prostate Cancer Dream Team, Armenia J, Wankowicz SAM, Liu D, Gao J, Kundra R, et al. The long tail of oncogenic drivers in prostate cancer. Nat Genet. 2018;50: 645–651.

114. Abeshouse A, Ahn J, Akbani R, Ally A, Amin S, Andry CD, et al. The Molecular Taxonomy of Primary Prostate Cancer. Cell. 11/2015;163: 1011–1025.

115. Baca SC, Takeda DY, Seo J-H, Hwang J, Ku SY, Arafeh R, et al. Reprogramming of the FOXA1 cistrome in treatment-emergent neuroendocrine prostate cancer. Nat Commun. 2021;12: 1979.

116. Augello MA, Liu D, Deonarine LD, Robinson BD, Huang D, Stelloo S, et al. CHD1 Loss Alters AR Binding at Lineage-Specific Enhancers and Modulates Distinct Transcriptional Programs to Drive Prostate Tumorigenesis. Cancer Cell. 04/2019;35: 603-617.e8.

117. Pomerantz MM, Li F, Takeda DY, Lenci R, Chonkar A, Chabot M, et al. The androgen receptor cistrome is extensively reprogrammed in human prostate tumorigenesis. Nat Genet. 11/2015;47: 1346–1351.

118. Wilson S, Fan L, Sahgal N, Qi J, Filipp FV. The histone demethylase *KDM3A* regulates the transcriptional program of the androgen receptor in prostate cancer cells. Oncotarget. 2017;8: 30328–30343.

119. Giles KA, Gould CM, Achinger-Kawecka J, Page SG, Kafer GR, Rogers S, et al. BRG1 knockdown inhibits proliferation through multiple cellular pathways in prostate cancer. Clin Epigenetics. 2021;13: 37.

120. Asangani IA, Dommeti VL, Wang X, Malik R, Cieslik M, Yang R, et al. Therapeutic targeting of BET bromodomain proteins in castration-resistant prostate cancer. Nature. 2014;510: 278–282.

121. Xiao L, Parolia A, Qiao Y, Bawa P, Eyunni S, Mannan R, et al. Targeting SWI/SNF ATPases in enhancer-addicted prostate cancer. Nature. 2021. doi:10.1038/s41586-021-04246-z

122. Schübeler D. Function and information content of DNA methylation. Nature. 2015;517: 321–326.

123. Michalak EM, Burr ML, Bannister AJ, Dawson MA. The roles of DNA, RNA and histone methylation in ageing and cancer. Nat Rev Mol Cell Biol. 2019;20: 573–589.

124. Yadav T, Quivy J-P, Almouzni G. Chromatin plasticity: A versatile landscape that underlies cell fate and identity. Science. 2018;361: 1332–1336.

125. Stillman B. Histone Modifications: Insights into Their Influence on Gene Expression. Cell. 2018;175: 6–9.

126. Flavahan WA, Gaskell E, Bernstein BE. Epigenetic plasticity and the hallmarks of cancer. Science. 2017;357. doi:10.1126/science.aal2380

127. Chang S, Yim S, Park H. The cancer driver genes IDH1/2, JARID1C/ KDM5C, and UTX/ KDM6A: crosstalk between histone demethylation and hypoxic reprogramming in cancer metabolism. Exp Mol Med. 2019;51: 1–17.

128. Falkenberg KJ, Johnstone RW. Histone deacetylases and their inhibitors in cancer, neurological diseases and immune disorders. Nat Rev Drug Discov. 9/2014;13: 673–691.

129. Greenberg MVC, Bourc'his D. The diverse roles of DNA methylation in mammalian development and disease. Nat Rev Mol Cell Biol. 2019;20: 590–607.

130. Sandoval J, Esteller M. Cancer epigenomics: beyond genomics. Curr Opin Genet Dev. 2012;22: 50–55.

131. Wu X, Zhang Y. TET-mediated active DNA demethylation: mechanism, function and beyond. Nat Rev Genet. 2017;18: 517–534.

132. Ren R, Horton JR, Zhang X, Blumenthal RM, Cheng X. Detecting and interpreting DNA methylation marks. Curr Opin Struct Biol. 2018;53: 88–99.

133. Barth TK, Imhof A. Fast signals and slow marks: the dynamics of histone modifications. Trends Biochem Sci. 2010;35: 618–626.

134. Guccione E, Richard S. The regulation, functions and clinical relevance of arginine methylation. Nat Rev Mol Cell Biol. 10/2019;20: 642–657.

135. Hwang JW, Cho Y, Bae G-U, Kim S-N, Kim YK. Protein arginine methyltransferases: promising targets for cancer therapy. Exp Mol Med. 2021;53: 788–808.

136. Blanc RS, Richard S. Arginine Methylation: The Coming of Age. Mol Cell. 2017;65: 8–24.

137. Zurita-Lopez CI, Sandberg T, Kelly R, Clarke SG. Human protein arginine methyltransferase 7 (PRMT7) is a type III enzyme forming ω-NG-monomethylated arginine residues. J Biol Chem. 2012;287: 7859–7870.

138. Walport LJ, Hopkinson RJ, Chowdhury R, Schiller R, Ge W, Kawamura A, et al. Arginine demethylation is catalysed by a subset of JmjC histone lysine demethylases. Nat Commun. 9/2016;7: 11974.

139. Wapenaar H, Dekker FJ. Histone acetyltransferases: challenges in targeting bi-substrate enzymes. Clin Epigenetics. 2016;8: 59.

140. Drazic A, Myklebust LM, Ree R, Arnesen T. The world of protein acetylation. Biochim Biophys Acta. 2016;1864: 1372–1401.

141. Avvakumov N, Côté J. The MYST family of histone acetyltransferases and their intimate links to cancer. Oncogene. 2007;26: 5395–5407.

142. Sapountzi V, Logan IR, Robson CN. Cellular functions of TIP60. Int J Biochem Cell Biol. 2006;38: 1496–1509.

143. Ogryzko VV, Schiltz RL, Russanova V, Howard BH, Nakatani Y. The transcriptional coactivators p300 and CBP are histone acetyltransferases. Cell. 1996;87: 953–959.

144. Mottamal M, Zheng S, Huang TL, Wang G. Histone deacetylase inhibitors in clinical studies as templates for new anticancer agents. Molecules. 2015;20: 3898–3941.

145. Delcuve GP, Khan DH, Davie JR. Roles of histone deacetylases in epigenetic regulation: emerging paradigms from studies with inhibitors. Clin Epigenetics. 2012;4: 5.

146. Maolanon AR, Madsen AS, Olsen CA. Innovative Strategies for Selective Inhibition of Histone Deacetylases. Cell Chem Biol. 2016;23: 759–768.

147. Soshnikova NV, Sheynov AA, Tatarskiy EV, Georgieva SG. The DPF Domain As a Unique

Structural Unit Participating in Transcriptional Activation, Cell Differentiation, and Malignant Transformation. Acta Naturae. 2020;12: 57–65.

148. Sabari BR, Zhang D, Allis CD, Zhao Y. Metabolic regulation of gene expression through histone acylations. Nat Rev Mol Cell Biol. 2017;18: 90–101.

149. Cochran AG, Conery AR, Sims RJ. Bromodomains: a new target class for drug development. Nat Rev Drug Discov. 8/2019;18: 609–628.

150. Khan A, Bridgers JB, Strahl BD. Expanding the Reader Landscape of Histone Acylation. Structure . 2017. pp. 571–573.

151. Donati B, Lorenzini E, Ciarrocchi A. BRD4 and Cancer: going beyond transcriptional regulation. Mol Cancer. 2018;17: 164.

152. Shi J, Vakoc CR. The mechanisms behind the therapeutic activity of BET bromodomain inhibition. Mol Cell. 2014;54: 728–736.

153. Swatek KN, Komander D. Ubiquitin modifications. Cell Res. 2016;26: 399–422.

154. Di Croce L, Helin K. Transcriptional regulation by Polycomb group proteins. Nat Struct Mol Biol. 2013;20: 1147–1155.

155. Minsky N, Shema E, Field Y, Schuster M, Segal E, Oren M. Monoubiquitinated H2B is associated with the transcribed region of highly expressed genes in human cells. Nat Cell Biol. 2008;10: 483–488.

156. Soares LM, Buratowski S. Histone Crosstalk: H2Bub and H3K4 Methylation. Mol Cell. 03/2013;49: 1019–1020.

157. Smeenk G, Mailand N. Writers, Readers, and Erasers of Histone Ubiquitylation in DNA Double-Strand Break Repair. Front Genet. 2016;7: 122.

158. Daou S, Barbour H, Ahmed O, Masclef L, Baril C, Sen Nkwe N, et al. Monoubiquitination of ASXLs controls the deubiquitinase activity of the tumor suppressor BAP1. Nat Commun. 2018;9: 4385.

159. Cao J, Yan Q. Histone Ubiquitination and Deubiquitination in Transcription, DNA Damage Response, and Cancer. Front Oncol. 2012;2. doi:10.3389/fonc.2012.00026

160. Cubeñas-Potts C, Matunis MJ. SUMO: A Multifaceted Modifier of Chromatin Structure and

Function. Dev Cell. 01/2013;24: 1–12.

161. Gill G. Something about SUMO inhibits transcription. Curr Opin Genet Dev. 2005;15: 536–541.

162. Hyun K, Jeon J, Park K, Kim J. Writing, erasing and reading histone lysine methylations. Exp Mol Med. 4/2017;49: e324–e324.

163. Zhou VW, Goren A, Bernstein BE. Charting histone modifications and the functional organization of mammalian genomes. Nat Rev Genet. 2011;12: 7–18.

164. van Mierlo G, Veenstra GJC, Vermeulen M, Marks H. The Complexity of PRC2 Subcomplexes. Trends Cell Biol. 2019;29: 660–671.

165. Rao RC, Dou Y. Hijacked in cancer: the KMT2 (MLL) family of methyltransferases. Nat Rev Cancer. 2015;15: 334–346.

166. Cenik BK, Shilatifard A. COMPASS and SWI/SNF complexes in development and disease. Nat Rev Genet. 2021;22: 38–58.

167. Wood K, Tellier M, Murphy S. DOT1L and H3K79 Methylation in Transcription and Genomic Stability. Biomolecules. 2018;8. doi:10.3390/biom8010011

168. Kaniskan HÜ, Martini ML, Jin J. Inhibitors of Protein Methyltransferases and Demethylases. Chem Rev. 2018;118: 989–1068.

169. Shi Y, Lan F, Matson C, Mulligan P, Whetstine JR, Cole PA, et al. Histone demethylation mediated by the nuclear amine oxidase homolog LSD1. Cell. 2004;119: 941–953.

170. Klose RJ, Kallin EM, Zhang Y. JmjC-domain-containing proteins and histone demethylation. Nat Rev Genet. 2006;7: 715–727.

171. Metzger E, Wissmann M, Yin N, Müller JM, Schneider R, Peters AHFM, et al. LSD1 demethylates repressive histone marks to promote androgen-receptor-dependent transcription. Nature. 2005;437: 436–439.

172. Anand R, Marmorstein R. Structure and mechanism of lysine-specific demethylase enzymes. J Biol Chem. 2007;282: 35425–35429.

173. Fang Y, Liao G, Yu B. LSD1/KDM1A inhibitors in clinical trials: advances and prospects. J Hematol Oncol. 2019;12: 129.

174. Punnia-Moorthy G, Hersey P, Emran AA, Tiffen J. Lysine Demethylases: Promising Drug Targets in Melanoma and Other Cancers. Front Genet. 2021;12: 680633.

175. Whetstine JR, Nottke A, Lan F, Huarte M, Smolikov S, Chen Z, et al. Reversal of histone lysine trimethylation by the JMJD2 family of histone demethylases. Cell. 2006;125: 467–481.

176. Williams ST, Walport LJ, Hopkinson RJ, Madden SK, Chowdhury R, Schofield CJ, et al. Studies on the catalytic domains of multiple JmjC oxygenases using peptide substrates. Epigenetics. 2014;9: 1596–1603.

177. Maes T, Carceller E, Salas J, Ortega A, Buesa C. Advances in the development of histone lysine demethylase inhibitors. Curr Opin Pharmacol. 2015;23: 52–60.

178. Horton JR, Upadhyay AK, Qi HH, Zhang X, Shi Y, Cheng X. Enzymatic and structural insights for substrate specificity of a family of jumonji histone lysine demethylases. Nat Struct Mol Biol. 2010;17: 38–43.

179. Xiang Y, Zhu Z, Han G, Lin H, Xu L, Chen CD. JMJD3 is a histone H3K27 demethylase. Cell Res. 2007;17: 850–857.

180. Seward DJ, Cubberley G, Kim S, Schonewald M, Zhang L, Tripet B, et al. Demethylation of trimethylated histone H3 Lys4 in vivo by JARID1 JmjC proteins. Nat Struct Mol Biol. 2007;14: 240–242.

181. Dorosz J, Kristensen LH, Aduri NG, Mirza O, Lousen R, Bucciarelli S, et al. Molecular architecture of the Jumonji C family histone demethylase KDM5B. Sci Rep. 2019;9: 4019.

182. D'Oto A, Tian Q-W, Davidoff AM, Yang J. Histone demethylases and their roles in cancer epigenetics. J Med Oncol Ther. 2016;1: 34–40.

183. Park SY, Park J-W, Chun Y-S. Jumonji histone demethylases as emerging therapeutic targets. Pharmacol Res. 2016;105: 146–151.

184. Thinnes CC, England KS, Kawamura A, Chowdhury R, Schofield CJ, Hopkinson RJ. Targeting histone lysine demethylases - progress, challenges, and the future. Biochim Biophys Acta. 2014;1839: 1416–1432.

185. Rose NR, Woon ECY, Tumber A, Walport LJ, Chowdhury R, Li XS, et al. Plant growth regulator daminozide is a selective inhibitor of human KDM2/7 histone demethylases. J

Med Chem. 2012;55: 6639–6643.

186. Kawamura A, Münzel M, Kojima T, Yapp C, Bhushan B, Goto Y, et al. Highly selective inhibition of histone demethylases by de novo macrocyclic peptides. Nat Commun. 2017;8: 14773.

187. Souto JA, Sarno F, Nebbioso A, Papulino C, Álvarez R, Lombino J, et al. A New Family of Jumonji C Domain-Containing KDM Inhibitors Inspired by Natural Product Purpurogallin. Front Chem. 2020;8: 312.

188. Clapier CR, Iwasa J, Cairns BR, Peterson CL. Mechanisms of action and regulation of ATP-dependent chromatin-remodelling complexes. Nat Rev Mol Cell Biol. 2017;18: 407–422.

189. Hasan N, Ahuja N. The Emerging Roles of ATP-Dependent Chromatin Remodeling Complexes in Pancreatic Cancer. Cancers . 2019;11. doi:10.3390/cancers11121859

190. Kadoch C, Crabtree GR. Mammalian SWI/SNF chromatin remodeling complexes and cancer: Mechanistic insights gained from human genomics. Sci Adv. 2015;1: e1500447.

191. Innis SM, Cabot B. GBAF, a small BAF sub-complex with big implications: a systematic review. Epigenetics Chromatin. 2020;13: 48.

192. Centore RC, Sandoval GJ, Soares LMM, Kadoch C, Chan HM. Mammalian SWI/SNF Chromatin Remodeling Complexes: Emerging Mechanisms and Therapeutic Strategies. Trends Genet. 2020;36: 936–950.

193. Mashtalir N, Dao HT, Sankar A, Liu H, Corin AJ, Bagert JD, et al. Chromatin landscape signals differentially dictate the activities of mSWI/SNF family complexes. Science. 2021;373: 306–315.

194. Mashtalir N, D'Avino AR, Michel BC, Luo J, Pan J, Otto JE, et al. Modular Organization and Assembly of SWI/SNF Family Chromatin Remodeling Complexes. Cell. 2018;175: 1272-1288.e20.

195. Pan J, McKenzie ZM, D'Avino AR, Mashtalir N, Lareau CA, St Pierre R, et al. The ATPase module of mammalian SWI/SNF family complexes mediates subcomplex identity and catalytic activity-independent genomic targeting. Nat Genet. 2019;51: 618–626.

196. Alfert A, Moreno N, Kerl K. The BAF complex in development and disease. Epigenetics Chromatin. 2019;12: 19.

197. Yoo AS, Staahl BT, Chen L, Crabtree GR. MicroRNA-mediated switching of chromatin-remodelling complexes in neural development. Nature. 2009;460: 642–646.

198. Ho L, Ronan JL, Wu J, Staahl BT, Chen L, Kuo A, et al. An embryonic stem cell chromatin remodeling complex, esBAF, is essential for embryonic stem cell self-renewal and pluripotency. Proc Natl Acad Sci U S A. 2009;106: 5181–5186.

199. Wanior M, Krämer A, Knapp S, Joerger AC. Exploiting vulnerabilities of SWI/SNF chromatin remodelling complexes for cancer therapy. Oncogene. 2021;40: 3637–3654.

200. Mashtalir N, Suzuki H, Farrell DP, Sankar A, Luo J, Filipovski M, et al. A Structural Model of the Endogenous Human BAF Complex Informs Disease Mechanisms. Cell. 2020;183: 802-817.e24.

201. Chen G, Zhou H, Liu B, Wang Y, Zhao J, Giancotti FG, et al. A heterotrimeric SMARCB1-SMARCC2 subcomplex is required for the assembly and tumor suppression function of the BAF chromatin-remodeling complex. Cell Discov. 2020;6: 66.

202. Schick S, Rendeiro AF, Runggatscher K, Ringler A, Boidol B, Hinkel M, et al. Systematic characterization of BAF mutations provides insights into intracomplex synthetic lethalities in human cancers. Nat Genet. 2019;51: 1399–1410.

203. Shain AH, Pollack JR. The spectrum of SWI/SNF mutations, ubiquitous in human cancers. PLoS One. 2013;8: e55119.

204. Grasso CS, Wu Y-M, Robinson DR, Cao X, Dhanasekaran SM, Khan AP, et al. The mutational landscape of lethal castration-resistant prostate cancer. Nature. 2012;487: 239–243.

205. Yegnasubramanian S, De Marzo AM, Nelson WG. Prostate Cancer Epigenetics: From Basic Mechanisms to Clinical Implications. Cold Spring Harb Perspect Med. 2019;9. doi:10.1101/cshperspect.a030445

206. Ruggero K, Farran-Matas S, Martinez-Tebar A, Aytes A. Epigenetic Regulation in Prostate Cancer Progression. Curr Mol Bio Rep. 6/2018;4: 101–115.

207. Simon Baumgart, Bernard Haendler. Exploiting Epigenetic Alterations in Prostate Cancer. IJMS. 2017;18: 1017.

208. Bianco-Miotto T, Chiam K, Buchanan G, Jindal S, Day TK, Thomas M, et al. Global levels

of specific histone modifications and an epigenetic gene signature predict prostate cancer progression and development. Cancer Epidemiol Biomarkers Prev. 2010;19: 2611–2622.

209. Ellinger J, Kahl P, von der Gathen J, Rogenhofer S, Heukamp LC, Gütgemann I, et al. Global levels of histone modifications predict prostate cancer recurrence. Prostate. 2010;70: 61–69.

210. Zhao SG, Chen WS, Li H, Foye A, Zhang M, Sjöström M, et al. The DNA methylation landscape of advanced prostate cancer. Nat Genet. 2020;52: 778–789.

211. Şeref C, Acar Ö, Kılıç M, Vural M, Sağlıcan Y, Saraç H, et al. Histologically benign PI-RADS 4 and 5 lesions contain cancer-associated epigenetic alterations. Prostate. 2021. doi:10.1002/pros.24255

212. Stelloo S, Nevedomskaya E, Kim Y, Schuurman K, Valle-Encinas E, Lobo J, et al. Integrative epigenetic taxonomy of primary prostate cancer. Nat Commun. 2018;9: 4900.

213. Launonen K-M, Paakinaho V, Sigismondo G, Malinen M, Sironen R, Hartikainen JM, et al. Chromatin-directed proteomics-identified network of endogenous androgen receptor in prostate cancer cells. Oncogene. 2021;40: 4567–4579.

214. Paltoglou S, Das R, Townley SL, Hickey TE, Tarulli GA, Coutinho I, et al. Novel Androgen Receptor Coregulator GRHL2 Exerts Both Oncogenic and Antimetastatic Functions in Prostate Cancer. Cancer Res. 2017;77: 3417–3430.

215. Stelloo S, Nevedomskaya E, Kim Y, Hoekman L, Bleijerveld OB, Mirza T, et al. Endogenous androgen receptor proteomic profiling reveals genomic subcomplex involved in prostate tumorigenesis. Oncogene. 2018;37: 313–322.

216. Gao L, Alumkal J. Epigenetic regulation of androgen receptor signaling in prostate cancer. Epigenetics. 2010;5: 100–104.

217. Jerónimo C, Bastian PJ, Bjartell A, Carbone GM, Catto JWF, Clark SJ, et al. Epigenetics in Prostate Cancer: Biologic and Clinical Relevance. Eur Urol. 10/2011;60: 753–766.

218. Yegnasubramanian S, Kowalski J, Gonzalgo ML, Zahurak M, Piantadosi S, Walsh PC, et al. Hypermethylation of CpG islands in primary and metastatic human prostate cancer. Cancer Res. 2004;64: 1975–1986.

219. Park JY. Promoter hypermethylation in prostate cancer. Cancer Control. 2010;17: 245–255.

220. Jeronimo C, Henrique R. A Quantitative Promoter Methylation Profile of Prostate Cancer. Vol. 2004;10: 8472–8478.

221. Nickerson ML, Das S, Im KM, Turan S, Berndt SI, Li H, et al. TET2 binds the androgen receptor and loss is associated with prostate cancer. Oncogene. 4/2017;36: 2172–2183.

222. Takayama K-I, Misawa A, Suzuki T, Takagi K, Hayashizaki Y, Fujimura T, et al. TET2 repression by androgen hormone regulates global hydroxymethylation status and prostate cancer progression. Nat Commun. 2015;6: 8219.

223. Valdés-Mora F, Clark SJ. Prostate cancer epigenetic biomarkers: next-generation technologies. Oncogene. 2015;34: 1609–1618.

224. Seligson DB, Horvath S, Shi T, Yu H, Tze S, Grunstein M, et al. Global histone modification patterns predict risk of prostate cancer recurrence. Nature. 2005;435: 1262–1266.

225. Pomerantz MM, Qiu X, Zhu Y, Takeda DY, Pan W, Baca SC, et al. Prostate cancer reactivates developmental epigenomic programs during metastatic progression. Nat Genet. 2020;52: 790–799.

226. Yu J, Yu J, Rhodes DR, Tomlins SA, Cao X, Chen G, et al. A polycomb repression signature in metastatic prostate cancer predicts cancer outcome. Cancer Res. 2007;67: 10657–10663.

227. van Leenders GJLH, Dukers D, Hessels D, van den Kieboom SWM, Hulsbergen CA, Witjes JA, et al. Polycomb-Group Oncogenes EZH2, BMI1, and RING1 Are Overexpressed in Prostate Cancer With Adverse Pathologic and Clinical Features. Eur Urol. 08/2007;52: 455–463.

228. Varambally S, Dhanasekaran SM, Zhou M, Barrette TR, Kumar-Sinha C, Sanda MG, et al. The polycomb group protein EZH2 is involved in progression of prostate cancer. Nature. 10/2002;419: 624–629.

229. Zhu S, Zhao D, Yan L, Jiang W, Kim J-S, Gu B, et al. BMI1 regulates androgen receptor in prostate cancer independently of the polycomb repressive complex 1. Nat Commun. 12/2018;9: 500.

230. Bryant RJ, Cross NA, Eaton CL, Hamdy FC, Cunliffe VT. EZH2 promotes proliferation and invasiveness of prostate cancer cells. Prostate. 2007;67: 547–556.

231. Xu K, Wu ZJ, Groner AC, He HH, Cai C, Lis RT, et al. EZH2 Oncogenic Activity in

Castration-Resistant Prostate Cancer Cells Is Polycomb-Independent. Science. 2012;338: 1465–1469.

232. Kong D, Heath E, Chen W, Cher ML, Powell I, Heilbrun L, et al. Loss of Let-7 Up-Regulates EZH2 in Prostate Cancer Consistent with the Acquisition of Cancer Stem Cell Signatures That Are Attenuated by BR-DIM. Katoh M, editor. PLoS One. 2012;7: e33729.

233. Dardenne E, Beltran H, Benelli M, Gayvert K, Berger A, Puca L, et al. N-Myc Induces an EZH2-Mediated Transcriptional Program Driving Neuroendocrine Prostate Cancer. Cancer Cell. 10/2016;30: 563–577.

234. Kim J, Lee Y, Lu X, Song B, Fong K-W, Cao Q, et al. Polycomb- and Methylation-Independent Roles of EZH2 as a Transcription Activator. Cell Rep. 2018;25: 2808-2820.e4.

235. Zhang Z, Zhou C, Li X, Barnes SD, Deng S, Hoover E, et al. Loss of CHD1 Promotes Heterogeneous Mechanisms of Resistance to AR-Targeted Therapy via Chromatin Dysregulation. Cancer Cell. 04/2020;37: 584-598.e11.

236. Malik R, Khan AP, Asangani IA, Cieślik M, Prensner JR, Wang X, et al. Targeting the MLL complex in castration-resistant prostate cancer. Nat Med. 2015;21: 344–352.

237. Jin L, Garcia J, Chan E, de la Cruz C, Segal E, Merchant M, et al. Therapeutic Targeting of the CBP/p300 Bromodomain Blocks the Growth of Castration-Resistant Prostate Cancer. Cancer Res. 2017;77: 5564–5575.

238. Xu S, Fan L, Jeon H-Y, Zhang F, Cui X, Mickle MB, et al. p300-Mediated Acetylation of Histone Demethylase JMJD1A Prevents Its Degradation by Ubiquitin Ligase STUB1 and Enhances Its Activity in Prostate Cancer. Cancer Res. 2020;80: 3074–3087.

239. Santer FR, Höschele PPS, Oh SJ, Erb HHH, Bouchal J, Cavarretta IT, et al. Inhibition of the acetyltransferases p300 and CBP reveals a targetable function for p300 in the survival and invasion pathways of prostate cancer cell lines. Mol Cancer Ther. 2011;10: 1644–1655.

240. Mounir Z, Korn JM, Westerling T, Lin F, Kirby CA, Schirle M, et al. ERG signaling in prostate cancer is driven through PRMT5-dependent methylation of the Androgen Receptor. Elife. 2016;5. doi:10.7554/eLife.13964

241. Wyce A, Degenhardt Y, Bai Y, Le B, Korenchuk S, Crouthame M-C, et al. Inhibition of BET bromodomain proteins as a therapeutic approach in prostate cancer. Oncotarget. 2013;4: 2419–2429.

242. Chan SC, Selth LA, Li Y, Nyquist MD, Miao L, Bradner JE, et al. Targeting chromatin binding regulation of constitutively active AR variants to overcome prostate cancer resistance to endocrine-based therapies. Nucleic Acids Res. 2015;43: 5880–5897.

243. Pawar A, Gollavilli PN, Wang S, Asangani IA. Resistance to BET Inhibitor Leads to Alternative Therapeutic Vulnerabilities in Castration-Resistant Prostate Cancer. Cell Rep. 02/2018;22: 2236–2245.

244. Cai C, He HH, Gao S, Chen S, Yu Z, Gao Y, et al. Lysine-Specific Demethylase 1 Has Dual Functions as a Major Regulator of Androgen Receptor Transcriptional Activity. Cell Rep. 2014;9: 1618–1627.

245. Shi Y-J, Matson C, Lan F, Iwase S, Baba T, Shi Y. Regulation of LSD1 histone demethylase activity by its associated factors. Mol Cell. 2005;19: 857–864.

246. Wissmann M, Yin N, Müller JM, Greschik H, Fodor BD, Jenuwein T, et al. Cooperative demethylation by JMJD2C and LSD1 promotes androgen receptor-dependent gene expression. Nat Cell Biol. 3/2007;9: 347–353.

247. Metzger E, Yin N, Wissmann M, Kunowska N, Fischer K, Friedrichs N, et al. Phosphorylation of histone H3 at threonine 11 establishes a novel chromatin mark for transcriptional regulation. Nat Cell Biol. 2008;10: 53–60.

248. Metzger E, Imhof A, Patel D, Kahl P, Hoffmeyer K, Friedrichs N, et al. Phosphorylation of histone H3T6 by PKCβ I controls demethylation at histone H3K4. Nature. 2010;464: 792–796.

249. Metzger E, Willmann D, McMillan J, Forne I, Metzger P, Gerhardt S, et al. Assembly of methylated KDM1A and CHD1 drives androgen receptor–dependent transcription and translocation. Nat Struct Mol Biol. 2/2016;23: 132–139.

250. Cai C, He HH, Chen S, Coleman I, Wang H, Fang Z, et al. Androgen Receptor Gene Expression in Prostate Cancer Is Directly Suppressed by the Androgen Receptor Through Recruitment of Lysine-Specific Demethylase 1. Cancer Cell. 10/2011;20: 457–471.

251. Sehrawat A, Gao L, Wang Y, Bankhead A, McWeeney SK, King CJ, et al. LSD1 activates a lethal prostate cancer gene network independently of its demethylase function. Proc Natl Acad Sci U S A. 2018;115: E4179–E4188.

252. Willmann D, Lim S, Wetzel S, Metzger E, Jandausch A, Wilk W, et al. Impairment of

prostate cancer cell growth by a selective and reversible lysine-specific demethylase 1 inhibitor. Int J Cancer. 2012;131: 2704–2709.

253. Liang Y, Ahmed M, Guo H, Soares F, Hua JT, Gao S, et al. LSD1-Mediated Epigenetic Reprogramming Drives CENPE Expression and Prostate Cancer Progression. Cancer Res. 2017;77: 5479–5490.

254. Yamane K, Toumazou C, Tsukada Y-I, Erdjument-Bromage H, Tempst P, Wong J, et al. JHDM2A, a JmjC-Containing H3K9 Demethylase, Facilitates Transcription Activation by Androgen Receptor. Cell. 05/2006;125: 483–495.

255. Lee H-Y, Yang EG, Park H. Hypoxia enhances the expression of prostate-specific antigen by modifying the quantity and catalytic activity of Jumonji C domain-containing histone demethylases. Carcinogenesis. 2013;34: 2706–2715.

256. Fan L, Peng G, Sahgal N, Fazli L, Gleave M, Zhang Y, et al. Regulation of c-Myc expression by the histone demethylase JMJD1A is essential for prostate cancer cell growth and survival. Oncogene. 2016;35: 2441–2452.

257. Saraç H, Morova T, Pires E, McCullagh J, Kaplan A, Cingöz A, et al. Systematic characterization of chromatin modifying enzymes identifies KDM3B as a critical regulator in castration resistant prostate cancer. Oncogene. 3/2020;39: 2187–2201.

258. Fan L, Zhang F, Xu S, Cui X, Hussain A, Fazli L, et al. Histone demethylase JMJD1A promotes alternative splicing of AR variant 7 (AR-V7) in prostate cancer cells. Proc Natl Acad Sci U S A. 2018;115: E4584–E4593.

259. Fan L, Xu S, Zhang F, Cui X, Fazli L, Gleave M, et al. Histone demethylase JMJD1A promotes expression of DNA repair factors and radio-resistance of prostate cancer cells. Cell Death Dis. 2020;11: 214.

260. Lin C-Y, Wang B-J, Chen B-C, Tseng J-C, Jiang SS, Tsai KK, et al. Histone Demethylase KDM4C Stimulates the Proliferation of Prostate Cancer Cells via Activation of AKT and c-Myc. Cancers . 2019;11. doi:10.3390/cancers11111785

261. Shin S, Janknecht R. Activation of androgen receptor by histone demethylases JMJD2A and JMJD2D. Biochem Biophys Res Commun. 08/2007;359: 742–746.

262. Kim T-D, Jin F, Shin S, Oh S, Lightfoot SA, Grande JP, et al. Histone demethylase JMJD2A drives prostate tumorigenesis through transcription factor ETV1. J Clin Invest. 2016;126:

706–720.

263. Kim T-D, Shin S, Janknecht R. ETS transcription factor ERG cooperates with histone demethylase KDM4A. Oncol Rep. 06/2016;35: 3679–3688.

264. Duan L, Rai G, Roggero C, Zhang Q-J, Wei Q, Ma SH, et al. KDM4/JMJD2 Histone Demethylase Inhibitors Block Prostate Tumor Growth by Suppressing the Expression of AR and BMYB-Regulated Genes. Chem Biol. 09/2015;22: 1185–1196.

265. Coffey K, Rogerson L, Ryan-Munden C, Alkharaif D, Stockley J, Heer R, et al. The lysine demethylase, KDM4B, is a key molecule in androgen receptor signalling and turnover. Nucleic Acids Res. 4/2013;41: 4433–4446.

266. Li N, Dhar SS, Chen T-Y, Kan P-Y, Wei Y, Kim J-H, et al. JARID1D Is a Suppressor and Prognostic Marker of Prostate Cancer Invasion and Metastasis. Cancer Res. 2016;76: 831–843.

267. Komura K, Jeong SH, Hinohara K, Qu F, Wang X, Hiraki M, et al. Resistance to docetaxel in prostate cancer is associated with androgen receptor activation and loss of KDM5D expression. Proc Natl Acad Sci U S A. 2016;113: 6259–6264.

268. Xiang Y, Zhu Z, Han G, Ye X, Xu B, Peng Z, et al. JARID1B is a histone H3 lysine 4 demethylase up-regulated in prostate cancer. Proceedings of the National Academy of Sciences. 2007;104: 19226–19231.

269. Stein J, Majores M, Rohde M, Lim S, Schneider S, Krappe E, et al. KDM5C Is Overexpressed in Prostate Cancer and Is a Prognostic Marker for Prostate-Specific Antigen-Relapse Following Radical Prostatectomy. Am J Pathol. 09/2014;184: 2430–2437.

270. Morozov VM, Li Y, Clowers MM, Ishov AM. Inhibitor of H3K27 demethylase JMJD3/UTX GSK-J4 is a potential therapeutic option for castration resistant prostate cancer. Oncotarget. 2017;8: 62131–62142.

271. Daures M, Idrissou M, Judes G, Rifaï K, Penault-Llorca F, Bignon Y-J, et al. A new metabolic gene signature in prostate cancer regulated by JMJD3 and EZH2. Oncotarget. 2018;9: 23413–23425.

272. Cao Z, Shi X, Tian F, Fang Y, Wu JB, Mrdenovic S, et al. KDM6B is an androgen regulated gene and plays oncogenic roles by demethylating H3K27me3 at cyclin D1 promoter in prostate cancer. Cell Death Dis. 2021;12: 2.

273. Sun D, Layer R, Mueller AC, Cichewicz MA, Negishi M, Paschal BM, et al. Regulation of several androgen-induced genes through the repression of the miR-99a/let-7c/miR-125b-2 miRNA cluster in prostate cancer cells. Oncogene. 2014;33: 1448–1457.

274. Dutta A, Le Magnen C, Mitrofanova A, Ouyang X, Califano A, Abate-Shen C. Identification of an NKX3.1-G9a-UTY transcriptional regulatory network that controls prostate differentiation. Science. 2016;352: 1576–1580.

275. Björkman M, Östling P, Härmä V, Virtanen J, Mpindi J-P, Rantala J, et al. Systematic knockdown of epigenetic enzymes identifies a novel histone demethylase PHF8 overexpressed in prostate cancer with an impact on cell proliferation, migration and invasion. Oncogene. 7/2012;31: 3444–3456.

276. Ma Q, Chen Z, Jia G, Lu X, Xie X, Jin W. The histone demethylase PHF8 promotes prostate cancer cell growth by activating the oncomiR miR-125b. Onco Targets Ther. 2015;8: 1979–1988.

277. Tong D, Liu Q, Liu G, Yuan W, Wang L, Guo Y, et al. The HIF/PHF8/AR axis promotes prostate cancer progression. Oncogenesis. 12/2016;5: e283–e283.

278. Lee K-H, Hong S, Kang M, Jeong CW, Ku JH, Kim H-H, et al. Histone demethylase KDM7A controls androgen receptor activity and tumor growth in prostate cancer. Int J Cancer. 2018;143: 2849–2861.

279. Ozawa M, Fukuda T, Sakamoto R, Honda H, Yoshida N. The Histone Demethylase FBXL10 Regulates the Proliferation of Spermatogonia and Ensures Long-Term Sustainable Spermatogenesis in Mice. Biol Reprod. 2016;94: 92.

280. Ge R, Wang Z, Zeng Q, Xu X, Olumi AF. F-box protein 10, an NF-κB-dependent anti-apoptotic protein, regulates TRAIL-induced apoptosis through modulating c-Fos/c-FLIP pathway. Cell Death Differ. 2011;18: 1184–1195.

281. Wang H-J, Pochampalli M, Wang L-Y, Zou JX, Li P-S, Hsu S-C, et al. KDM8/JMJD5 as a dual coactivator of AR and PKM2 integrates AR/EZH2 network and tumor metabolism in CRPC. Oncogene. 2019;38: 17–32.

282. Sinha KM, Bagheri-Yarmand R, Lahiri S, Lu Y, Zhang M, Amra S, et al. Oncogenic and osteolytic functions of histone demethylase NO66 in castration-resistant prostate cancer. Oncogene. 2019;38: 5038–5049.

283. Kadoch C, Hargreaves DC, Hodges C, Elias L, Ho L, Ranish J, et al. Proteomic and bioinformatic analysis of mammalian SWI/SNF complexes identifies extensive roles in human malignancy. Nat Genet. 2013;45: 592–601.

284. Cyrta J, Augspach A, De Filippo MR, Prandi D, Thienger P, Benelli M, et al. Role of specialized composition of SWI/SNF complexes in prostate cancer lineage plasticity. Nat Commun. 2020;11: 5549.

285. Barbieri CE, Baca SC, Lawrence MS, Demichelis F, Blattner M, Theurillat J-P, et al. Exome sequencing identifies recurrent SPOP, FOXA1 and MED12 mutations in prostate cancer. Nat Genet. 6/2012;44: 685–689.

286. Sun A, Tawfik O, Gayed B, Thrasher JB, Hoestje S, Li C, et al. Aberrant expression of SWI/SNF catalytic subunits BRG1/BRM is associated with tumor development and increased invasiveness in prostate cancers. Prostate. 2007;67: 203–213.

287. Muthuswami R, Bailey L, Rakesh R, Imbalzano AN, Nickerson JA, Hockensmith JW. BRG1 is a prognostic indicator and a potential therapeutic target for prostate cancer. J Cell Physiol. 2019;234: 15194–15205.

288. Ding Y, Li N, Dong B, Guo W, Wei H, Chen Q, et al. Chromatin remodeling ATPase BRG1 and PTEN are synthetic lethal in prostate cancer. J Clin Invest. 2019;129: 759–773.

289. Sandoval GJ, Pulice JL, Pakula H, Schenone M, Takeda DY, Pop M, et al. Binding of TMPRSS2-ERG to BAF Chromatin Remodeling Complexes Mediates Prostate Oncogenesis. Mol Cell. 2018;71: 554-566.e7.

290. Lv D, Song X, Huang B, Yu Y-Z, Shu F, Wang C, et al. HMGB1 Promotes Prostate Cancer Development and Metastasis by Interacting with Brahma-Related Gene 1 and Activating the Akt Signaling Pathway. Theranostics. 2019;9: 5166–5182.

291. Dai Y, Ngo D, Jacob J, Forman LW, Faller DV. Prohibitin and the SWI/SNF ATPase subunit BRG1 are required for effective androgen antagonist-mediated transcriptional repression of androgen receptor-regulated genes. Carcinogenesis. 2008;29: 1725–1733.

292. Shen H, Powers N, Saini N, Comstock CES, Sharma A, Weaver K, et al. The SWI/SNF ATPase Brm Is a Gatekeeper of Proliferative Control in Prostate Cancer. Cancer Res. 2008;68: 10154–10162.

293. Giles KA, Gould CM, Du Q, Skvortsova K, Song JZ, Maddugoda MP, et al. Integrated

epigenomic analysis stratifies chromatin remodellers into distinct functional groups. Epigenetics Chromatin. 2019;12: 12.

294. Heebøll S, Borre M, Ottosen PD, Andersen CL, Mansilla F, Dyrskjøt L, et al. SMARCC1 expression is upregulated in prostate cancer and positively correlated with tumour recurrence and dedifferentiation. Histol Histopathol. 2008;23: 1069–1076.

295. Hansen RL, Heeboll S, Ottosen PD, Dyrskjøt L, Borre M. Smarcc1 expression: A significant predictor of disease-specific survival in patients with clinically localized prostate cancer treated with no intention to cure. Scand J Urol Nephrol. 2011;45: 91–96.

296. Mota STS, Vecchi L, Zóia MAP, Oliveira FM, Alves DA, Dornelas BC, et al. New Insights into the Role of Polybromo-1 in Prostate Cancer. Int J Mol Sci. 2019;20: 2852.

297. van de Wijngaart DJ, Dubbink HJ, Molier M, de Vos C, Trapman J, Jenster G. Functional Screening of FxxLF-Like Peptide Motifs Identifies SMARCD1/BAF60a as an Androgen Receptor Cofactor that Modulates TMPRSS2 Expression. Mol Endocrinol. 2009;23: 1776–1786.

298. Alpsoy A, Utturkar SM, Carter BC, Dhiman A, Torregrosa-Allen SE, Currie MP, et al. BRD9 Is a Critical Regulator of Androgen Receptor Signaling and Prostate Cancer Progression. Cancer Res. 2021;81: 820–833.

299. Meister G, Tuschl T. Mechanisms of gene silencing by double-stranded RNA. Nature. 2004;431: 343–349.

300. O'Brien J, Hayder H, Zayed Y, Peng C. Overview of MicroRNA biogenesis, mechanisms of actions, and circulation. Front Endocrinol (Lausanne). 2018;9: 402.

301. Davidson BL, McCray PB Jr. Current prospects for RNA interference-based therapies. Nat Rev Genet. 2011;12: 329–340.

302. Amarzguioui M, Rossi JJ, Kim D. Approaches for chemically synthesized siRNA and vector-mediated RNAi. FEBS Lett. 2005;579: 5974–5981.

303. Kim DH, Rossi JJ. Strategies for silencing human disease using RNA interference. Nat Rev Genet. 2007;8: 173–184.

304. Lam JKW, Chow MYT, Zhang Y, Leung SWS. siRNA Versus miRNA as Therapeutics for Gene Silencing. Mol Ther Nucleic Acids. 2015;4: e252.

305. Schlabach MR, Luo J, Solimini NL, Hu G, Xu Q, Li MZ, et al. Cancer proliferation gene discovery through functional genomics. Science. 2008;319: 620–624.

306. Mendes-Pereira AM, Sims D, Dexter T, Fenwick K, Assiotis I, Kozarewa I, et al. Genome-wide functional screen identifies a compendium of genes affecting sensitivity to tamoxifen. Proc Natl Acad Sci U S A. 2012;109: 2730–2735.

307. Kodama M, Kodama T, Newberg JY, Katayama H, Kobayashi M, Hanash SM, et al. In vivo loss-of-function screens identify KPNB1 as a new druggable oncogene in epithelial ovarian cancer. Proc Natl Acad Sci U S A. 2017;114: E7301–E7310.

308. Evers B, Jastrzebski K, Heijmans JPM, Grernrum W, Beijersbergen RL, Bernards R. CRISPR knockout screening outperforms shRNA and CRISPRi in identifying essential genes. Nat Biotechnol. 2016;34: 631–633.

309. Grimm D, Streetz KL, Jopling CL, Storm TA, Pandey K, Davis CR, et al. Fatality in mice due to oversaturation of cellular microRNA/short hairpin RNA pathways. Nature. 2006;441: 537–541.

310. de Veer MJ, Sledz CA, Williams BRG. Detection of foreign RNA: implications for RNAi. Immunol Cell Biol. 2005;83: 224–228.

311. Cong L, Zhou R, Kuo Y-C, Cunniff M, Zhang F. Comprehensive interrogation of natural TALE DNA-binding modules and transcriptional repressor domains. Nat Commun. 2012;3: 968.

312. Cox DBT, Platt RJ, Zhang F. Therapeutic genome editing: prospects and challenges. Nat Med. 2015;21: 121–131.

313. Komor AC, Badran AH, Liu DR. CRISPR-based technologies for the manipulation of eukaryotic genomes. Cell. 2017;169: 559.

314. Doudna JA, Charpentier E. Genome editing. The new frontier of genome engineering with CRISPR-Cas9. Science. 2014;346: 1258096.

315. Makarova KS, Haft DH, Barrangou R, Brouns SJJ, Charpentier E, Horvath P, et al. Evolution and classification of the CRISPR-Cas systems. Nat Rev Microbiol. 2011;9: 467–477.

316. Makarova KS, Wolf YI, Alkhnbashi OS, Costa F, Shah SA, Saunders SJ, et al. An updated

evolutionary classification of CRISPR-Cas systems. Nat Rev Microbiol. 2015;13: 722–736.

317. Makarova KS, Wolf YI, Iranzo J, Shmakov SA, Alkhnbashi OS, Brouns SJJ, et al. Evolutionary classification of CRISPR-Cas systems: a burst of class 2 and derived variants. Nat Rev Microbiol. 2020;18: 67–83.

318. Hsu PD, Lander ES, Zhang F. Development and applications of CRISPR-Cas9 for genome engineering. Cell. 2014;157: 1262–1278.

319. Nishimasu H, Ran FA, Hsu PD, Konermann S, Shehata SI, Dohmae N, et al. Crystal structure of Cas9 in complex with guide RNA and target DNA. Cell. 2014;156: 935–949.

320. Anders C, Niewoehner O, Duerst A, Jinek M. Structural basis of PAM-dependent target DNA recognition by the Cas9 endonuclease. Nature. 2014;513: 569–573.

321. Mali P, Yang L, Esvelt KM, Aach J, Guell M, DiCarlo JE, et al. RNA-guided human genome engineering via Cas9. Science. 2013;339: 823–826.

322. Cong L, Ran FA, Cox D, Lin S, Barretto R, Habib N, et al. Multiplex genome engineering using CRISPR/Cas systems. Science. 2013;339: 819–823.

323. Yu C, Liu Y, Ma T, Liu K, Xu S, Zhang Y, et al. Small molecules enhance CRISPR genome editing in pluripotent stem cells. Cell Stem Cell. 2015;16: 142–147.

324. Li G, Liu D, Zhang X, Quan R, Zhong C, Mo J, et al. Suppressing Ku70/Ku80 expression elevates homology-directed repair efficiency in primary fibroblasts. Int J Biochem Cell Biol. 2018;99: 154–160.

325. Robert F, Barbeau M, Éthier S, Dostie J, Pelletier J. Pharmacological inhibition of DNA-PK stimulates Cas9-mediated genome editing. Genome Med. 2015;7: 93.

326. Maruyama T, Dougan SK, Truttmann MC, Bilate AM, Ingram JR, Ploegh HL. Increasing the efficiency of precise genome editing with CRISPR-Cas9 by inhibition of nonhomologous end joining. Nat Biotechnol. 2015;33: 538–542.

327. Chu VT, Weber T, Wefers B, Wurst W, Sander S, Rajewsky K, et al. Increasing the efficiency of homology-directed repair for CRISPR-Cas9-induced precise gene editing in mammalian cells. Nat Biotechnol. 2015;33: 543–548.

328. Hu JH, Miller SM, Geurts MH, Tang W, Chen L, Sun N, et al. Evolved Cas9 variants with broad PAM compatibility and high DNA specificity. Nature. 2018;556: 57–63.

329. Doench JG, Fusi N, Sullender M, Hegde M, Vaimberg EW, Donovan KF, et al. Optimized sgRNA design to maximize activity and minimize off-target effects of CRISPR-Cas9. Nat Biotechnol. 2016;34: 184–191.

330. Uddin F, Rudin CM, Sen T. CRISPR Gene Therapy: Applications, Limitations, and Implications for the Future. Front Oncol. 2020;10: 1387.

331. Wang T, Wei JJ, Sabatini DM, Lander ES. Genetic screens in human cells using the CRISPR-Cas9 system. Science. 2014;343: 80–84.

332. Shalem O, Sanjana NE, Hartenian E, Shi X, Scott DA, Mikkelsen 2. Tarjei S., et al. Genome-Scale CRISPR-Cas9 Knockout Screening in Human Cells. ., PLOS Genet. 2008;4: e9.

333. Sanjana NE, Shalem O, Zhang F. Improved vectors and genome-wide libraries for CRISPR screening. Nat Methods. 2014;11: 783–784.

334. Li F, Huang Q, Luster TA, Hu H, Zhang H, Ng W-L, et al. In Vivo Epigenetic CRISPR Screen Identifies Asf1a as an Immunotherapeutic Target in Kras-Mutant Lung Adenocarcinoma. Cancer Discov. 2020;10: 270–287.

335. Joung J, Konermann S, Gootenberg JS, Abudayyeh OO, Platt RJ, Brigham MD, et al. Genome-scale CRISPR-Cas9 knockout and transcriptional activation screening. Nat Protoc. 2017;12: 828–863.

336. Patel SJ, Sanjana NE, Kishton RJ, Eidizadeh A, Vodnala SK, Cam M, et al. Identification of essential genes for cancer immunotherapy. Nature. 2017;548: 537–542.

337. Hart T, Chandrashekhar M, Aregger M, Steinhart Z, Brown KR, MacLeod G, et al. High-Resolution CRISPR Screens Reveal Fitness Genes and Genotype-Specific Cancer Liabilities. Cell. 2015;163: 1515–1526.

338. Behan FM, Iorio F, Picco G, Gonçalves E, Beaver CM, Migliardi G, et al. Prioritization of cancer therapeutic targets using CRISPR-Cas9 screens. Nature. 2019;568: 511–516.

339. Tsherniak A, Vazquez F, Montgomery PG, Weir BA, Kryukov G, Cowley GS, et al. Defining a Cancer Dependency Map. Cell. 2017;170: 564-576.e16.

340. DepMap: The Cancer Dependency Map Project at Broad Institute. [cited 15 Sep 2021]. Available: https://depmap.org/portal/

341. Fei T, Li W, Peng J, Xiao T, Chen C-H, Wu A, et al. Deciphering essential cistromes using

genome-wide CRISPR screens. Proc Natl Acad Sci U S A. 2019;116: 25186–25195.

342. Henser-Brownhill T, Monserrat J, Scaffidi P. Generation of an arrayed CRISPR-Cas9 library targeting epigenetic regulators: from high-content screens to in vivo assays. Epigenetics. 2017;12: 1065–1075.

343. Yedier-Bayram O, Gokbayrak B, Aksu AC, Cavga AD, Kayabolen A, Kala EY, et al. EPIKOL, a chromatin-focused CRISPR/Cas9-based screening platform, to identify cancer-specific epigenetic vulnerabilities. bioRxiv. Cancer Biology; 2021. p. 2021.05.14.444239. doi:10.1101/2021.05.14.444239

344. Horoszewicz JS, Leong SS, Kawinski E, Karr JP, Rosenthal H, Chu TM, et al. LNCaP model of human prostatic carcinoma. Cancer Res. 1983;43: 1809–1818.

345. Culig Z, Hoffmann J, Erdel M, Eder IE, Hobisch A, Hittmair A, et al. Switch from antagonist to agonist of the androgen receptor bicalutamide is associated with prostate tumour progression in a new model system. Br J Cancer. 1999;81: 242–251.

346. Kuruma H, Matsumoto H, Shiota M, Bishop J, Lamoureux F, Thomas C, et al. A novel antiandrogen, Compound 30, suppresses castration-resistant and MDV3100-resistant prostate cancer growth in vitro and in vivo. Mol Cancer Ther. 2013;12: 567–576.

347. Sramkoski RM, Pretlow TG, Giaconia JM, Pretlow TP, Schwartz S, Sy M-S, et al. A new human prostate carcinoma cell line, 22Rv1. In Vitro Cellular & Developmental Biology - Animal. 1999;35: 403–409.

348. Stone KR, Mickey DD, Wunderli H, Mickey GH, Paulson DF. Isolation of a human prostate carcinoma cell line (DU 145). Int J Cancer. 1978;21: 274–281.

349. Bello D, Webber MM, Kleinman HK, Wartinger DD, Rhim JS. Androgen responsive adult human prostatic epithelial cell lines immortalized by human papillomavirus 18. Carcinogenesis. 1997;18: 1215–1223.

350. Medvedeva YA, Lennartsson A, Ehsani R, Kulakovskiy IV, Vorontsov IE, Panahandeh P, et al. EpiFactors: a comprehensive database of human epigenetic factors and complexes. Database . 2015;2015: bav067.

351. Rauscher B, Heigwer F, Breinig M, Winter J, Boutros M. GenomeCRISPR - a database for high-throughput CRISPR/Cas9 screens. Nucleic Acids Res. 2017;45: D679–D686.

352. Stemmer M, Thumberger T, Del Sol Keyer M, Wittbrodt J, Mateo JL. CCTop: An Intuitive, Flexible and Reliable CRISPR/Cas9 Target Prediction Tool. PLoS One. 2015;10: e0124633.

353. Heigwer F, Kerr G, Boutros M. E-CRISP: fast CRISPR target site identification. Nat Methods. 2014;11: 122–123.

354. Figliozzi RW, Chen F, Chi A, Hsia S-CV. Using the inverse Poisson distribution to calculate multiplicity of infection and viral replication by a high-throughput fluorescent imaging system. Virol Sin. 2016;31: 180–183.

355. Li W, Xu H, Xiao T, Cong L, Love MI, Zhang F, et al. MAGeCK enables robust identification of essential genes from genome-scale CRISPR/Cas9 knockout screens. Genome Biol. 2014;15: 554.

356. Love MI, Huber W, Anders S. Moderated estimation of fold change and dispersion for RNA-seq data with DESeq2. Genome Biol. 2014;15: 550.

357. Subramanian A, Tamayo P, Mootha VK, Mukherjee S, Ebert BL, Gillette MA, et al. Gene set enrichment analysis: a knowledge-based approach for interpreting genome-wide expression profiles. Proc Natl Acad Sci U S A. 2005;102: 15545–15550.

358. Li H, Durbin R. Fast and accurate short read alignment with Burrows-Wheeler transform. Bioinformatics. 2009;25: 1754–1760.

359. Zhang Y, Liu T, Meyer CA, Eeckhoute J, Johnson DS, Bernstein BE, et al. Model-based analysis of ChIP-Seq (MACS). Genome Biol. 2008;9: R137.

360. Quinlan AR, Hall IM. BEDTools: a flexible suite of utilities for comparing genomic features. Bioinformatics. 2010;26: 841–842.

361. Zheng R, Wan C, Mei S, Qin Q, Wu Q, Sun H, et al. Cistrome Data Browser: expanded datasets and new tools for gene regulatory analysis. Nucleic Acids Res. 2019;47: D729–D735.

362. Mei S, Qin Q, Wu Q, Sun H, Zheng R, Zang C, et al. Cistrome Data Browser: a data portal for ChIP-Seq and chromatin accessibility data in human and mouse. Nucleic Acids Res. 2017;45: D658–D662.

363. Heinz S, Benner C, Spann N, Bertolino E, Lin YC, Laslo P, et al. Simple combinations of lineage-determining transcription factors prime cis-regulatory elements required for

macrophage and B cell identities. Mol Cell. 2010;38: 576–589.

364. Bailey TL, Johnson J, Grant CE, Noble WS. The MEME suite. Nucleic Acids Res. 2015;43: W39-49.

365. Maina PK, Shao P, Liu Q, Fazli L, Tyler S, Nasir M, et al. c-MYC drives histone demethylase PHF8 during neuroendocrine differentiation and in castration-resistant prostate cancer. Oncotarget. 2016;7. doi:10.18632/oncotarget.12310

366. Ellis L, Loda M. LSD1: A single target to combat lineage plasticity in lethal prostate cancer. Proceedings of the National Academy of Sciences of the United States of America. 2018. pp. 4530–4531.

367. Prinz F, Schlange T, Asadullah K. Believe it or not: how much can we rely on published data on potential drug targets? Nature reviews. Drug discovery. Springer Science and Business Media LLC; 2011. p. 712.

368. Begley CG, Ellis LM. Drug development: Raise standards for preclinical cancer research. Nature. 2012;483: 531–533.

369. Errington TM, Mathur M, Soderberg CK, Denis A, Perfito N, Iorns E, et al. Investigating the replicability of preclinical cancer biology. Elife. 2021;10: e71601.

370. Scher HI, Fizazi K, Saad F, Taplin M-E, Sternberg CN, Miller K, et al. Increased Survival with Enzalutamide in Prostate Cancer after Chemotherapy. Cabot RC, Harris NL, Rosenberg ES, Shepard J-AO, Cort AM, Ebeling SH, et al., editors. N Engl J Med. 2012;367: 1187–1197.

371. Ku SY, Rosario S, Wang Y, Mu P, Seshadri M, Goodrich ZW, et al. Rb1 and Trp53 cooperate to suppress prostate cancer lineage plasticity, metastasis, and antiandrogen resistance. Science. 2017;355: 78–83.

372. Shi J, Wang E, Milazzo JP, Wang Z, Kinney JB, Vakoc CR. Discovery of cancer drug targets by CRISPR-Cas9 screening of protein domains. Nat Biotechnol. 2015;33: 661–667.

373. Bai Y, Zhang Z, Cheng L, Wang R, Chen X, Kong Y, et al. Inhibition of enhancer of zeste homolog 2 (EZH2) overcomes enzalutamide resistance in castration-resistant prostate cancer. J Biol Chem. 2019;294: 9911–9923.

374. Layer RM, Pedersen BS, DiSera T, Marth GT, Gertz J, Quinlan AR. GIGGLE: a search

engine for large-scale integrated genome analysis. Nat Methods. 2018;15: 123–126.

375. Corces MR, Granja JM, Shams S, Louie BH, Seoane JA, Zhou W, et al. The chromatin accessibility landscape of primary human cancers. Science. 2018;362: eaav1898.

376. Cejas P, Xie Y, Font-Tello A, Lim K, Syamala S, Qiu X, et al. Subtype heterogeneity and epigenetic convergence in neuroendocrine prostate cancer. Nat Commun. 2021;12: 5775.

377. Jin ML, Kim YW, Jeong KW. BAF53A regulates androgen receptor-mediated gene expression and proliferation in LNCaP cells. Biochem Biophys Res Commun. 2018;505: 618–623.

378. Link KA, Balasubramaniam S, Sharma A, Comstock CES, Godoy-Tundidor S, Powers N, et al. Targeting the BAF57 SWI/SNF Subunit in Prostate Cancer: A Novel Platform to Control Androgen Receptor Activity. Cancer Res. 2008;68: 4551–4558.